Use Authorization

In presenting this dissertation in partial fulfillment of the requirements for an advanced degree at Idaho State University, I agree that the Library shall make it freely available for inspection. I further state that permission to download and/or print my dissertation for scholarly purposes may be granted by the Dean of the Graduate School, Dean of my academic division, or by the University Librarian. It is understood that any copying or publication of this dissertation for financial gain shall not be allowed without my written permission.

Signature ___________________________________

Date ____

SIMULATING EXPERIMENTAL BREEDER REACTOR II

APPROACH-TO-CRITICAL

by

Bilguun Byambadorj

A dissertation

submitted in partial fulfillment

of the requirements for the degree of

Doctor of Philosophy in the Department Nuclear Science and Engineering

Idaho State University

Fall 2017

Copyright

Copyright (2017) Bilguun Byambadorj

Committee Approval

To the Graduate Faculty:

The members of the committee appointed to examine the dissertation of BILGUUN BYAMBADORJ find it satisfactory and recommend that it be accepted.

Chad Pope,

Major Advisor

George Imel,

Committee Member

Jay Kunze,

Committee Member

Mary Lou Dunzik-Gougar,

Committee Member

James Mahar,

Graduate Faculty Representative

Vita

Bilguun Byambadorj was born in Ulaanbaatar, Mongolia, in 1988. After graduating high school in 2005, he attended National University of Mongolia for two years as nuclear technology major. He then enrolled at Dickinson State University in North Dakota, and received a Bachelor of Science in Mathematics and a minor in Information and Technology. He enrolled at ISU in nuclear engineering in Fall 2011 first as an undergraduate. After completing certain undergraduate engineering courses, he then enrolled as a graduate student in Fall 2012. He received his master of science degree in nuclear science and engineering in December 2014.

Dedication

I dedicate my dissertation work to my mother, Batkhishig, and father, Byambadorj, for their endless support and encouragement. I also dedicate this work to my beautiful wife, Enkhmaa, and my little brother, Tsenguun.

Acknowledgement

I would like to acknowledge and thank Dr. Chad Pope for his encouragement, countless hours of support and patience throughout this work and my academic career. A special thanks to Dr. George Imel for his professional advice and guidance throughout this work. Thank you Dr. Jay Kunze, Dr. Mary Lou Dunzik-Gougar, and Dr. James Mahar for being my committee.

I would like to acknowledge and thank Michael Smith from Argonne National Laboratory for his countless hours of technical support on my research work. I would like to thank Edward Lum, Ryan Stewart, and Quinton Beaulieu for their support.

Finally, I would like to acknowledge and thank my parents for their endless encouragement and support throughout this work and throughout my entire life.

Table of Contents

List of Figures

ABSTRACT

The research presented here focuses on simulating approach-to-critical experiment of Experimental Breeder Reactor II using DIF3D computer code and applying Modified Source Multiplication method.

Historical EBR-II approach-to-critical measured data was obtained from Argonne National Laboratory reports. The dry and wet critical experiment reports include reactor fuel loading configurations, neutron source and detector locations, and count rates of each detector.

Traditional approach-to-critical experiment of EBR-II was simulated, and neutron flux and adjoint flux were calculated by using DIF3D. The MSM correction factor was calculated. The measured 1/M data was corrected.

Finally, the improvement factor (IF) was developed to assist in confirming the improvement from ASM to MSM.

1. Introduction

When nuclear reactors startup, the approach-to-critical procedure is used to confirm expected behavior. The critical mass can also be determined by performing an approach-to-critical experiment. Traditionally, the Amplified Source Multiplication (ASM) method was used to predict reactor criticality. The major drawback with the ASM method is that detector efficiency and source importance were assumed to be constant in each fuel loading stage and were not included in the calculation. The Modified Source Multiplication (MSM) method, a better version of ASM, corrects the ASM result by applying source importance and detector efficiency. This research focuses on performing an approach-to-critical simulation of EBR-II using the nodal analysis computer code DIF3D and applying MSM. The research includes a) description of the dry and wet critical experiment of EBR-II, b) development of DIF3D models of EBR-II to simulate the approach-to-critical experiment, c) and development of MSM correction factors.

Before the EBR-II DIF3D model was built, the code needed to be tested for simulation. A simple hexagonal lattice model consisting of uranium fuel and stainless-steel reflector regions was modeled using both DIF3D and KENO VI. The eigenvalue calculation results confirmed DIF3D was successfully compiled and can be used for approach-to-critical simulation.

The EBR-II dry and wet critical experiment models were built by using engineering drawings and "An Integrated Experimental Fast Reactor Nuclear Power Station".[1] The EBR-II driver assemblies had 48.08wt% enriched ^{235}U and blanket assemblies had 0.3wt% depleted uranium fuel.

When ASM method is used to predict criticality, the detector efficiency and source strength are assumed to be constant. The ratio of count rates of two consecutive fuel loading stage is calculated as 1/M. The ASM approach-to-critical of EBR-II using measured data was compared to DIF3D simulation. Normalized 1/M curves show that the DIF3D simulation is close to measured data. More information is provided in Section 5.5.

Every detector in the system predicts different criticality when using ASM method. The MSM method does not assume constant detector efficiency and source strength, and MSM method corrects the ASM critical predictions. With the correction, every detector in the system has closer count rates and predicts consistent criticality. The MSM method and correction factor are discussed in Section 2.2 in more detail. The MSM correction was applied to measured EBR-II approach-to-critical experiment data.

The research results show that using the MSM method is indeed a better choice than ASM method to predict reactor criticality. The improvement factor (IF) was developed to assist in confirming the improvement in the prediction. The MSM predictions of the criticality are more consistent than the ASM predictions according to the IF. The improvement factor will be discussed in Section 6.3 in more detail.

The following sections of this dissertation provide a discussion of the ASM and MSM methodology, a description of EBR-II and a discussion of the EBR-II approach-to-critical experiments. Section 5 provides a chronologically based discussion of the simulation model development that occurred as part of this research project. The chronological development is provided to show the challenges and pitfalls associated with the model development. Results are presented in section 6 including development of a new method IF of evaluating the effectiveness of applying MSM correction factors.

1.1 Problem Description

The ASM method assumes detector efficiency and source importance are constant with each fuel addition. However, when performing an approach-to-critical experiment, and when simulating using computer code, the detector efficiency and source importance change with fuel addition. The source importance changes because it is a function of adjoint flux. The adjoint flux changes due to the amount of fuel in the system. The detector efficiency changes because the flux changes due to the amount of fuel in the system.

Monte Carlo method based simulation codes such as MCNP and KENO are not well suited for adjoint flux calculations which is necessary for determining source and detector importance. MCNP does not calculate adjoint flux with a kcode tally. KENO also does not calculate adjoint flux with criticality calculation. The adjoint flux can be calculated in multi-group KENO when calculating k. Also, the importance values can be calculated in KENO and MCNP using the iterated fission probability method which was recently added to both codes. However, these techniques have only been integrated into the codes for use in sensitivity analysis. Modification of the codes to support MSM related calculations requires access to the source code which is typically not provided to non. US. citizens. These issues lead to use of deterministic computer codes such as DIF3D.

DIF3D is an Argonne National Laboratory discrete ordinates and nodal analysis code for both neutron diffusion and transport problems. Additional detail on DIF3D is provided in Section 5.

1.2 Background

Every nuclear reactor is started with an approach-to-critical process. The reactor starts in a subcritical configuration with a neutron source present. The reactor slowly approaches a critical configuration as operators add fuel. The process can be simulated by using computer codes such as DIF3D. The ASM method is used to predict the critical configuration. The problem with the ASM method is a lack of inclusion of source importance and detector efficiency. The source importance and detector efficiency change as reactor changes when adding fuel. The MSM method accounts for source importance and detector efficiency changes in the reactor. The MSM method has its own weakness. Pre-calculated source importance and detector efficiency are needed for MSM correction. Fortunately, in a fast neutron spectrum, hexagonal geometry, DIF3D can be used to calculate the source importance and detector efficiency for each configuration. The MSM method is used widely around the world.

Both ASM and MSM methods were used in the French, CEA (Commissariat à l'Energie Atomique) EOLE and MASURCA critical facilities for the determination of reactivity worth by using fission chambers in subcritical configurations.[2] The standard deviation of the reactivity worth calculated by the MSM method is ten times smaller than the standard deviation of the reactivity worth calculated using the ASM method. These techniques were used to determine the reactivity effect of various perturbations from an unperturbed state. They were based on relative measurements of count rate variations between an unperturbed configuration and a perturbed configuration. The consistency of the MSM calculation and the associated corrections were judged by three indicators: the first indicator addresses the dispersion in inferred reactivities by the ASM when several detectors are used. The dispersion can be improved when MSM factors are considered. The second indicator addresses the discrepancy between the calculated reactivity and the final MSM-corrected experimental reactivity. The last indicator addresses the calculation-to-experiment discrepancy of the reaction rate ratios between the perturbed configuration and the reference configuration.

In Italy, Imel, G., et al. demonstrated the MSM correction for sensitivity of a TRIGA reactor core. “The TRIGA reactor at the Casaccia Center of ENEA was studied in a number of configurations ranging from k_{eff} approximately 0.993 to 0.93”.[3] A set of experiments were begun not knowing how sensitive the TRIGA reactor would be to core geometry changes, control rod perturbations, etc.

The MSM correction is not necessarily a perfect solution to the source importance and detector efficiency. “The MSM method was tested in calculation of rod worth using an educational reactor in Kyung Hee University, AGN-201K. For this study, a revised nuclear data library and a neutron transport code system, TRANSX-PARTISN, were used for the calculation of correction factors for various control rod positions and source locations”.[4] Experiments were designed and performed to enhance errors in ASM from the location effects of source and detectors. The forward, adjoint, and fixed source fluxes were solved for the MSM correction factor calculation. The maximum difference in correction factors were less than 1%, and therefore, the correction in sub-critical measurement was not done effectively.

“The MSM is applied to the prototype FBR Monju**.** This static method to estimate the reactivity in sub-critical conditions has already given good results on commercial pressurized water reactors. The MSM consists both in the extraction of the fundamental mode seen by a detector to avoid the effect of higher modes near sources, and the correction of flux distortion effects due to control rod movement between different reactor states".[5] Among Monju's unique characters that have an influence on the MSM factors are: the presence of two californium sources near the core and the position of the detector, which is located far from the core outside of the reactor vessel.

The EBR-II dry and wet critical experiments measured results coupled with DIF3D simulation provide a unique source of detailed fast spectrum reactor approach-to-critical measurements where development of MSM correction factors can be determined and evaluated.

1.3 Method

To calculate MSM correction factors for a better prediction of EBR-II criticality, a simulation model and measured results are needed. The approach-to-critical experiment will be simulated by DIF3D. The source importance and detector efficiency can be calculated from DIF3D simulation results.

2. Subcritical Multiplication

Subcritical multiplication is a theory that represents the changes in the neutron population in a subcritical reactor through reactivity changes. A system is subcritical if, for any nonzero initial neutron population, the expected population, at later times as time goes to infinity, will die out unless it is sustained by either an internal or external neutron source.[6] If a neutron source is added to the reactor, the neutron population will be both fission neutrons and source neutrons:

$$N = S + Fission\ Neutrons \tag{1}$$

Where:

N – Total number of neutrons in the reactor per generation

S – Number of neutrons from the source

The number of neutrons generated from fission is:

$$N_i * k$$

Where:

k –Multiplication factor

The total number of neutrons in the next generation according to Equation 1 is:

$$N_{i+1} = S + N_i * k$$

The total number of neutrons in the n^{th} generation will become:

$$N_n = S * (1 + k + k^2 + k^3 + \cdots + k^n) \tag{2}$$

The subcritical multiplication factor, M, is the factor by which the neutron population increases:

$$M = 1 + k + k^2 + k^3 + \cdots + k^n$$

When k is greater than 1, M approaches infinity. When k is less than 1, the subcritical multiplication factor converges to:

$$M = \frac{1}{1-k} \tag{3}$$

Thus, N will become:

$$N = \frac{S}{1-k}$$

When M approaches infinity, k approaches 1, but 1/M will approach 0. Thus, a 1/M versus fissile mass plot is used when approaching criticality.

2.1 Amplified Source Multiplication

Example: Assume there is a neutron source which releases 100 neutrons in each generation and k=0.7 (subcritical). After the first generation, there will be N*k fission neutrons in the second generation and the total number of neutrons in particular generation will be represented as Equation 2. In second generation, there will be 100 neutrons from the source and 70 fission neutrons which are produced from fission in first generation. In third generation, there will be 100 neutrons from the source, 70 fission neutrons from second generation which were produced from fission from 100 source neutrons, and 49 fission neutrons from fission of 70 fission neutrons which were produced from first generation. Starting with the 13^{th} generation, the number of neutrons in each generation converges to 330. After few generations, the neutrons in the system will be constant. The total neutron population, fission neutrons and source neutrons in each generation are shown in Table 1.

Table 1. Total Number of Neutrons versus Number of Generations

Generation	1	2	3	4	5	6	7	8	9	10	11	12	13	14	15
Source neutrons	100	100	100	100	100	100	100	100	100	100	100	100	100	100	100
Fission Neutrons		70	70 49	70 49 34	70 49 34 24	70 49 34 24 17	70 49 34 24 17 12	70 49 34 24 17 12 8	70 49 34 24 17 12 8 6	70 49 34 24 17 12 8 6 4	70 49 34 24 17 12 8 6 4 3	70 49 34 24 17 12 8 6 4 3 2	70 49 34 24 17 12 8 6 4 3 2 1	70 49 34 24 17 12 8 6 4 3 2 1 0	70 49 34 24 17 12 8 6 4 3 2 1 0
Total Neutrons	100	170	219	253	277	294	306	314	320	324	327	329	330	330	330

Since the subcritical multiplication factor (M) and the effective neutron multiplication factor (k_{eff}) are related, approach to criticality can be performed through monitoring the subcritical multiplication factor. The k_{eff} will approach unity as positive reactivity is added to a subcritical reactor. According to Equation 3, as k_{eff} gets close to one, the subcritical multiplication factor becomes larger. When the reactor is close to criticality, M increases faster for step insertions of positive reactivity. When the reactor becomes critical, M will be infinite. For this reason, calculating and plotting M during approach to criticality is not possible because M is infinite when the reactor becomes critical. Thus, the inverse of the subcritical multiplication factor (1/M) is used for plotting and monitoring, since as M approaches to infinity, 1/M approaches 0.

The neutron detectors used to monitor the number of neutrons in the core do not count every single neutron in the system. The count rate the detector will see is shown by Equation 4.

$$CR = \eta S \frac{1}{1 - k_{eff}} \tag{4}$$

Where:

η – Detector efficiency

If the detector efficiency and source strength are assumed to be constant from generation to generation, the ratio between two count rates will cancel the detector efficiency and source strength terms.

$$\frac{CR_1}{CR_2} = \frac{\eta S \frac{1}{1 - k_1}}{\eta S \frac{1}{1 - k_2}} = \frac{M_1}{M_2} \tag{5}$$

A reference count rate will be needed to simplify the above equation. If CR_1 is substituted with the count rate of the initial configuration (CR_0), then k_0 will equal to 0 and M_0 will equal to 1. Thus $1/M_2$ can be evaluated using count rates as:

$$\frac{CR_0}{CR_2} = \frac{1}{M_2}$$

In general:

$$\frac{CR_0}{CR_i} = \frac{1}{M_i} \tag{6}$$

Example:

Assume the initial count rate, CR_0, is 20 counts per second, along with count rates as a function of control rod position as shown in Table 2.

Table 2. Count Rates in each Control Rod Position

Rod Position (inches)	Count Rates (cps)
1	22
3	27
5	33
7	39
9	54
11	94
15	200

The 1/M values calculated for each rod position are listed in Table 3.

Table 3. Calculated 1/M Value

Rod Position (inches)	Count Rate (cps)	1/M
0	20	1
1	22	0.909
3	27	0.741
5	33	0.606
7	39	0.513
9	54	0.370
11	94	0.213
15	200	0.100

The values in Table 3 can be plotted as shown in Figure 1 with 1/M in the y-axis and rod position in the x-axis. The x-intercept of the extrapolation between two consecutive points is the prediction of criticality.

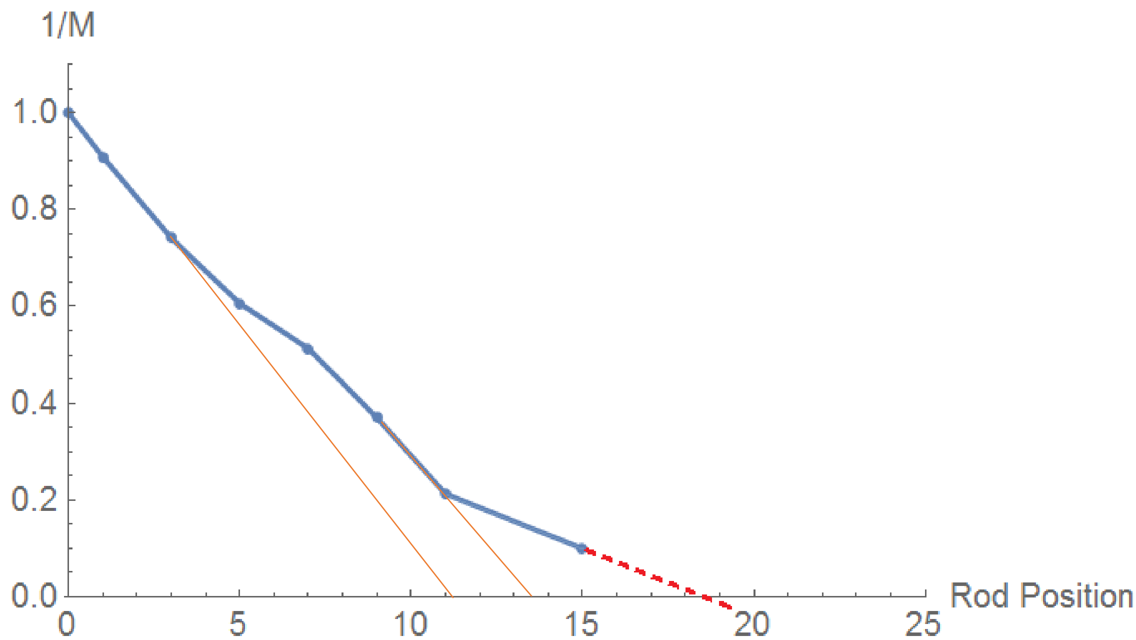

Figure 1. The 1/M value as a function of control rod position.

The extrapolation of the last pair of points is more accurate than that of the previous pairs because the 1/M values of the last two points are close to 0 and reactor is close to criticality. It is shown that the system will go critical when control rod position reaches 18.5 inches. "The general rule of thumb for adding more fuel during approach-to-critical is to add **no more than** half of the additional amount of fuel needed to achieve criticality **with the control rods in the least reactive position**. For example, if 1/M curve predicts that reactor needs 6 more fuel assemblies to achieve criticality **with the control rods in the least reactive position**, operator should add **no more than** 3 fuel assemblies, and then take the count rate."

The ASM method can be used for either adding more fuel assemblies or moving the control rods in the system. Nuclear reactor approach-to-critical experiments do not actually start with no fuel in the core when $k^{-}_{eff} = 0$. In fact, it starts with a subcritical configuration where $k_{eff} > 0$. Also, simulating approach-to-critical with $k_{eff} = 0$ is a very poor choice, because the $k = 0$ has no physical or mathematical meaning. A better approach is a starting point with a significant k (> 0.9).

2.2 Modified Source Multiplication

The detector efficiency and source importance is not always constant during approach-to-critical, in fact, they are different with each new core configuration. The detector efficiency is a ratio of detected neutrons and total neutrons in the system. The total number of neutrons in the system is a fixed value established by the source and M. The detectors only count those neutrons which interact with the detector. Thus, the number of neutrons detected is always much smaller than the total number of neutrons.

Assume a system consists of fuel assemblies, three detectors and a source as shown in Figure 2.

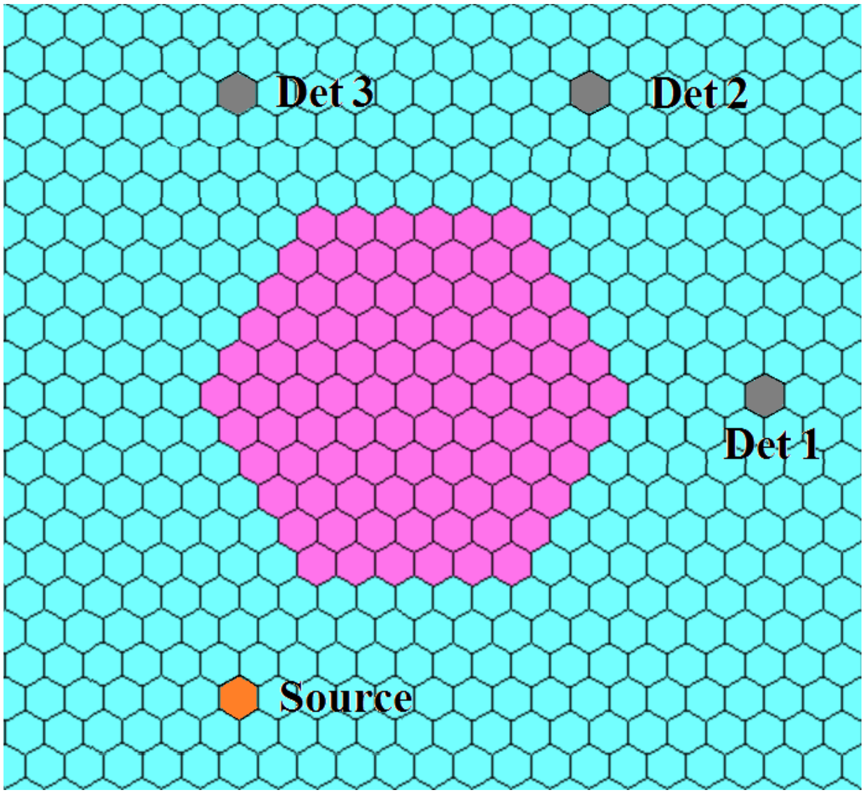

Figure 2. A hexagonal lattice fuel configuration with neutron source and detectors (Pink is fuel and teal is sodium).

In this system, detector #1 and #3 have the same efficiency based on symmetry. Detector #2 will have different efficiency due to its location in relation to the source.

Now, we add fuel on one side of the core region as shown in Figure 3. The detectors #1 and #3 will no longer have equal efficiency due to the added fuel. The number of fission neutrons counted in detector #1 and #3 will be different. Similarly, detector #2 will experience an altered efficiency due to the core configuration change. The source importance will also change due to change in fission neutrons and adjoint flux.

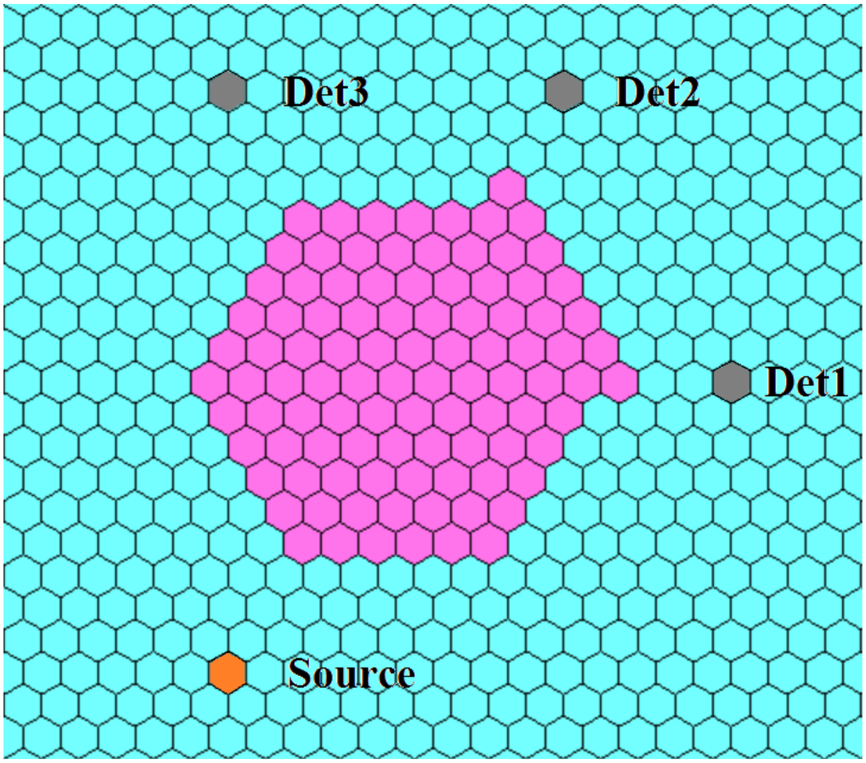

Figure 3. A hypothetical model with added fuel assemblies.

Now we have 3 detectors each with different counts but the total neutron population is the same for all. Thus, the efficiency is different between detectors and also different from prior configurations.

In this case, equation 5 cannot be used to eliminate detector efficiency and source strength. Thus, we have the following equation:

$$\frac{CR_1}{CR_2} = \frac{\eta_1 S_1 \dfrac{1}{1-k_1}}{\eta_2 S_2 \dfrac{1}{1-k_2}} = \frac{\eta_1 S_1 (1-k_2)}{\eta_2 S_2 (1-k_1)} = \frac{\eta_1 S_1 M_1}{\eta_2 S_2 M_2} \tag{7}$$

The modified source multiplication (MSM) factor is the change in the ηS term between two states. To obtain the physical meaning, these terms need to be mathematically defined.

$$\eta = \frac{Detected\ Neutrons}{Total\ Number\ of\ Neutrons} = \frac{\int \Sigma_d \phi}{\int \nu \Sigma_f \phi} = \frac{\langle \Sigma_d \phi \rangle}{\langle F \phi \rangle} \tag{8}$$

Where:

Σ_d – Detector Cross Section

As shown in equation 8, the symbol of inner product, < >, means the integral over all the reactor space and energy. A new term, source importance, needs to be defined using the adjoint flux ϕ^*:

$$Source\ Importance = \frac{Average\ Source\ Neutrons}{Fission\ Neutrons} = \frac{\langle \phi^* S \rangle}{\langle \phi^* F\phi \rangle} \quad (9)$$

The "effective" source neutrons can be represented by multiplying source importance by total fission neutron rate:

$$S_{eff} = \frac{\langle \phi^* S \rangle}{\langle \phi^* F\phi \rangle} \langle F\phi \rangle \qquad (10)$$

The MSM correction factor can be found by multiplying efficiency by the effective source term:

$$\eta S_{eff} = \frac{\langle \phi^* S \rangle}{\langle \phi^* \mathrm{F}\phi \rangle} \langle \mathrm{F}\phi \rangle \frac{\langle \Sigma_d \phi \rangle}{\langle \mathrm{F}\phi \rangle} = \frac{\langle \phi^* S \rangle}{\langle \phi^* \mathrm{F}\phi \rangle} \langle \Sigma_d \phi \rangle \qquad (11)$$

The adjoint flux at position r is a measure of how effective an absorber inserted at position r in the reactor is in changing the reactivity of the core. It means the adjoint flux is the "importance" of the point r with respect to reactivity changes. It is not limited to only absorbers in the reactor.

The application of the MSM correction factors is discussed in Section 6.

3. Detailed Description of EBR-II

The Experimental Breeder Reactor II (EBR-II) was a sodium cooled, fast spectrum, breeder reactor. It had a maximum thermal output of 62.5 MW and produced approximately

20 MWe. The EBR-II power plant complex was located in Idaho, and the plant included a complete, remotely-operated fuel-processing and fuel-element fabrication facility. It was the first reactor in the US to operate on a closed fuel cycle.

The EBR-II reactor core consisted of 637 hexagonal assemblies. The assemblies were divided into three regions: core, inner blanket, and outer blanket. Later, the core was reconfigured to support irradiation activities. As shown in Figure 4, the control rods were located at the outer edge of the core region and two safety rods were located at the third row of the core region.

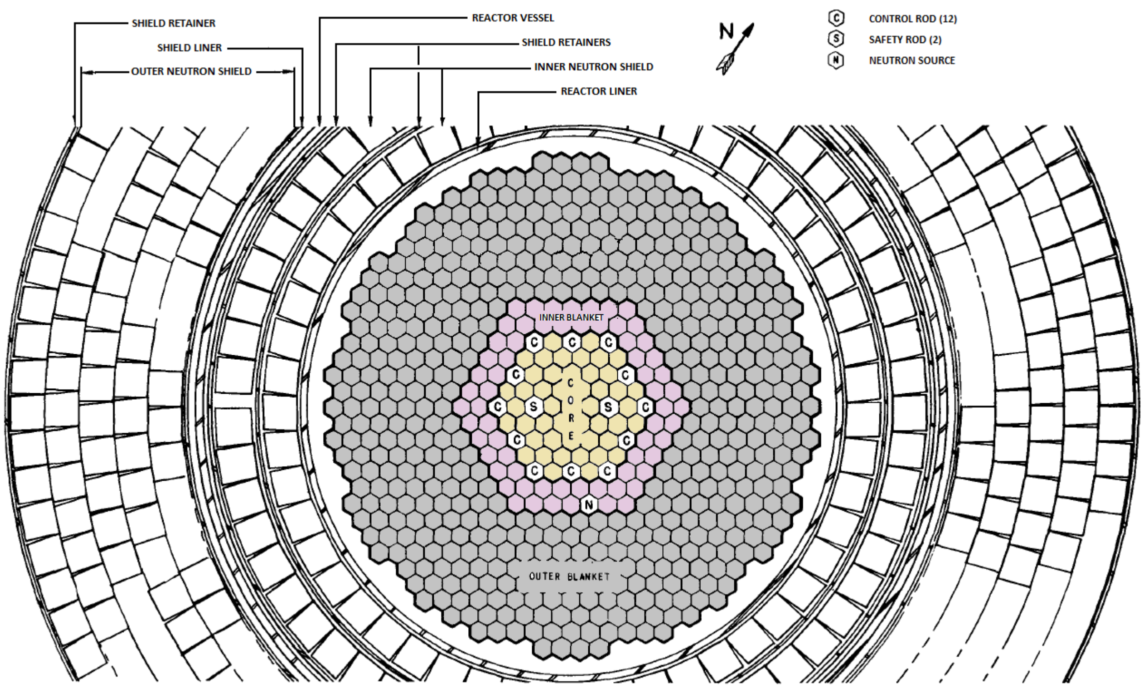

Figure 4. The EBR-II reactor core configuration.

The approach-to-critical experiments core used for this analysis consisted of two safety rods, 11 regular control rods, one special control rod, 47 driver subassemblies, 66 inner blanket subassemblies and 510 outer blanket subassemblies.

3.1 Driver Subassembly

The driver subassembly, as shown in Figure 5, consisted of three regions containing fissile materials: upper blanket, driver, and lower blanket region. The over-all length of the driver subassembly was 233.24-cm. The fuel region consists of 91 fuel elements in a hexagonal lattice.

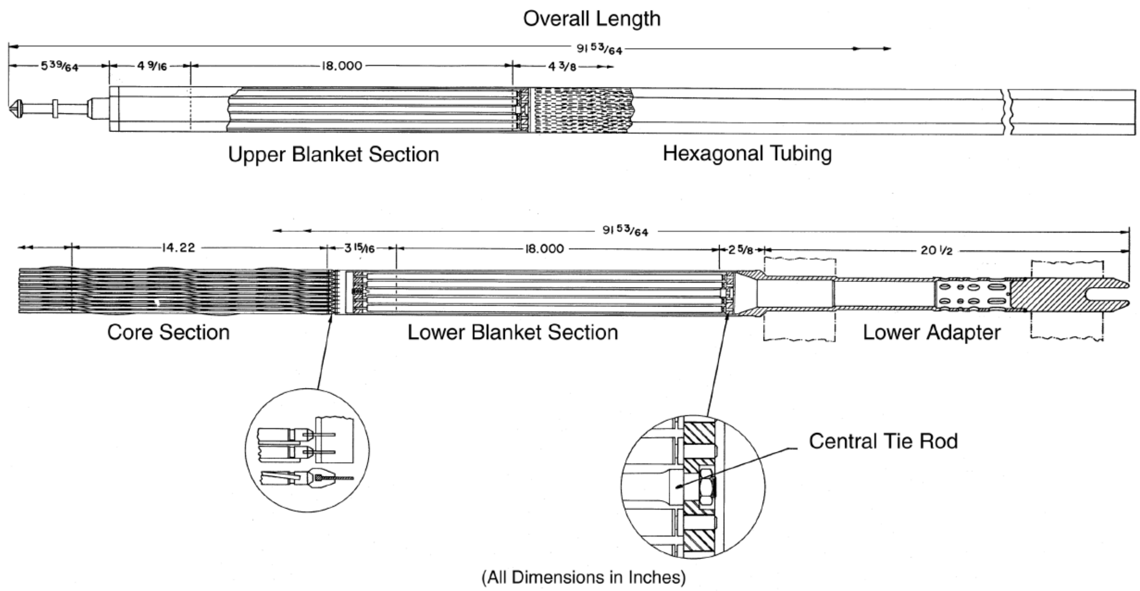

Figure 5**.** Driver fuel subassembly (all dimensions are in inches).

An individual fuel element, as shown in Figure 6, was 44.07-cm long not including spade in the bottom. The fuel element consisted of fuel slug, sodium gap, stainless-steel 316 cladding, stainless-steel 316 cap and stainless-steel 316 wire wrap. The report "The EBR-II Dry Critical Experiments Experimental Results" indicate that the fresh fuel slug was 95wt% uranium and 5wt% fissium alloy.[7] Fissium is a given name to a mixture of fission product elements (atomic numbers 40 to 47) as shown in Table 4. The uranium is 48.08% enriched ^{235}U. The active fuel region was 36.12-cm long, and fuel slug diameter was 0.366-cm.

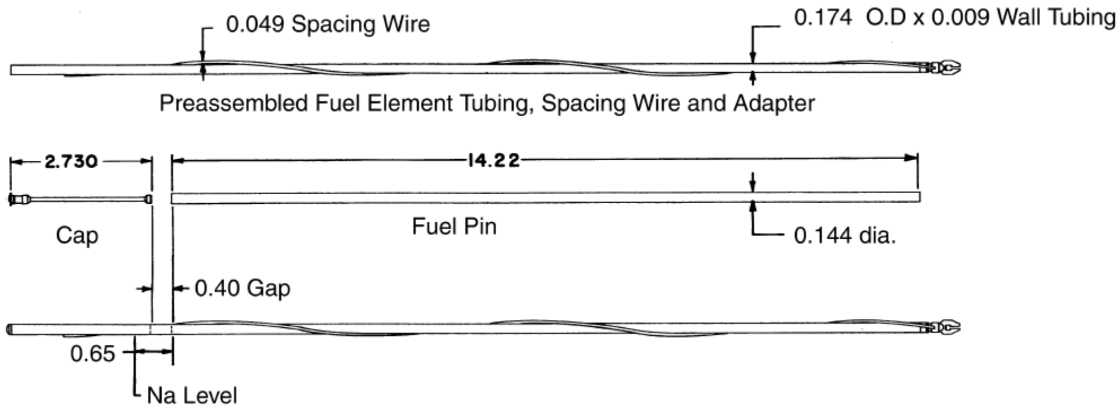

Figure 6. Driver fuel element (all dimensions are in inches).

Table 4. Uranium-Fissium Alloy Composition

Elements	Weight %
Uranium	95.00
Molybdenum	2.46
Ruthenium	1.96
Palladium	0.19
Zirconium	0.10
Niobium	0.01

The upper and lower blanket regions were geometrically identical to each other. Both consisted of 19 pin-type elements in a hexagonal lattice. The blanket elements, as shown in Figure 7, were about 3.78 inches longer and had 2.2 times bigger diameter than a fuel element. It consisted of stainless-steel 316 cladding, depleted uranium, sodium gap, and stainless-steel 316 plug springs. The blanket slug, 0.3% depleted uranium, was 45.72-cm in length and 0.803-cm in diameter.

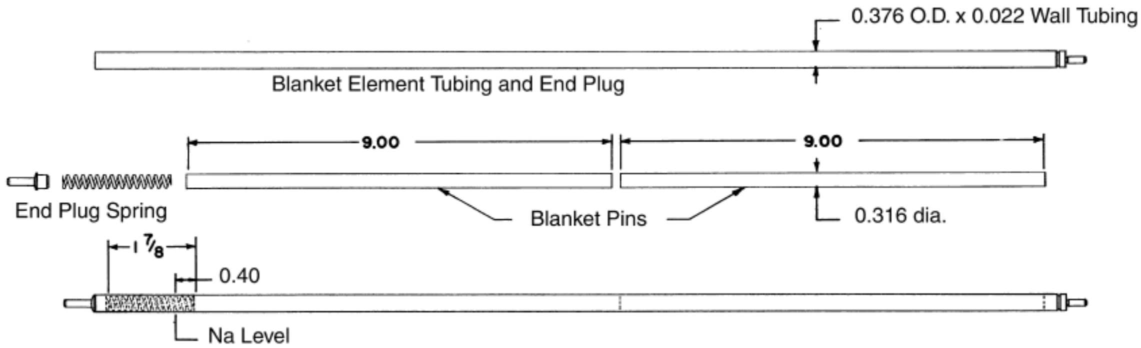

Figure 7. Upper and lower blanket element (all dimensions are in inches).

3.2 Control Subassembly

Each EBR-II control rod had its own electrical-mechanical drive mechanism. There were 11 control rods and one special control rod during critical experiments. The control rods were arranged that one drive mechanism operates at any given time except reactor scram when all 12 drive mechanisms operate together. Each control rod moved 14 inches (35.56 cm) vertically with a constant speed. Control rods were disconnected from their drive mechanisms, when they were in the least reactive position, during fuel handling operations. Figure 8 shows the control rod motion. The control assembly consisted of two hexagonal tubes. The smaller one contains the fuel elements and fits into a normal driver size hexagonal tube. When the control rod is moved up by 14 inches, the fuel section of the control rod is 0.25 inches (0.635 cm) below the driver fuel region. When a control rod is at the least reactive position, the top of the control rod fuel section is aligned with the bottom of the driver fuel section.

The control rod fuel section consists of 61 fuel elements in a hexagonal lattice. The fuel element is a standard driver fuel element which consists of 90wt% uranium and 10wt% fissium fuel slug, stainless-steel 316 cladding, wire-wrap and end plug.

Since the control rods are fuel, they are inserted into the core to add reactivity and lowered below the core region to remove reactivity. This is different than poison control rods used in LWR's.

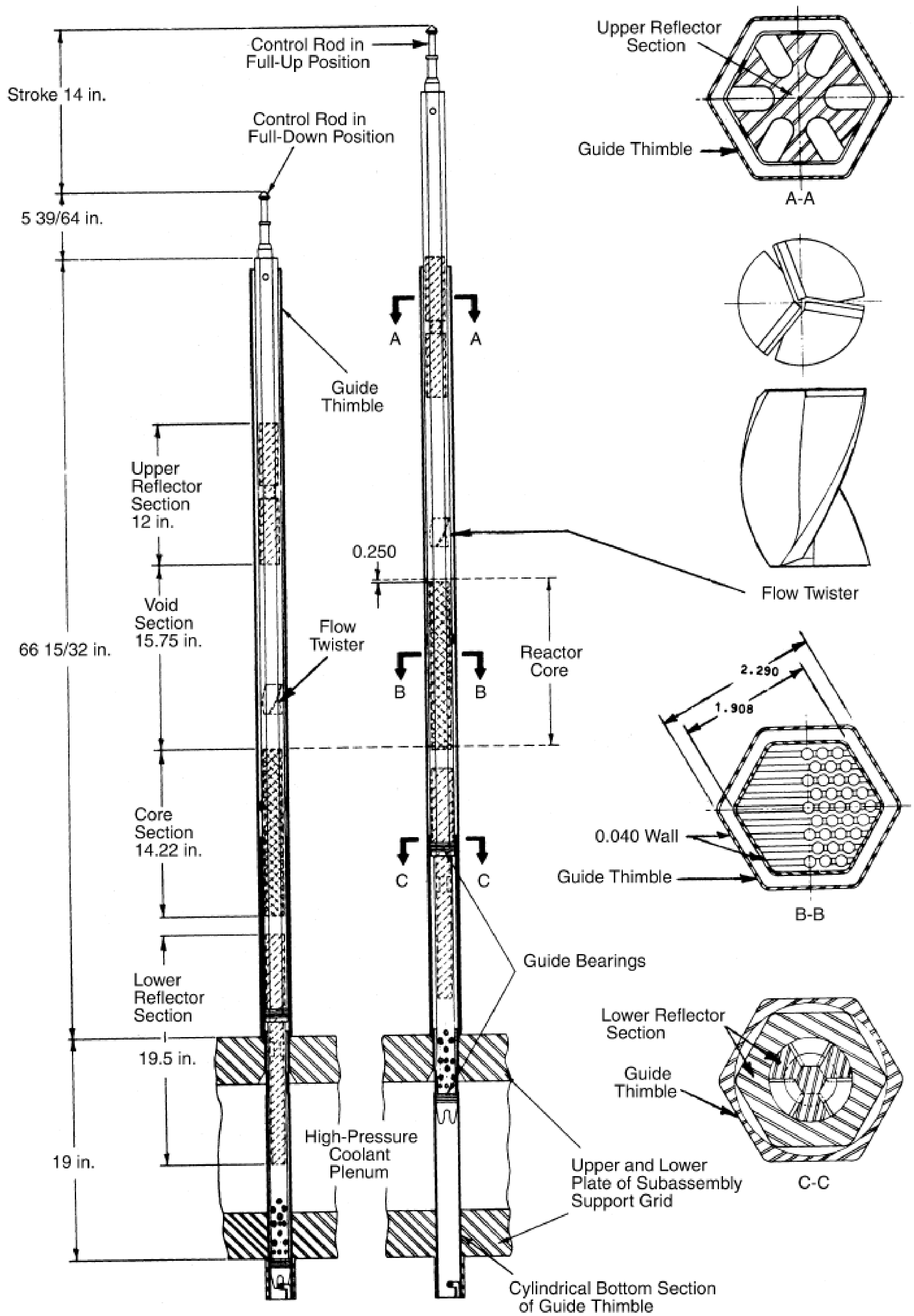

Figure 8. Control rod (all dimensions are in inches).

Above the fuel section, there is a void and upper reflector section. It is different for the one special control rod. These sections of the special control rod had B_4C poison elements. There were 7 poison elements in the special control rod in a triangular lattice. As shown in Figure 9, the capsule contains B_4C poison and a stainless-steel shield. The upper reflector section of a regular control rod consists of stainless-steel reflector. The special control rod contains B_4C poison capsules instead of stainless-steel reflector.

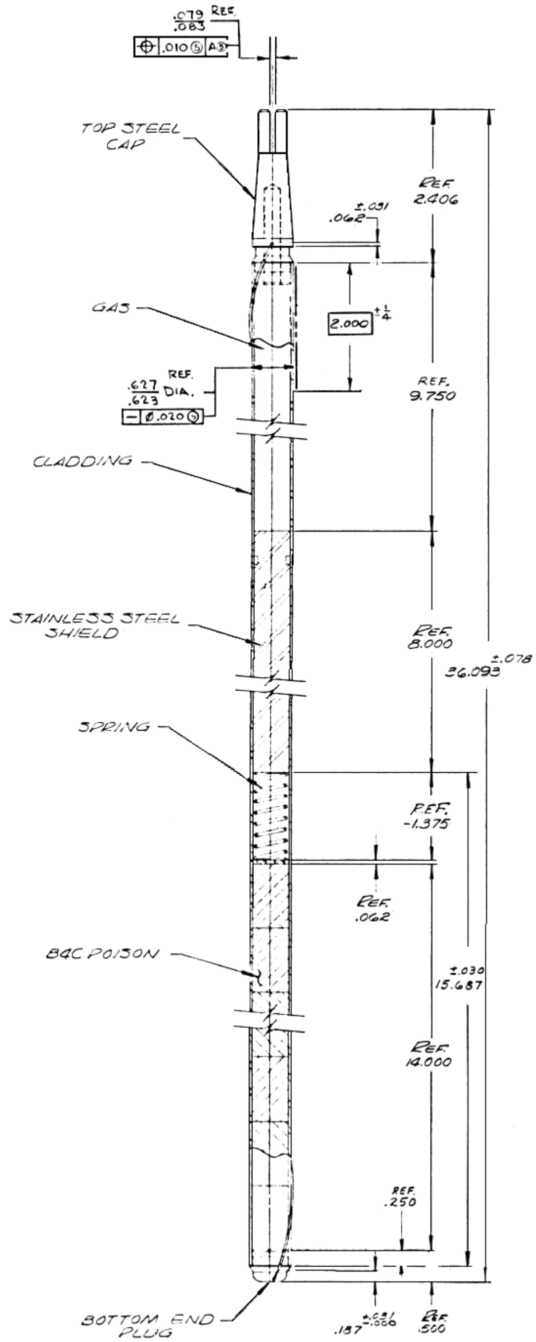

Figure 9. B_4C capsule (all dimensions are in inches).

3.3 Safety Subassembly

The EBR-II safety subassemblies consisted of a safety rod and guide thimble. In certain ways, the safety rods were almost identical to control rods, except the length of the void section and the design of the lower end, as shown in Figure 10. The safety rod drive system is below the reactor core; thus, it would not interfere with fuel loading or control rod mechanisms which are on the top of the reactor. Both safety rods were fully inserted into the reactor, at the most reactive position, during normal reactor operations and fuel handling. The two safety rods were moved together with a single drive mechanism. The purpose of the safety rod was to shut down the reactor from unintended critical condition during refueling.

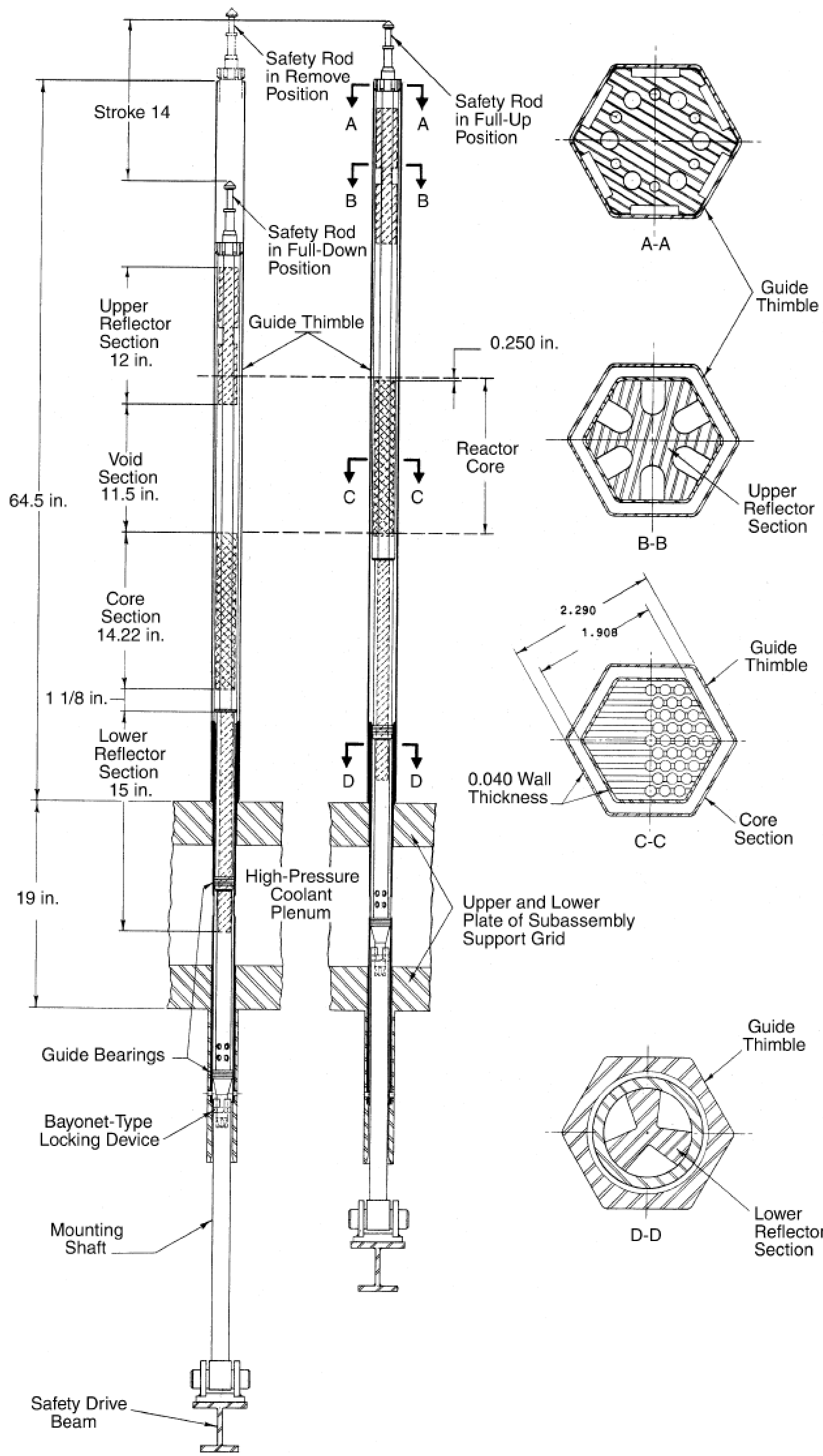

Figure 10. Safety rod.

3.4 Inner and Outer Blanket

As shown in Figure 11, the inner and outer blanket subassemblies consisted of 19 depleted uranium fuel elements in triangular lattice, a bottom adapter, and an upper pole piece. The only difference between inner and outer blanket subassemblies was the bottom adapter and the coolant flow design as shown in Figure 12.

The blanket elements were about 3.6 times longer and 2.5 times larger diameter than the driver fuel elements. Each blanket element was 158.59-cm long, and 1.1-cm in diameter. The blanket element consisted of five fuel pins each 27.94-cm long, sodium gap, stainless-steel 316 spring, bottom end spade and top end cap. The depleted uranium fuel consisted of 0.3wt% ^{235}U and 99.7wt% ^{238}U.

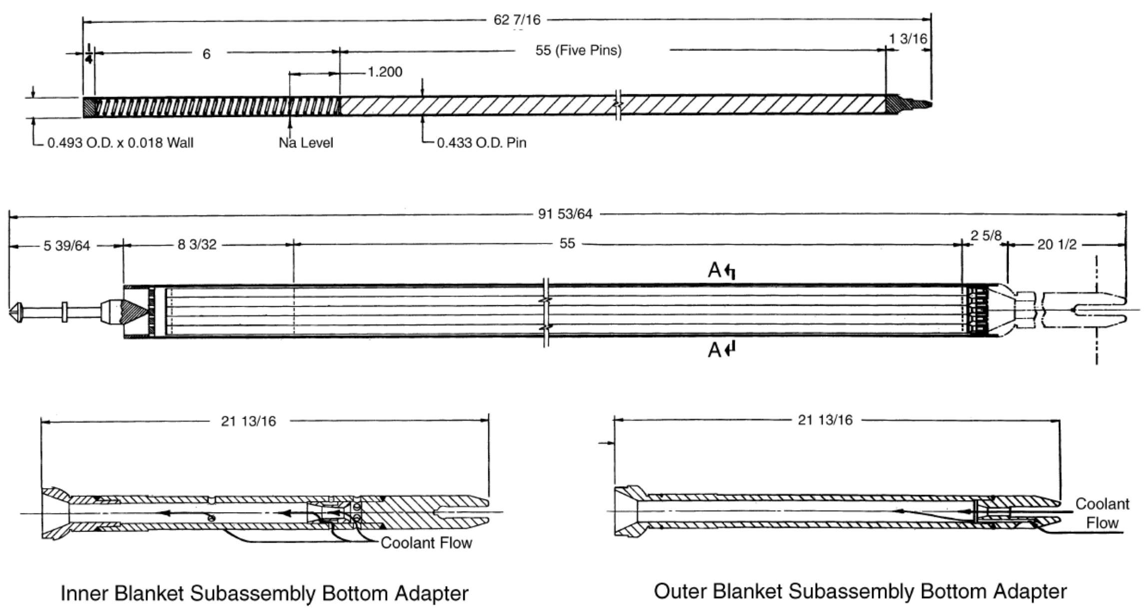

Figure 11. Inner and outer blanket subassemblies (all dimensions are in inches).

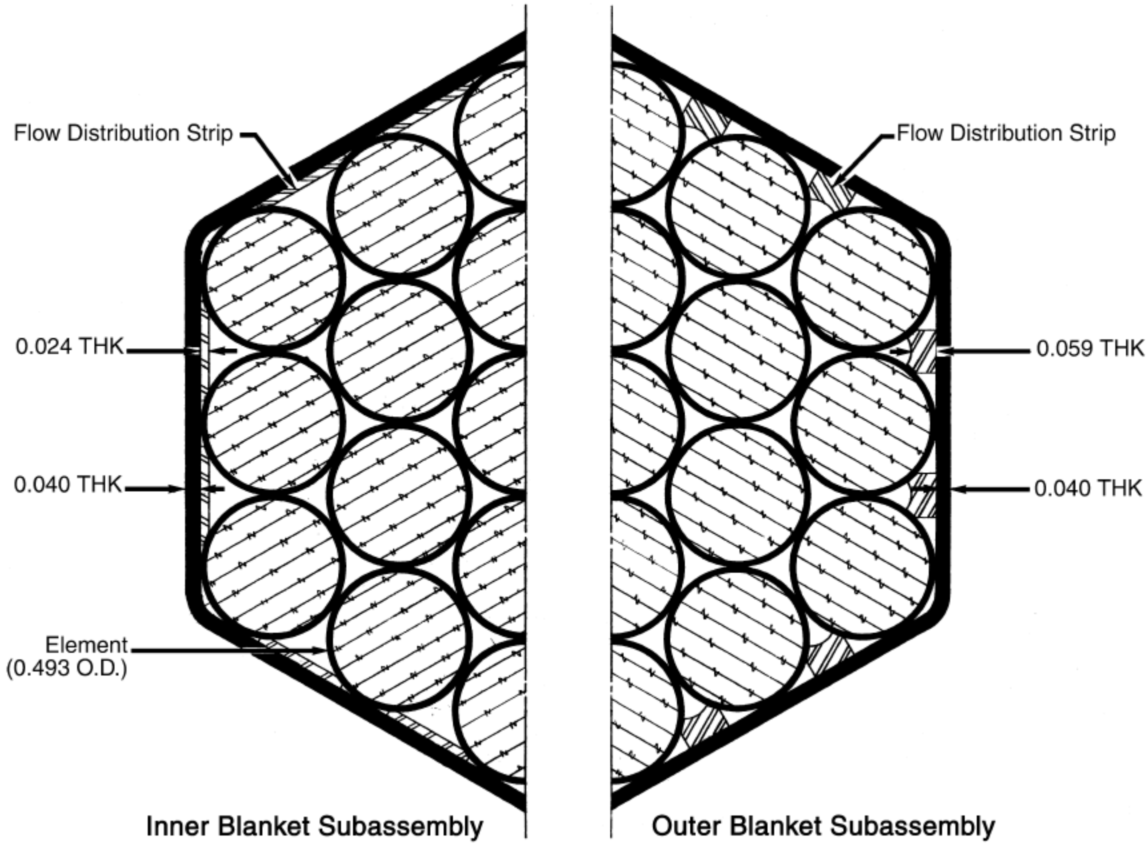

Figure 12. Inner and outer blanket subassembly cross-sectional view (all dimensions are in inches).

4. EBR-II Critical Experiment

The approach-to-critical experiments of EBR-II were zero power experiments. According to "EBR-II Dry Critical Experiments Experimental Program, Experimental Procedures and Safety Consideration"[8] report, there were two objectives to these experiments:

1. *To determine information relating to the performance of the system without sodium coolant, for future comparison with information derived with sodium coolant. By comparison, it will then be possible to ascertain various sodium effects on the neutronics of the system.*
2. *To determine and/or verify certain operational data to permit modification or improvement of the system (neutron shield, instrumentation, etc.) prior to the introduction of sodium into the system. After sodium filling it will be difficult to alter, modify, or correct many of the system components.*

There were some significant considerations regarding the experiment such as a) the maximum reactor power level should be less than 1 kW, b) there should not be any initial contamination of the fissionable or fertile materials with fission products or plutonium, with no significant quantities of these material generated during critical experiments, and c) the dry critical reactor mass is larger than wet critical reactor mass, so the core must be at least 20% larger in diameter than it is considered for the reactor with sodium present.

4.1 Dry Critical Experiment

The EBR-II reactor achieved dry criticality on September 30, 1961. The reactor started up with no sodium coolant in the vessel. The experiment used the same components and fuel as normal power operations. This operation was simplified due to low power level

(<1 kW). Since the reactor did not have liquid sodium coolant, special in-core instruments were used to obtain more accurate information of the core during operation.

Since the dry critical mass of ^{235}U was 47.9 kg larger than wet critical mass, additional 17 enriched subassemblies were needed. These enriched subassemblies were loaded in the inner blanket region. However, there was no specific engineering drawings of the enriched inner blanket subassembly. It was mentioned in the "EBR-II Dry Critical Experiments"[8] report that there were indeed inner blanket subassemblies which were highly enriched. The ^{235}U amount was equal to that of a driver subassembly.

Prior to the critical experiment, the core was loaded with stainless-steel dummy subassemblies, natural uranium subassemblies, inner and outer blanket subassemblies. The approach-to-critical experiment was started with the two safety rods inserted into their most reactive positions, all control rods were inserted in their least reactive positions and one driver subassembly was at the center location as shown in Figure 13. An antimony-124 beryllium neutron source rod was located in 7th row. The source strength was 270 Ci and a half-life of 60 days. During the critical experiment, the source strength decayed 13%, and all count rates were corrected to 189 Ci source strength.

In a dry critical experiment, it was possible to use in-core neutron detectors. BF_3 neutron detectors were located in inner blanket row 6 and 7, and outer blanket row 11 and 13.

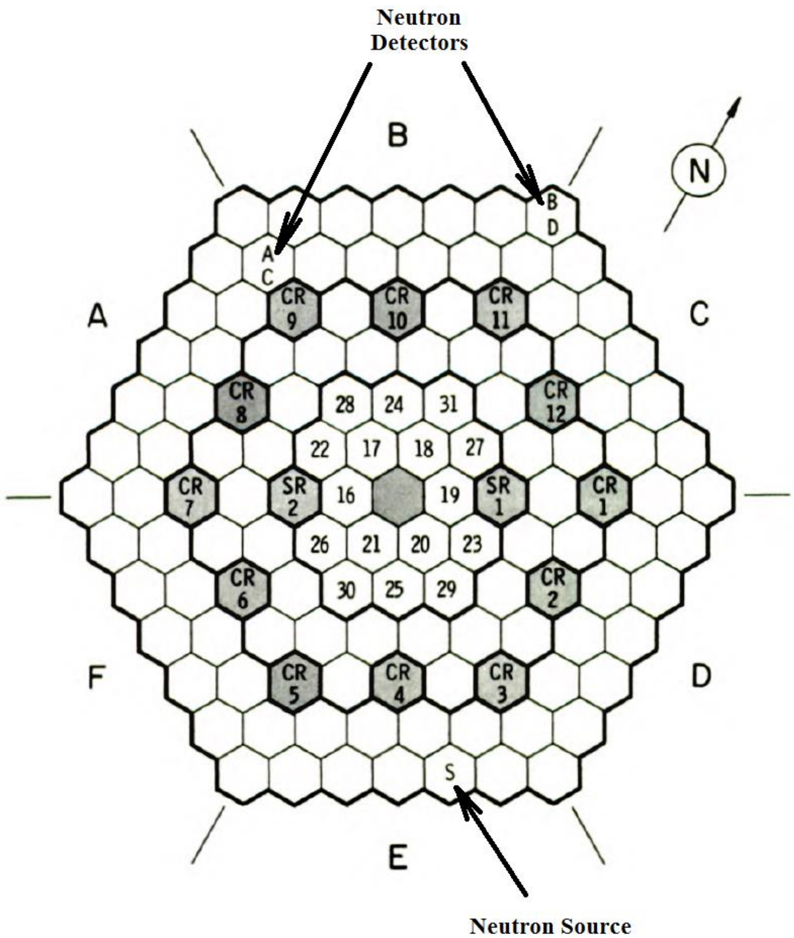

Figure 13. Dry critical experiment, approach-to-critical loading #1.

From this point on, driver and enriched inner blanket subassemblies were added to the core as symmetric as possible. The core configurations are shown in Figure 14 and Figure 15. Since EBR-II subassemblies were only locked at the bottom, a single subassembly was allowed to be removed during fuel loading.

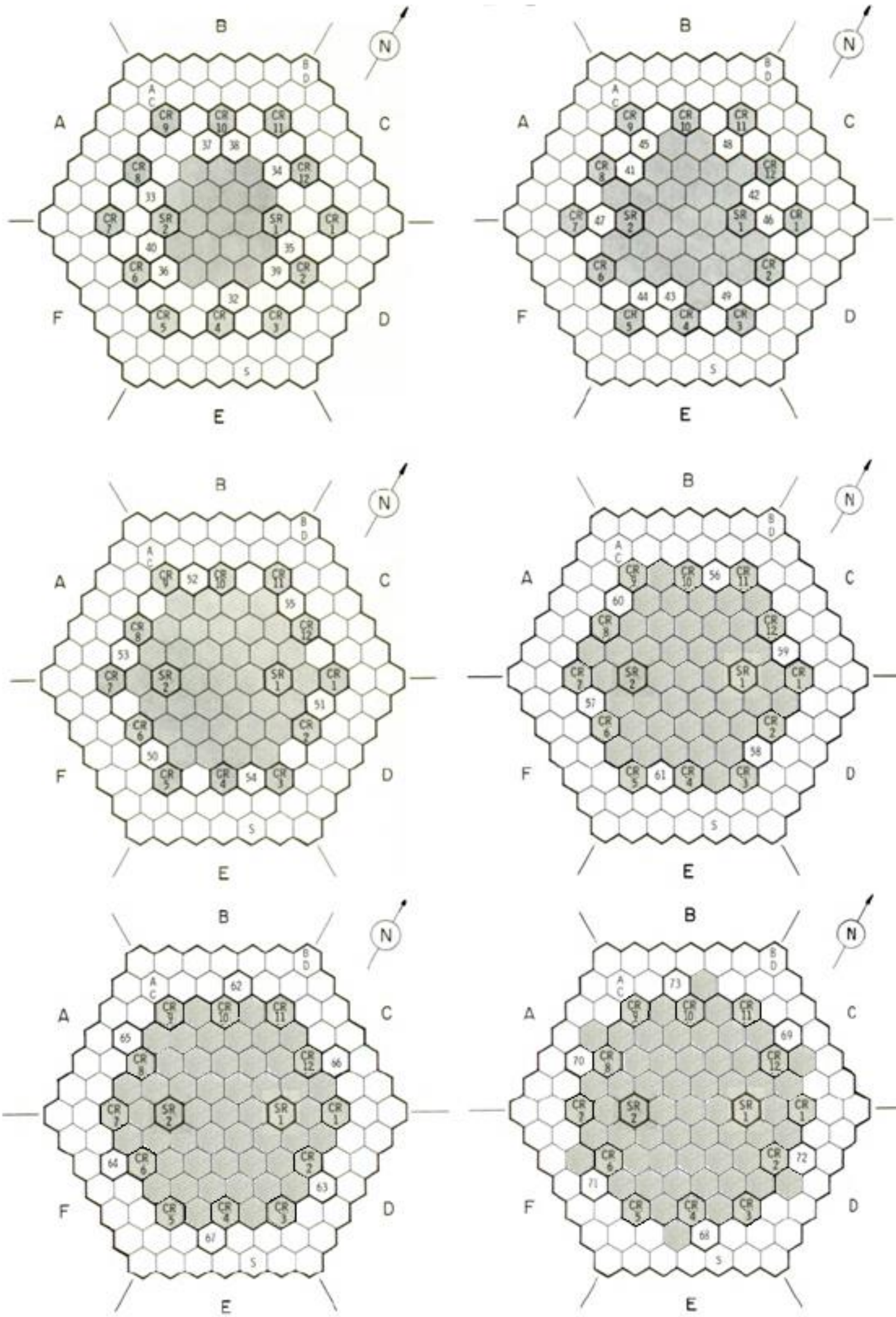

Figure 14. Dry critical experiment, approach-to-critical loading #2 - #7.

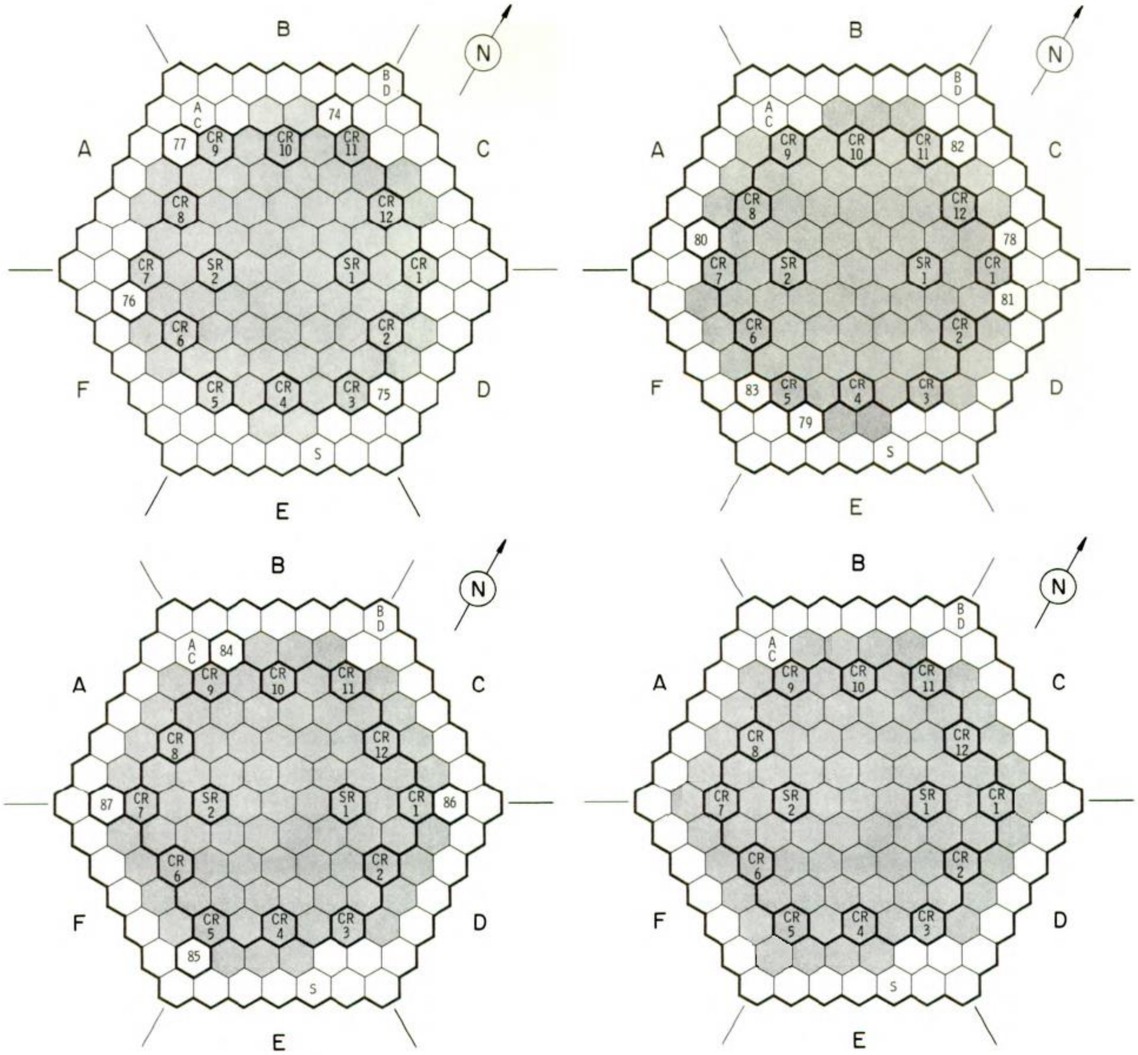

Figure 15. Dry critical experiment, approach-to-critical loading #8 - #11.

The amount of ^{235}U loaded into the core is shown in Table 5.

Table 5. Dry Critical Experiment Fuel Subassembly Loading Increment

Loading No.	Number of Subassemblies Added/Loading	Total Number of Subassemblies	Total Kg of ^{235}U
1	15	15	29.21
2	16	31	74.18
3	9	40	99.49
4	9	49	124.98
5	6	55	141.86
6	6	61	158.81
7	6	67	175.73
8	6	73	192.67
9	4	77	203.95
10	6	83	220.88
11	4	87	232.18

4.2 Wet Critical Experiment

The wet critical experiments were performed after various dry critical experiments.[9] The reactor was filled by liquid sodium coolant and similar low-power experiments were performed. These experiments were designed to provide two types of information: a) the data that are necessary for operating power reactor system such as control rod worth, nuclear instrument response and neutron source strength, and b) the general information such as total worth of the sodium coolant and critical size of the reactor. The wet critical experiments were performed at 600 °F.

Although, the dry and wet critical experiments were similar, there were some differences such as core loading, neutron source strength and location, and detector locations. As shown in Figure 16, the neutron detectors were located in thimbles J1, J2 and J3. There were five detectors total; three fission and two BF_3 detectors. Two of the fission detectors were in J1 thimble, one fission and one BF_3 detectors were in J2 thimble, and one

BF_3 detector was in J3 thimble. There were three antimony-beryllium neutron sources located in subassemblies in row 7 and 8.

The core was filled with dummy driver, natural uranium driver, inner and outer blanket subassemblies before the critical experiment. The core loading started with loading two safety rods and 12 control rods containing total of 26.5 kg of ^{235}U. Then the three neutron sources were loaded in reactor locations 8-E-2, 7-E-3 and 7-E-5.

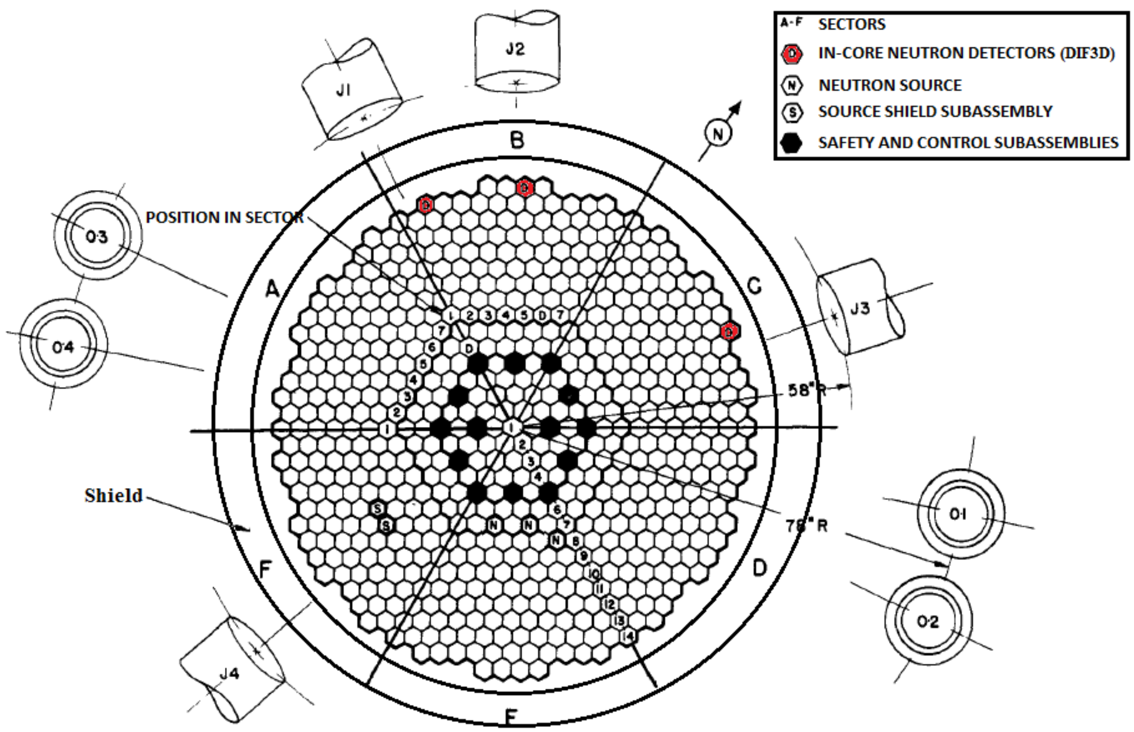

Figure 16. The EBR-II wet critical experiment core before loading fuel.

The counts were taken with all control rods up and down positions. The fuel loading increments and amount of ^{235}U are listed in Table 6.

Table 6. Wet Critical Experiment Fuel Subassembly Loading Increment

Loading No.	Number of Subassemblies Added/Loading	Total Number of Subassemblies	Total Kg of ^{235}U
1	14	14	26.50
2	17	31	74.28
3	6	37	91.09
4	6	43	108.04
5	6	49	124.96
6	6	55	141.93
7	5	60	155.99
8	4	64	167.29
9	3	67	175.79
10	3	70	184.29

The Figure 17 shows the wet critical fuel loading diagram. As shown in Table 6, the loading #1 (first column) has total of 14 subassemblies (third column). The subassemblies #1 to #14 in Figure 17 will be loaded. The loading #2 has total of 31 subassemblies. The subassemblies #15 to #31 will be added to the previous configuration.

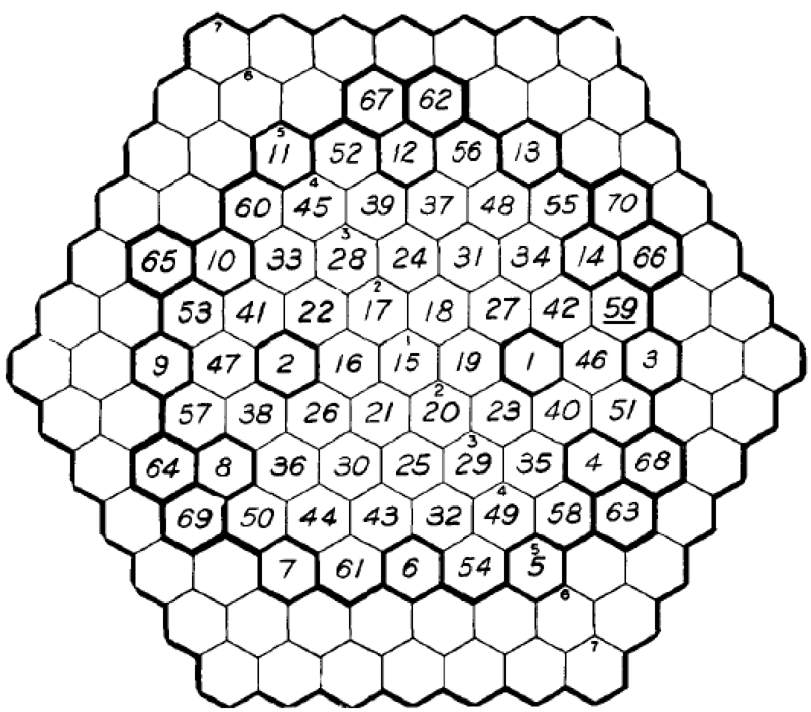

Figure 17. The wet critical experiment fuel loading diagram.

5. Benchmark Simulation Model

Deterministic reactor physics simulation codes such as DIF3D solve the Boltzmann transport equation using multi-group and finite difference methods.

The DIF3D VARIANT (VARIational Anisotropic Neutron Transport) code performs nodal neutron transport calculations using P_N theory in Cartesian and hexagonal two- and three-dimensional geometries.[10] It starts with the time independent form of Boltzmann transport equation:

$$\hat{\Omega} \cdot \vec{\nabla}\Phi(\vec{r},\hat{\Omega},E) + \Sigma_t(\vec{r},E)\Phi(\vec{r},\hat{\Omega},E) = \\ = \int\int \Sigma_s(\vec{r},\hat{\Omega}' \to \hat{\Omega}, E' \to E)\Phi(\vec{r},\hat{\Omega}',E')d\hat{\Omega}'dE' \\ + S(\vec{r},\hat{\Omega},E) \quad (12)$$

Where:

$\Phi(\vec{r},\hat{\Omega},E)$ – neutron angular flux

$\Sigma_t(\vec{r},E)$ – sum of all possible neutron reaction probabilities with energy E at the point $\vec{r}$

$\Sigma_s(\vec{r},\hat{\Omega}' \to \hat{\Omega}, E' \to E)$ – probability that a particle at $\vec{r}$ with energy E' traveling in the direction $\hat{\Omega}'$ is scattered into energy dE about E with direction $d\hat{\Omega}$ about $\hat{\Omega}$

$S(\vec{r},\hat{\Omega},E)$ – generic neutron source that includes fission, fixed and external sources.

The first step of solving the Boltzmann transport equation is discretizing space and energy as shown in Figure 18. The multi-group approach divides the energy range into G intervals with upper and lower energy cutoff at E_0 and E_G as shown below.

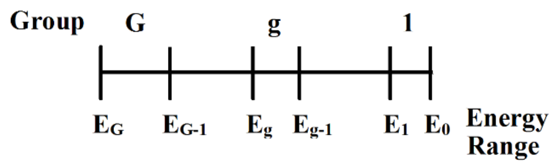

Figure 18. The splitting of the energy range into energy groups.

After applying the multi-group approach to the angular flux and source and cross sections, equation 12 becomes:

$$\hat{\Omega}\cdot\vec{\nabla}\Phi_g(\vec{r},\hat{\Omega})+\Sigma_{t,g}(\vec{r})\Phi_g(\vec{r},\hat{\Omega})= \sum_{g'=1}^{G}\Sigma_{s,g'\to g}(\vec{r})\varphi_g(\vec{r})+S_g(\vec{r},\hat{\Omega}) \qquad g=1..\mathrm{G} \tag{13}$$

Where the scalar flux is:

$$\varphi(\vec{r})=\int\Phi(\vec{r},\hat{\Omega})d\Omega \tag{14}$$

The first term of the Equation 13 is in derivative form. This can be simplified by the difference in a small mesh interval. The entire problem geometry can be dived into mesh intervals as shown in Figure 19. The neutron flux can then be solved at every mesh point.

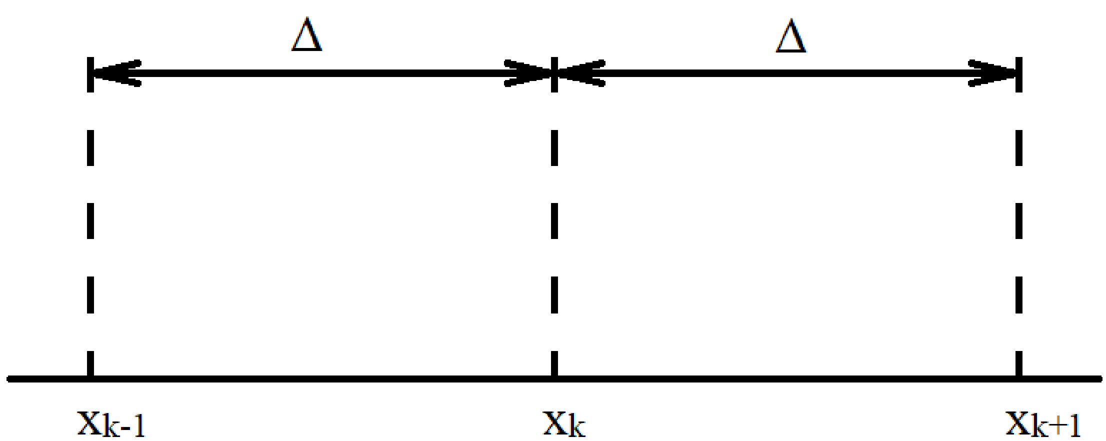

Figure 19. Spacial mesh interval.

The differential term can be represented as a finite difference:

$$\frac{\delta \Phi(\vec{r}, \hat{\Omega})}{\delta x}\Big|_{x_k} \approx \frac{\Phi_{k+1} - \Phi_{k-1}}{x_{k+1} - x_{k-1}} \tag{15}$$

Thus,

$$\Phi_k = \frac{\Phi_{k+1} - \Phi_{k-1}}{2} \tag{16}$$

Similarly, the angular dependence can be discretized and the Boltzmann transport equation can be solved numerically using DIF3D.

5.1 DIF3D Neutron Cross-Section Confirmation

Before simulating a nuclear reactor, the simulation tool must be confirmed to be working properly. A DIF3D model and using Argonne National Laboratory supplied neutron cross-section data was compared with a KENO VI[11] model. The problem specific cross-sections are generated by MC^2.[12] The EBR-II specific cross-section file was acquired from Argonne National Laboratory. This cross-section file was specific for hexagonal geometry simulations.

A simple critical model using a hexagonal lattice was built using both KENO VI and DIF3D. The model, as shown in Figure 20, was used for comparing the cross-sections and confirming DIF3D installation and execution. This model consisted of two regions; fuel region and stainless-steel reflector. For simplicity's sake, the stainless steel consisted of 12% Ni, 17% Cr, and 71% Fe. The fuel region consisted of 48.86% enriched ^{235}U. The initial model started with fuel region only. The initial composition was started with 50% enriched ^{235}U which produced k_{eff}=1.000 on KENO VI. On the other hand, the k_{eff} of an identical model on DIF3D was about 0.8. The fuel region was surrounded by stainless-steel reflector to reduce leakage. As reflectors being added, the k_{eff} from DIF3D increased significantly. But, the k_{eff} from KENO VI increased slightly. The ^{235}U atom density was slowly reduced to 48.86% enriched ^{235}U to make the model critical on KENO VI as reflectors kept being added.

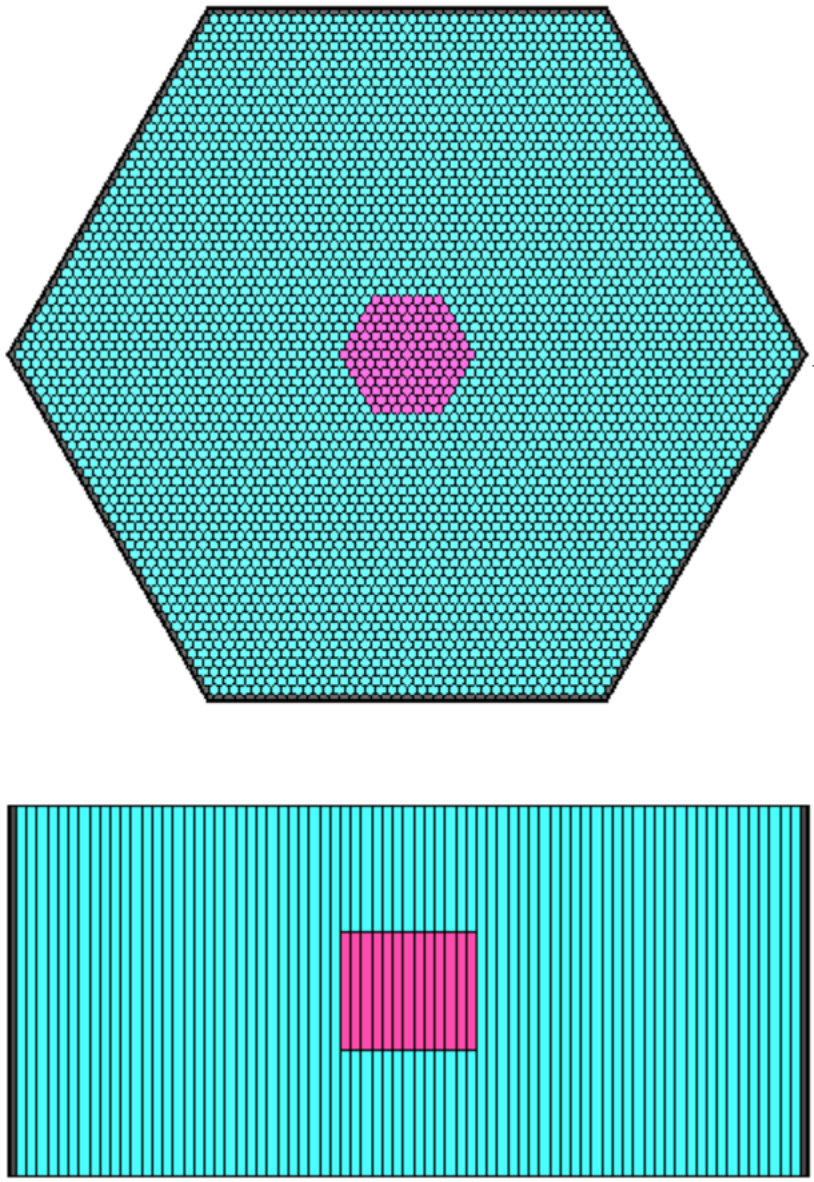

Figure 20. A simple hexagonal lattice for confirmation, pink is fuel, teal is stainless steel.

A simple hexagonal assembly consisting of a homogenized mixture of ^{235}U, ^{238}U and Na was used as a fuel assembly. The fuel region was surrounded by sodium and a stainless-steel reflector. The stainless-steel above and below sodium were 70 cm long. There were 7 rows (127 hexagons) of fuel assemblies in the model. The fuel assemblies are surrounded by 31 rows of stainless steel reflector to reduce leakage. Table 7 shows the effective multiplication factor was calculated using both KENO VI and DIF3D.

Table 7. K_{eff} Calculated from both KENO VI and DIF3D

Code	k_{eff}	Uncertainty
KENO VI	1.00021	±0.0003
DIF3D	0.99909	

In the KENO VI model, ENDF-v7 continuous energy cross section data was used. The model was run with 250 generations and 10,000 neutrons per generation. The first 50 generations were skipped to ensure convergence. On the other hand, the DIF3D model was run with 33 group specific cross-section data of EBR-II. The 8th order of the polynomial approximation of the source within the node, the 8th order of the polynomial approximation of the fluxes within the node, and the second order of the polynomial approximation of the leakage on the surfaces of the nodes were used. The P_3 flux and leakage expansions were selected.

The k_{eff} values from KENO VI and DIF3D confirm that DIF3D and EBR-II specific cross-section data can be used for simulation. Also, the DIF3D was compiled and executed properly.

5.2 DIF3D Model Development

Due to geometric limitations of DIF3D, the EBR-II model was homogenized. To be consistent with the physical subassemblies, each subassembly was divided into sections and then homogenized. The driver fuel subassembly was divided into 10 sections as shown in Figure 21. Sodium and stainless-steel pieces were added on the top and the bottom of the driver subassembly. Another DIF3D geometry limitation is that every subassembly must have the same height. The sodium region was added above and below each subassembly including safeties, inner and outer blanket to compensate for the motion of control rods. The list of material composition of the driver fuel subassembly is shown in Table 8.

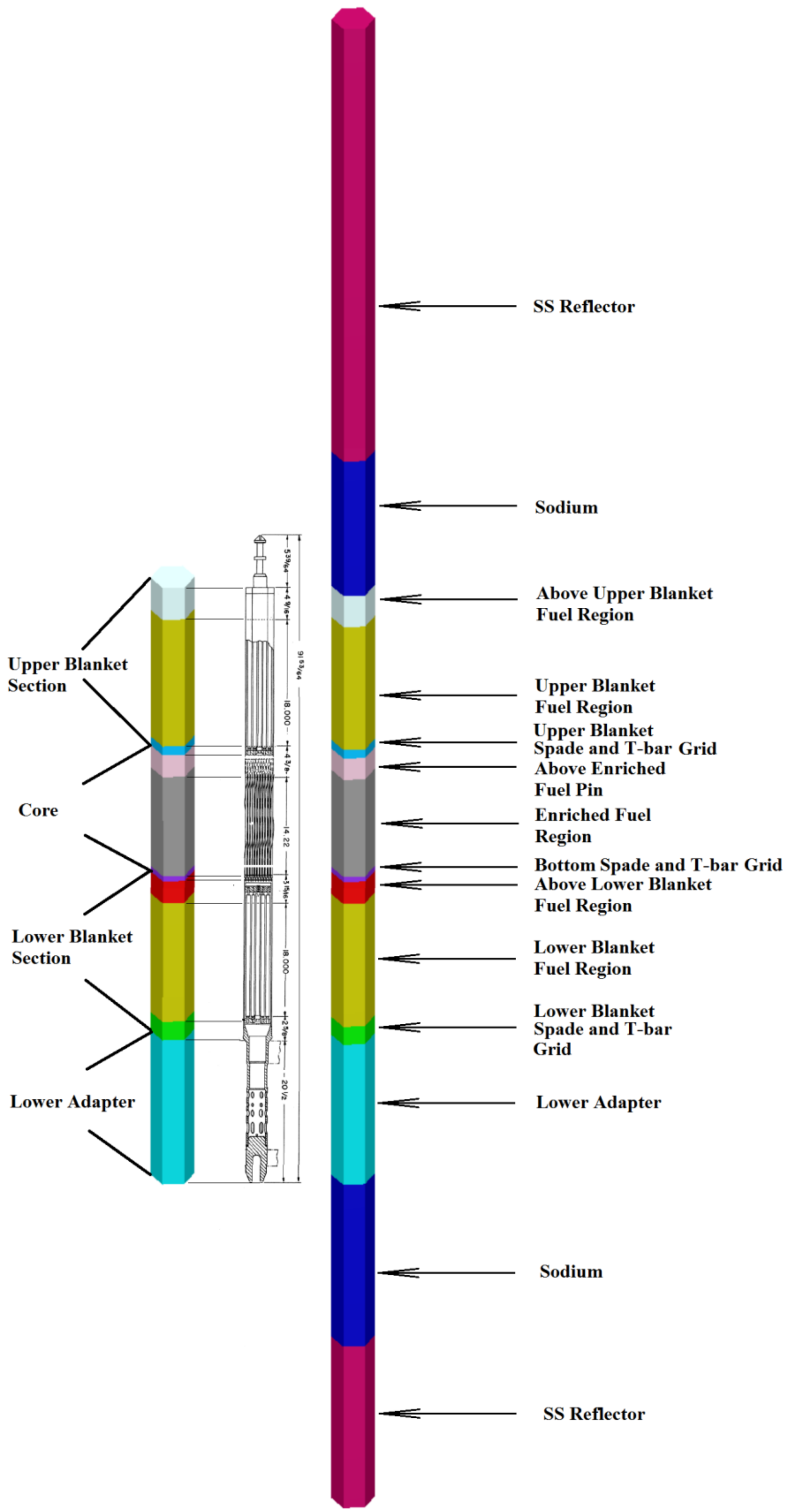

Figure 21. Homogenized driver fuel subassembly.

Table 8. Material Composition of Homogenized Driver Fuel Subassembly
(units in grams)

Materials	Above Upper Blanket Fuel Region	Upper Blanket Fuel Region	Upper Blanket Spade T-bar Grid	Above Enriched Fuel Region	Enriched Fuel Region	Bottom Spade and T-bar Grid	Above Lower Blanket Fuel Region	Lower Blanket Fuel Region	Lower Blanket Spade and -bar grid	Lower Adapter
^{235}U		23.43			2807.79			23.43		
^{238}U		7787.90			3032.04			7787.90		
Fs*					307.36					
Na	292.36	645.78	42..83	108.25	462.29	23.41	109.66	645.78	54.19	1410.58
Fe	131.73	1254.78	261.47	653.90	1196.63	172.14	669.42	1254.74	771.81	8610.62
Ni	22.26	212.08	44.19	110.52	202.25	29.09	113.14	212.08	130.45	1455.32
Cr	31.54	300.44	62..61	156.57	286.52	41.22	160.29	300.44	184.80	2061.70

Fs* is a shortcut of fissium.

Neutron leakage in a small reactor like EBR-II is significant. For example, "the neutron flux of a bare spherical reactor of 50 cm is given by $\varphi = 5 * 10^{13} * \frac{\sin(0.0628r)}{r}$ neutrons/cm^2-sec, where r is measured from the center of the reactor".[13] The number of neutrons escaping from this reactor is equal to $1.58 * 10^{15}$neutrons/sec. DIF3D could not solve problems with significant leakage due to application of boundary conditions in the hexagonal lattice geometry. To decrease the leakage, 60-cm long stainless-steel reflectors were added at the top and bottom of the EBR-II model and 9 rows of stainless-steel reflectors were placed around the core.

The inner and outer blanket subassemblies in the model were geometrically identical. As shown in Figure 22, the blanket subassembly is divided into five pieces: lower adapter, spade and t-bar grid, blanket fuel region, above blanket fuel region and top plug and then homogenized.

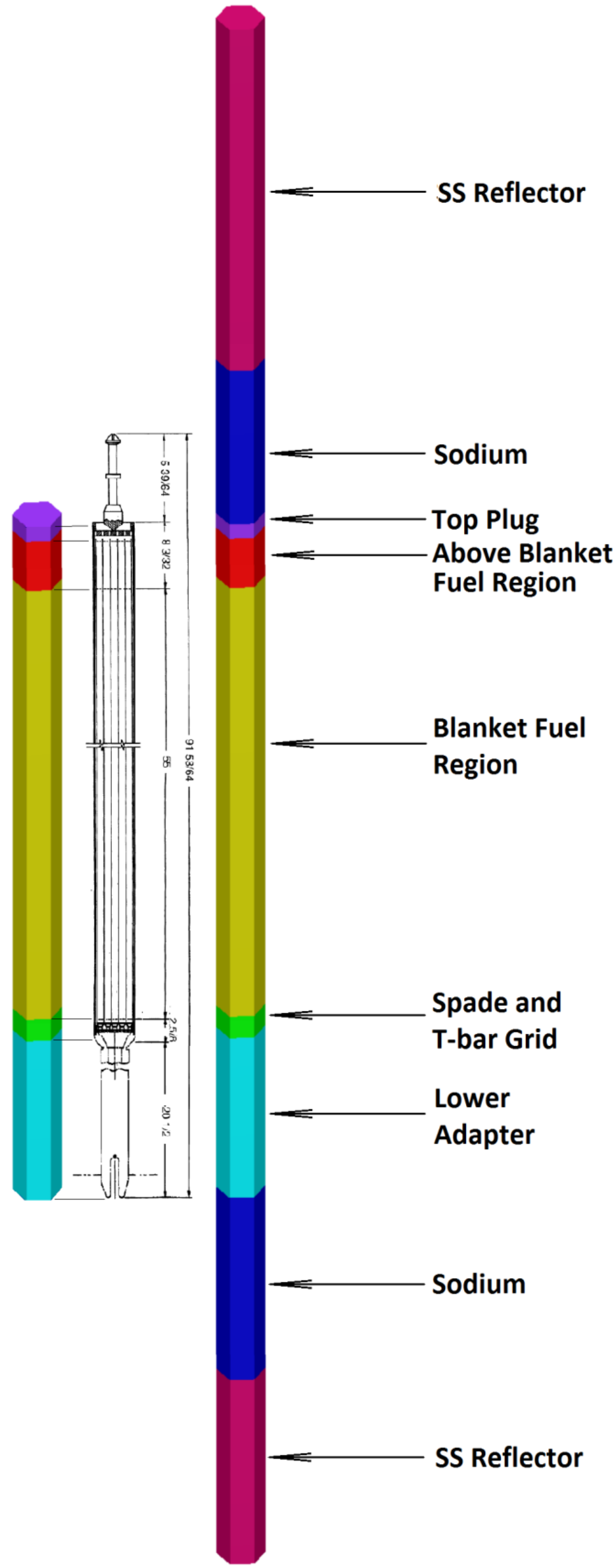

Figure 22. Homogenized blanket fuel subassembly.

The detailed material description of homogenized subassembly is listed in Table 9.

Table 9. Material Composition of Homogenized Driver Fuel Subassembly (units in grams)

Materials	Top Plug	Above Blanket Fuel Region	Blanket Fuel Region	Spade and T-bar Grid	Lower Adapter
^{235}U			94.31		
^{238}U			47060.36		
Na	38.08	126.73	760.39	54.19	1410.58
Fe	542.43	981.97	4190.80	771.81	8610.62
Ni	91.68	165.97	708.30	130.45	1455.32
Cr	129.88	235.12	1003.43	184.80	2061.70

Since the safety and the control rods were identical, the same geometrical model was used for both. The only difference between a regular control rod and the safety rod is the length of the lower adapter and the region above the upper reflector. In the homogenized model of safety and control rods, these regions have equal volume but different atom densities. Figure 23 shows the homogenized control and safety subassemblies. The material compositions of the homogenized safety and control rods are shown Table 10.

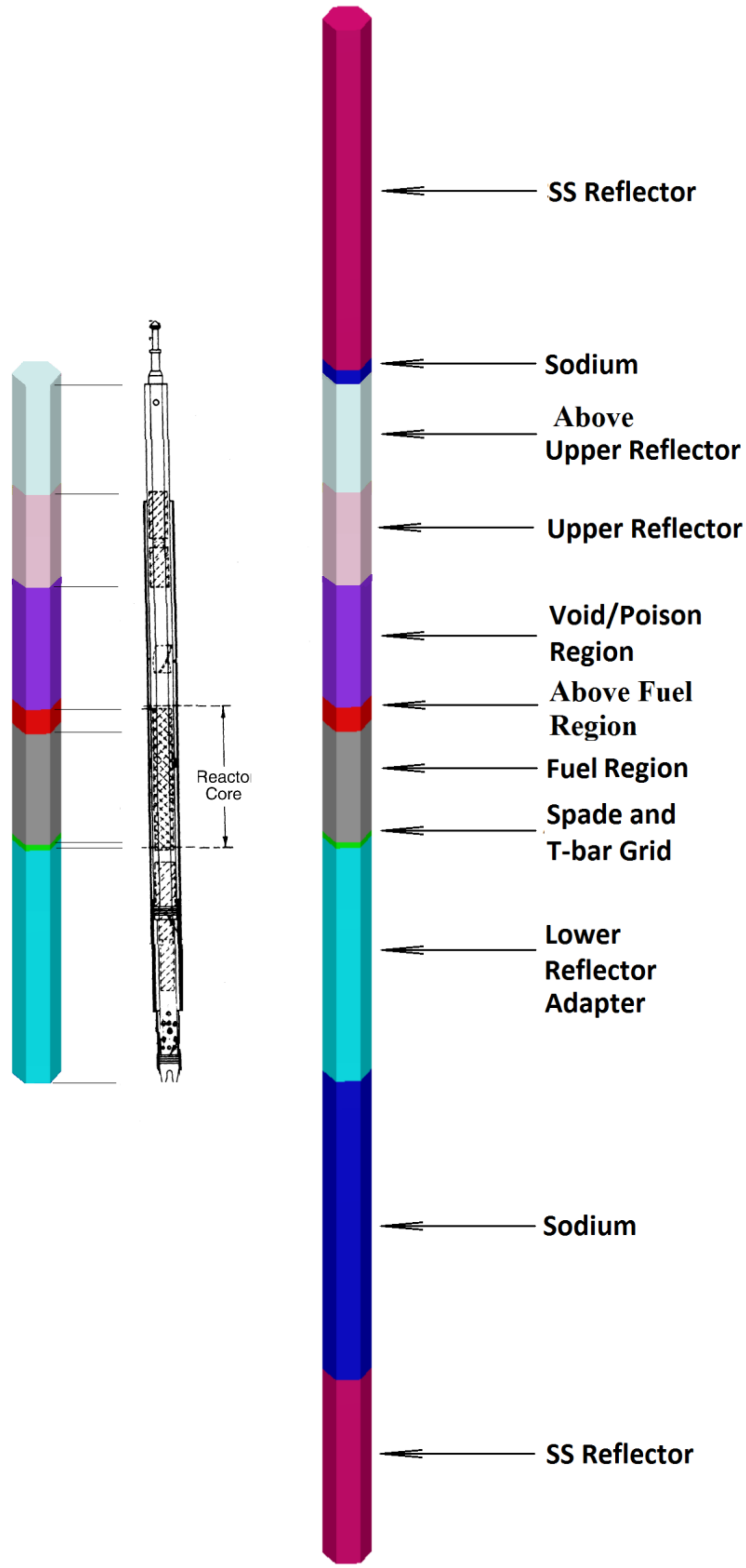

Figure 23. Homogenized control and safety subassemblies.

Table 10. Material Composition of Homogenized Control and Safety Subassembly (units in grams)

Materials	Above Upper Reflector	Upper Reflector	Void Region	Above Fuel Region	Enriched Fuel Region	Spade and T-bar Grid	Lower Reflector and Adapter
^{235}U					1882.14		
^{238}U					2032.46		
Fs*					206.03		
Na	879.57	301.69	947.45	126.40	554.49	28.59	403.18
Fe	596.57	3198.75	831.95	543.09	1278.06	140.49	9844.47
Ni	100.83	540.64	140.61	91.79	216.01	23.75	1663.85
Cr	142.84	765.90	199.20	130.03	306.02	33.64	2357.12

The motion of the control rod is shown in Figure 24.

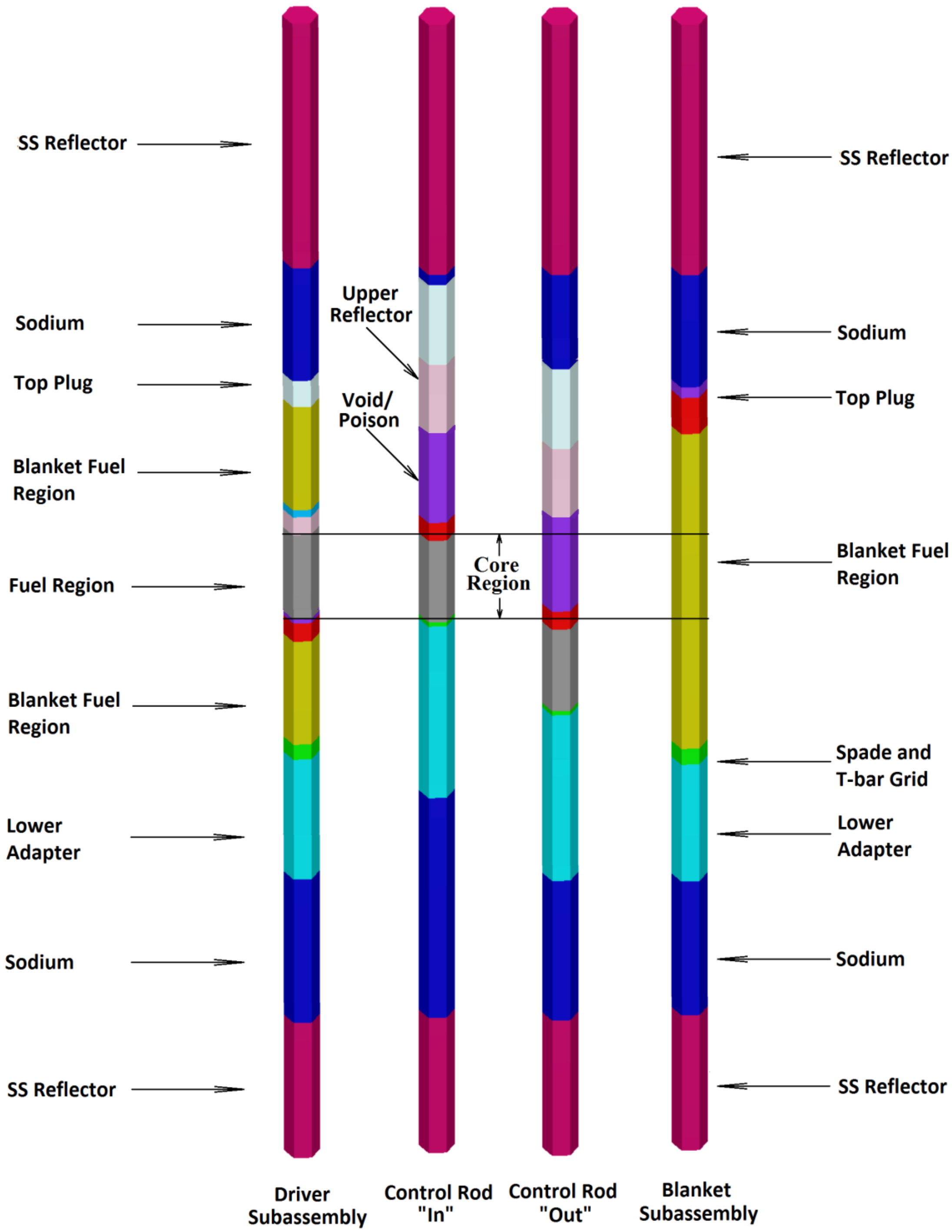

Figure 24. The control rod "in" and "out" positions respect to driver and blanket subassemblies.

5.3 Input File Description

The DIF3D input file consists of my different cards describing the problem. In this simulation, only basic three cards, A.DIF3D, A.HMG4C and A.NIP3, were used. The input file can be written in either free format or according to the formats specified for each card type.

5.3.1 A.DIF3D Description

The A.DIF3D contains the calculational parameters, storage containers, and edit sentinels.

```
UNFORM=A.DIF3D
01       33 GROUP 3D PROBLEM
02    20000000 100000000
03        1    2    0  4500   500    0  1000000000   0  0  90
04        1    0    0   00    000    00   000    1    1
05        1.0E-5     1.0E-5     1.0E-5
06        1.0      0.001       0.04  14.30000+6
12        80801                  33
```

The card numbers represent the following:

The type 01 card is used for problem title.

The type 02 card is used for storage and dump specifications.

- 20000000 – pointer container array size in fast core memory (FCM) in real*8 words
- 100000000 – the pointer container array size in core memory (ECM) in real*8 words

The type 03 card is used for the problem control parameters.

- 1 – fixed source problem
- 2 – both real and adjoint solution
- 0 – Chebyshev acceleration of outer iterations is on

- 4500 – minimum plane-block size in real*8 words for I/O transfer in the the concurrent inner iteration strategy
- 500 – maximum number of outer iteration
- 0 – restart flag is off
- 1000000000 – job time limit
- 0 – performs the estimated number of inner iterations for each group
- 0 – no acceleration of optimum overrelaxation factor calculation
- 90 – number of optimum overrelaxation factor estimation iteration control

The type 04 card is used for editing options.

- 1 – print problem description edits
- 0 – no geometry map edits for region to mesh interval
- 0 – no geometry map edits for zone to mesh interval
- 00 – no edits for the scattering and principal cross sections and principal cross sections edits
- 000 – no edits for the group balance edits integrated over the reactor, region balance edits by group and region balance edits totals
- 00 – no edits for both region power and average power density edits and power density by mesh interval edits
- 000 – no edits for flux edit by region and group including group and region totals, total flux edit by mesh interval, and total flux edit by mesh interval and group
- 1 – print edits for the zone averaged real flux
- 1 – print edits for region averaged flux

The type 05 card is used for convergence criteria.

- 1.0E-5 – the eigenvalue convergence criterion for steady state calculation
- 1.0E-5 – the pointwise fission source convergence criterion for steady state shape calculation
- 1.0E-5 – the average fission source convergence criterion for steady state shape calculation

The type 06 card is used for other floating-point data.

- 1.0 – the k_{eff} of reactor
- 0.001 – any pointwise fission source will be neglected in pointwise fission source convergence test if it is less than this factor time fission source
- 0.04 – error reduction factor to be achieved by each series of inner iterations for each group during a shape calculation
- 14.30000+6 – steady state reactor power (Watts)

The type 12 card is used for parameters for variational nodal option.

- 80801 – 8^{th} order source approximation, 8^{th} order flux approximation, and linear leakage approximation (DEFAULT)
- 33 – P3 flux expansion and P3 leakage expansion

5.3.2 A.NIP3 Description

The geometry description of DIF3D computer code is specified in A.NIP3. A small part of A.NIP3 used for EBR-II reactor geometry and the explanation of each card are shown below. The EBR-II input file is given in Appendix B.

```
DATASET=A.NIP3
01       33 GROUP FIXED-SOURCE TRANSPORT PROBLEM
02            0     0 50000      50000     0     0     0     0     0
03          120
04            2     2     2     2     2     2
09       Z     1   60.000
09       Z     1  120.000
09       Z     1  121.944
  Lower Blanket Fuel Region
14        DEPB  NA23I  0.000761778
14        DEPB  U235N  0.000044937U238N  0.014745338
14        DEPB  FE__R  0.010127125NI__R  0.001628561CR__R  0.002604296
15    DEPBB FR1BB
15    DEPB  FR1B
15    DEPBT FR1BT
15    FUELB FR1FB
15    FUEL  FR1F
15    FUELT FR1FT
15    DEPTB FR1TB
15    DEPT  FR1T
15    DEPTT FR1TT
19    SOURC1    1  33  662.517546E+07
29          5.80898     25     3
 DRIVER REGION
30     OREF    01                 0.0      60.000
30     BOTS    01              60.000     120.000
30      BOT    01             120.000     172.070
30    FR1BB    01              172.070     178.737
30     FR1B    01             178.737     224.457
30    FR1BT    01              224.457     232.553
30    FR1FB    01              232.553     234.458
30     FR1F    01             234.458     270.577
30    FR1FT    01              270.577     278.527
30    FR1TB    01              278.527     281.689
30     FR1T    01             281.689     327.409
30    FR1TT    01              327.409     338.998
30     TOPS    01             338.998     388.998
30     OREF    01             388.998     550.000
```

The card numbers represent the following:

The type 01 card is used for problem title.

The type 02 card is used for input processing specifications.

- 0 – no debugging printout
- 0 – no geometry processing module edits
- 50000 – size of main core storage array for geometry processing module
- 50000 – size of main core storage array for cross-section processing module
- 0 – size of bulk core storage array for cross-section processing modules
- 0 – no pointer debugging edits for cross-section processing module
- 0 – no cross-section processing edits
- 0 – no region/mesh interval printer-plotter map editing
- 0 – no zone/mesh interval printer-plotter map editing

The type 03 card is used for problem geometry.

- 120 – geometry type: hexagonal-z, full core in plane

The type 04 card is used for external boundary conditions.

- 2 – boundary condition at lower "x" boundary of reactor
- 2 - boundary condition at upper "x" boundary of reactor
- 2 – boundary condition at lower "y" boundary of reactor
- 2 - boundary condition at upper "y" boundary of reactor
- 2 – boundary condition at lower "z" boundary of reactor
- 2 – boundary condition at upper "z" boundary of reactor

The type 09 card is used for variable mesh structure.

- Z – coordinate direction
- 1 – number of interval
- 60.000 – upper coordinate

This card can be repeated for each interval.

The type 14 card is used for composition specification.

- DEPBB – composition label
- NA23I – material label
- 0.000761778 – atom density

This card can be repeated for all materials and compositions.

The type 15 card is used for region/composition correspondence.

- DEPB – composition label
- FR1B – region label defining region containing specified composition

The type 19 card is used for region or mesh distributed inhomogeneous source.

- SOURC1 – label or region where source is located
- 1 – higher-energy group number
- 33 – lower-energy group number
- 662.517546E+07 – isotopic source value in the specified mesh interval (neutrons per second per unit volume)

The type 29 card is used for hexagon dimension.

- 5.80898 – dimension of hexagon across flats
- 25 – total number of hexagonal rings
- 3 – 54 mesh points

The type 30 card is used for region definitions for arrays of hexagons.

- OREF – region label
- 01 – hexagonal ring number where region is located
- 0.0 – starting hexagon position for this region
- 60.000 – final hexagon position for this region

This card can be repeated for entire problem geometry.

5.3.3 A.HMG4C Description

HMG4C is designed to create a homogenized macroscopic cross-section for each composition.

```
UNFORM=A.HMG4C
01        TURN OFF HMG4C EDITS
02   999999    1    0    0    0    1
```

The card numbers represent the following:

The type 01 card is used for problem title.

The type 02 card is used for problem options

- 999999 – size of main core container array
- 1 – suppress all printing except diagnostics
- 0 – no COMPXS edit
- 0 – no ISOTXS edit
- 0 – no POINTR debugging edit
- 1 – use isotope fission vectors to compute composition fission vectors with total fission source weighting

5.4 Running DIF3D

The DIF3D model of the EBR-II reactor was run on Idaho National Laboratory's (INL) High Performance Computing (HPC) cluster. DIF3D calculated the flux and adjoint flux for the fixed-source problem. The run time for the simulation ranged between 3 hours to 8 hours depending on the amount of fuel in the reactor. The run time on a regular home computer with 32GB RAM was ranging between 8 hours to 2 days depending on the amount of fuel material. The process of installing DIF3D on the HPC required experience working in Linux environment. The detailed protocol is given in Appendix A.

5.5 Dry and Wet Critical Simulation Failures

The approach-to-critical simulation of EBR-II using the DIF3D computer code started with all control rods and safety rods inserted, and every outer blanket assembly inserted. The neutron flux was calculated in all detector positions. Figure 25 to Figure 28 show the 1/M of detectors 1 to 4 as a function of number of assemblies, respectively. As fuel was added to the reactor, the neutron flux increases and inverse flux decreases. First six data points of the plot show that as the number of fuel assemblies was increased, the inverse flux was decreased. But starting seventh data point, the inverse flux increased. After carefully reviewing the input file and atom density calculation, it was found that the ^{235}U and ^{238}U atom density calculation of blanket assemblies was missing division of 100 in the percentage calculation.

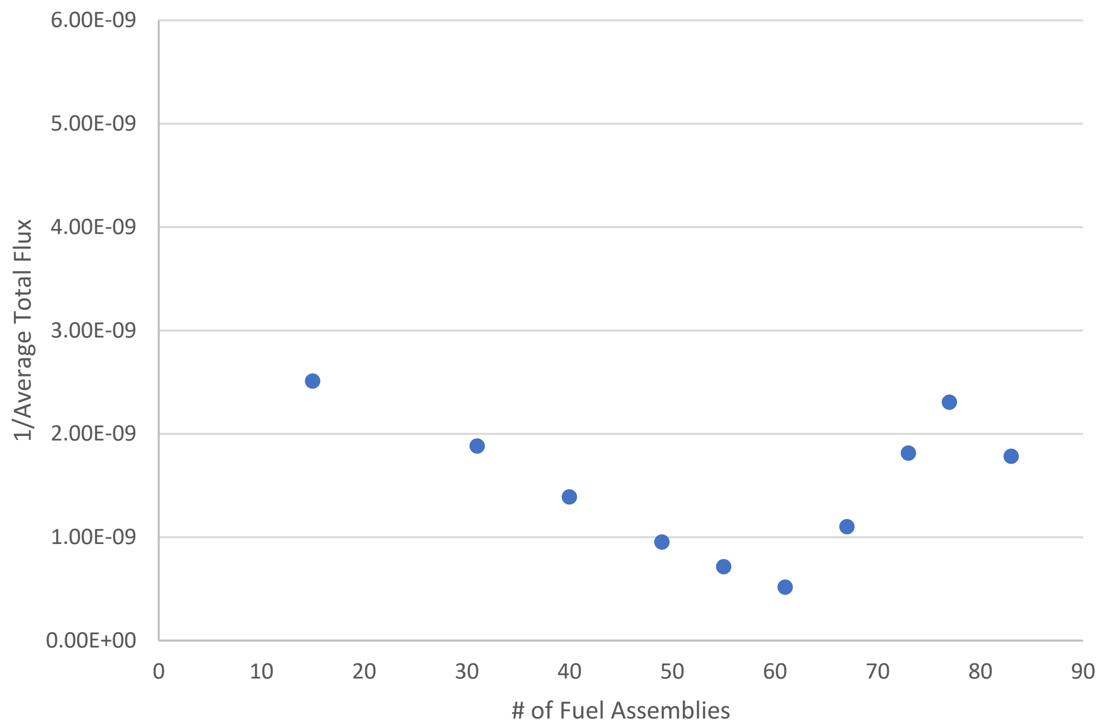

Figure 25. Dry critical experiment initial flux calculation in detector #1.

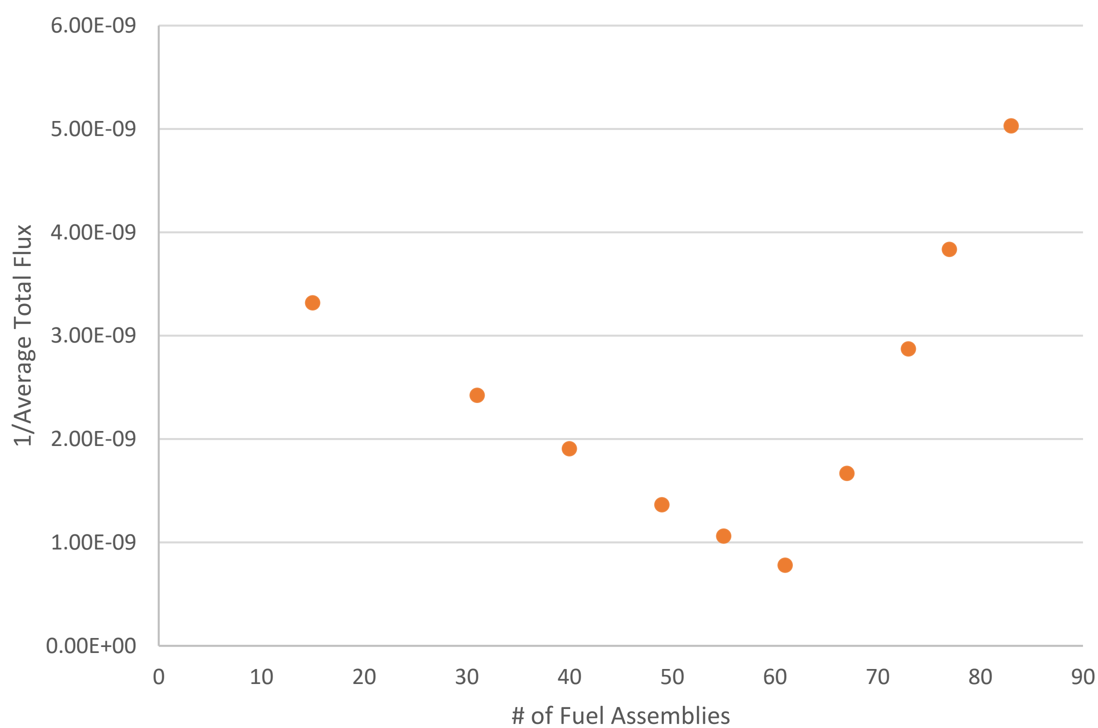

Figure 26. Dry critical experiment initial flux calculation in detector #2.

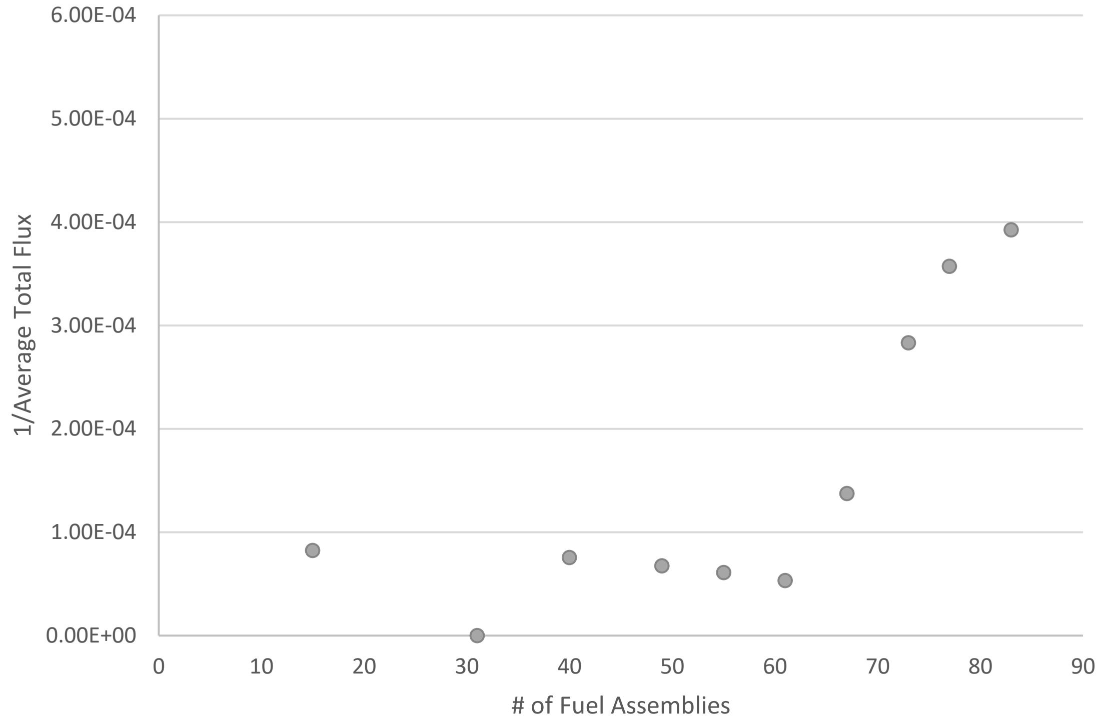

Figure 27. Dry critical experiment initial flux calculation in detector #3.

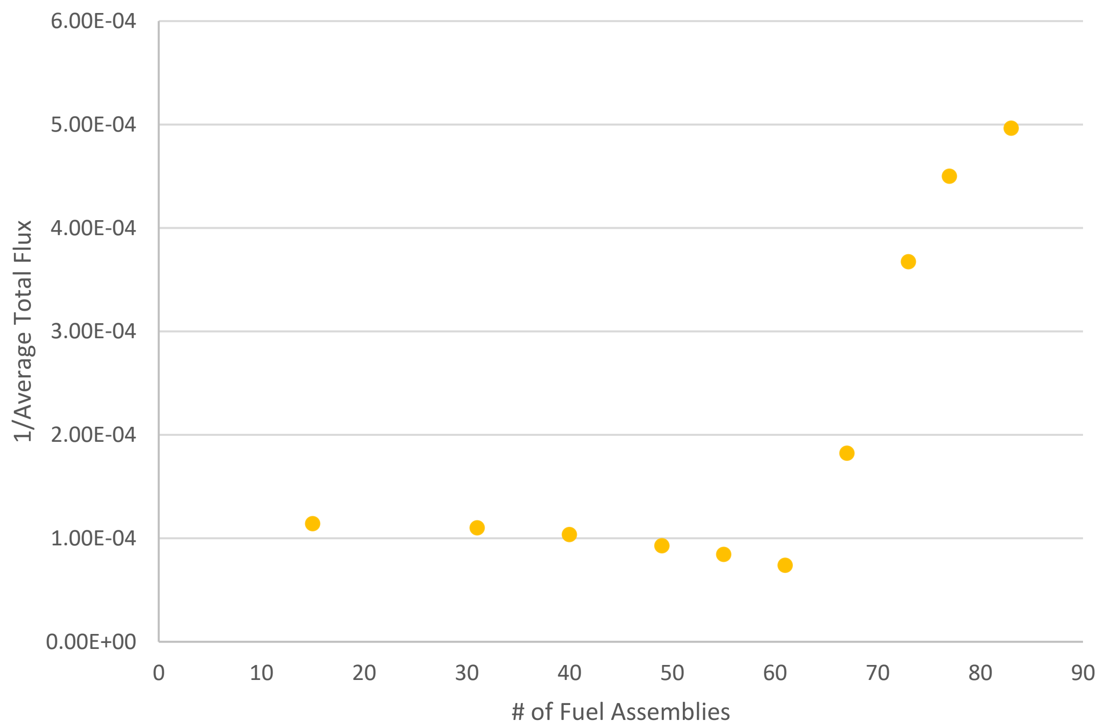

Figure 28. Dry critical experiment initial flux calculation in detector #4.

After fixing the error, both dry and wet critical experiment were simulated again. The wet critical experiment's detector responses are shown in Figure 29. The inverse flux value decreases as the number of fuel assemblies increases as expected. The dry critical experiment results improved compared to the previous simulation, however, the Figure 30 shows that the inverse flux value did not decrease after approaching 60 assemblies.

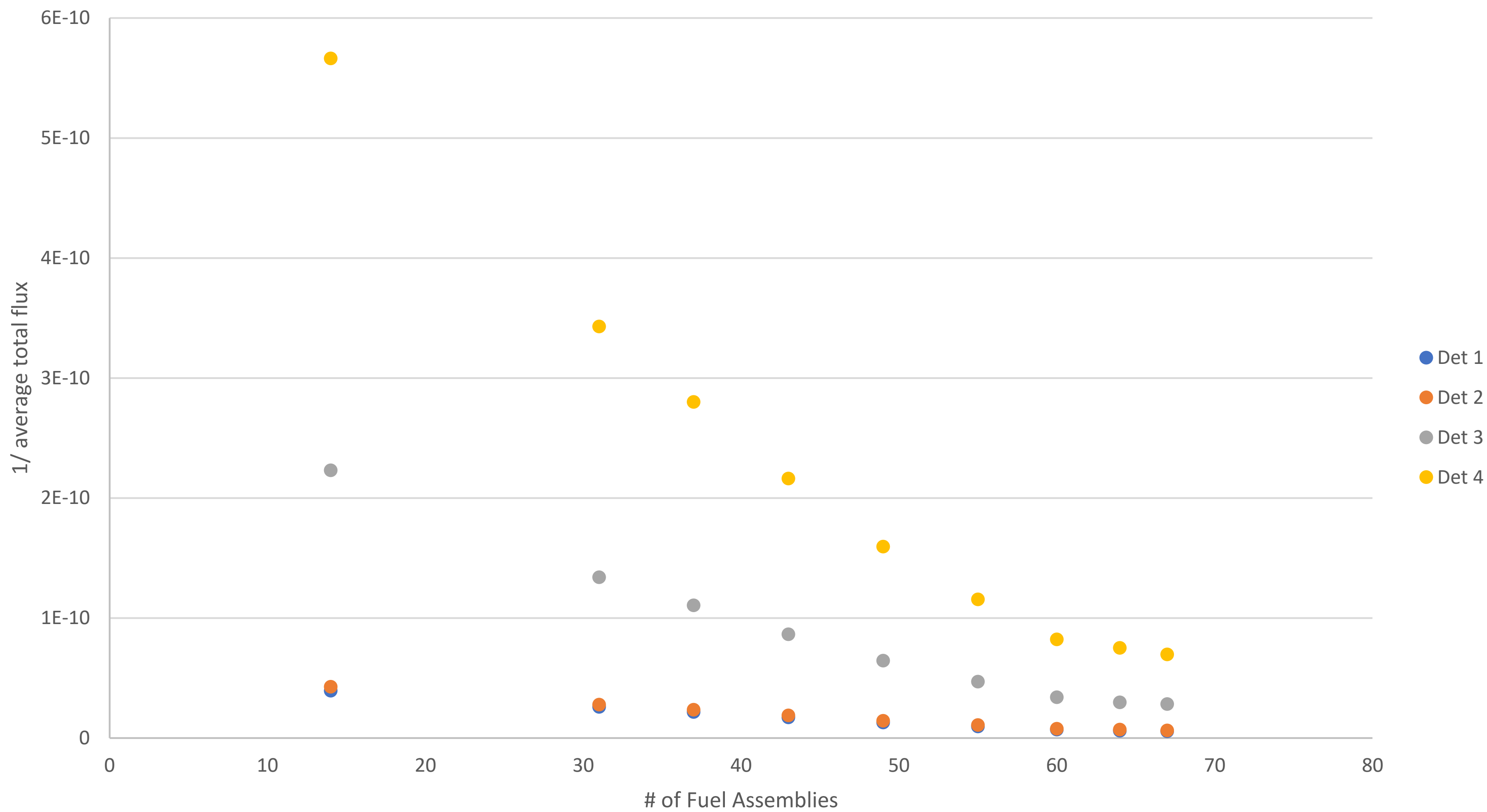

Figure 29. Wet critical experiment, CR* "in" position, 1/flux plot.

CR – Control Rods

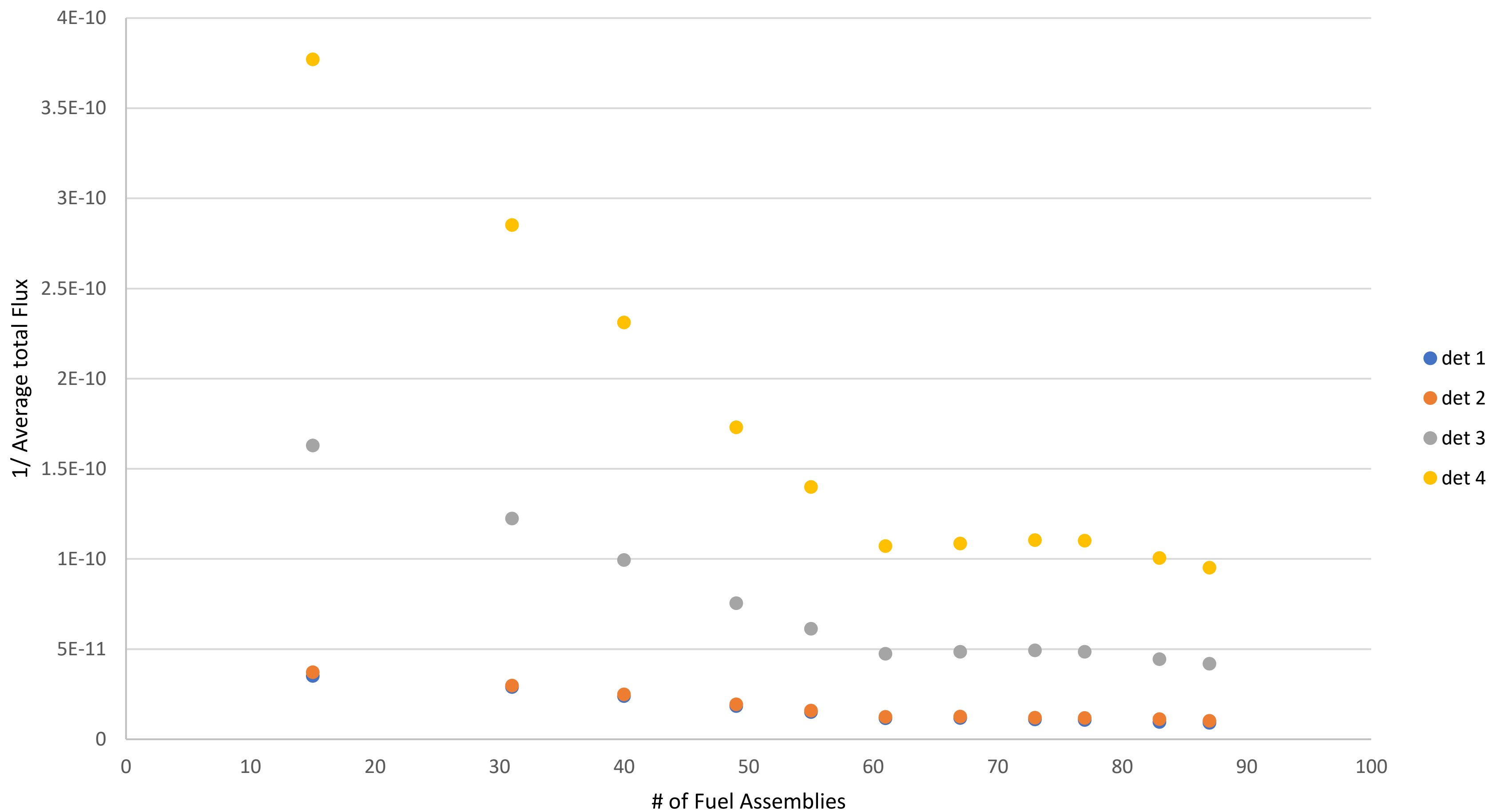

Figure 30. Dry critical experiment, CR "in" position, 1/flux plot.

However, the dry critical simulation result did not show as much increase in the inverse flux value, it was still not decreasing consistently as fuel being added. Both dry and wet critical experiment literature was reviewed again to help identify possible mistakes. From Figure 30, we can see that driver region fuel loading was going as predicted. However, when it came to adding the inner blanket region, the flux started decreasing. These calculations assumed enrichment of the inner blanket was 0.3% ^{235}U. However, the dry and wet critical experiment documents said that when they operated EBR-II during both dry and wet critical experiment, there was an assembly called “enriched inner blanket”. The enrichment of the enriched inner blanket assemblies was assumed to be the same as driver assembly enrichment, 48.08wt% ^{235}U. With the enrichment of inner blanket assembly increased to 48.08wt% ^{235}U, the simulation was ended with the result which is shown in Figure 31. The dimensions of the fuel slug remained same as inner blanket fuel slug.

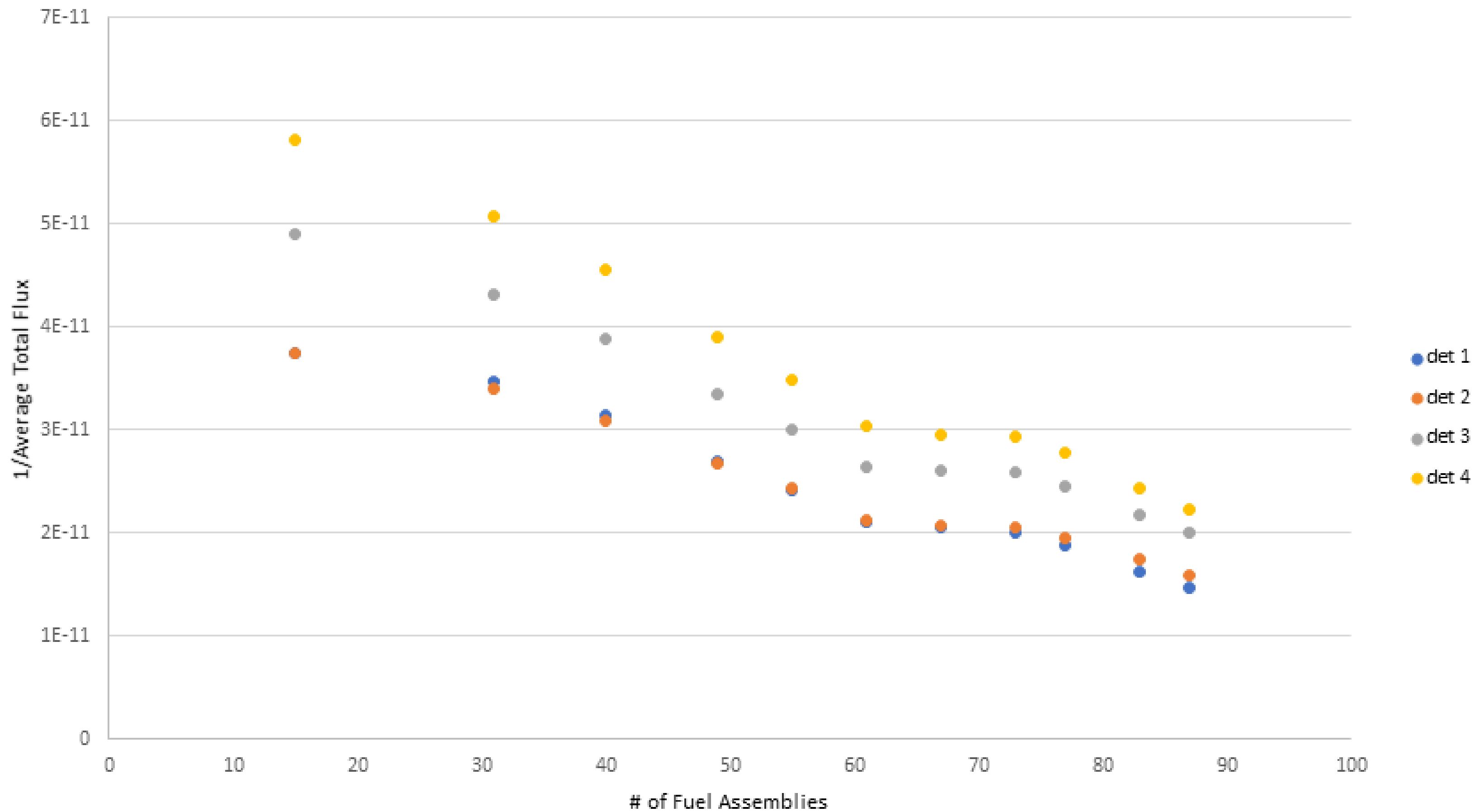

Figure 31. Dry critical experiment, CR "in" position, 1/flux plot with enriched inner blanket.

As Figure 31 shows, the data points are in a decreasing order, which we were not able to see before. But, the amount of ^{235}U was too large. A single enriched inner blanket assembly contained 22.6 kg of ^{235}U. From Table 5 and Table 6, the amount of ^{235}U is calculated to be 2.83 kg per inner blanket assembly. Because of it is greater length and 19 large pins, the 48.08% enriched inner blanket assembly had nearly 10 times more ^{235}U than the driver assembly. It was assumed that the "enriched inner blanket" assemblies were a regular driver assembly. Hence, instead of putting enriched inner blanket in the model, a regular driver assembly was used for comparison purposes. The revised dry and wet critical experiment results are shown in Figure 32 and Figure 33, respectively.

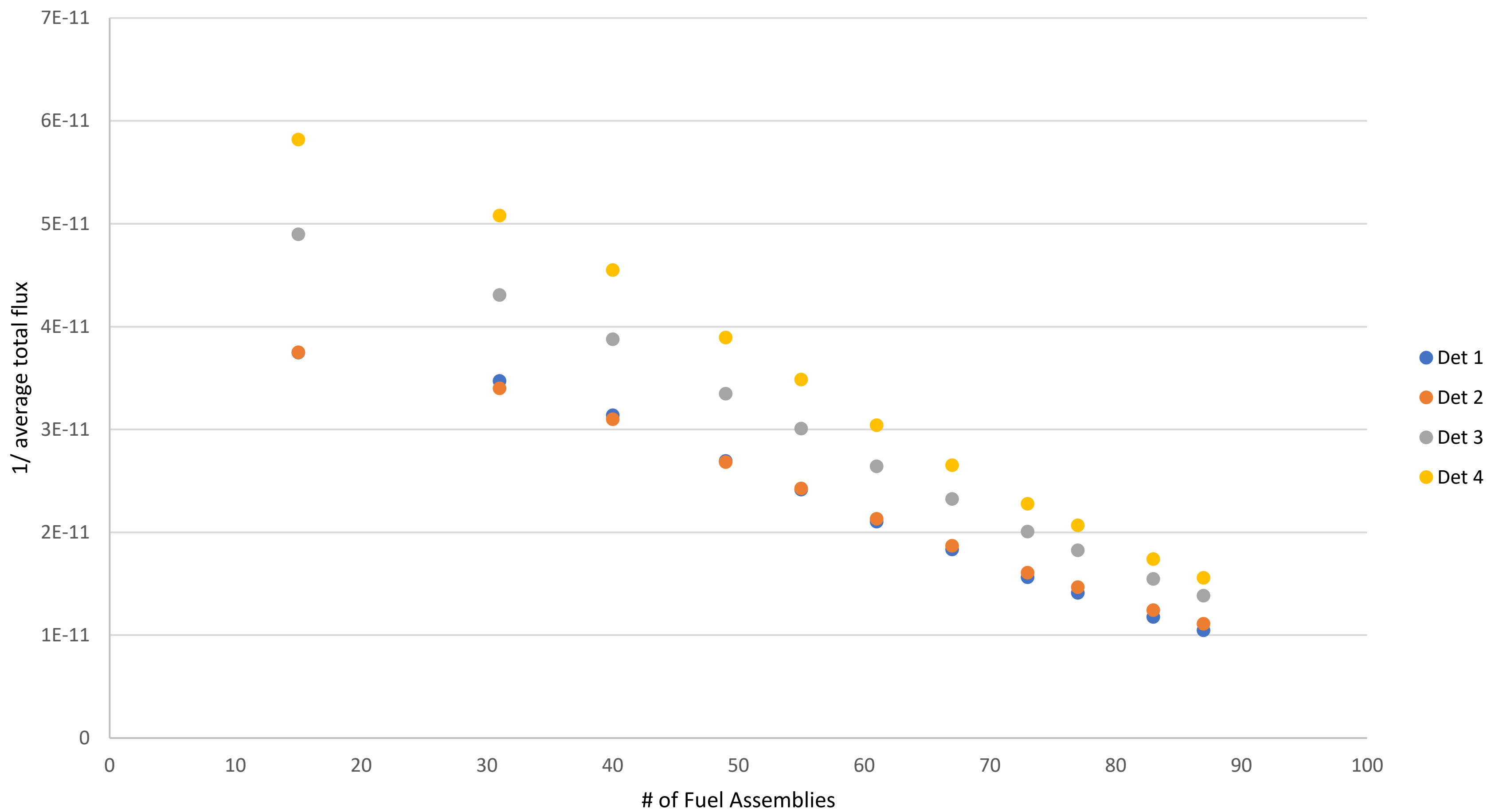

Figure 32. Dry critical experiment, CR "in" position, driver fuel subassemblies added as an inner blanket.

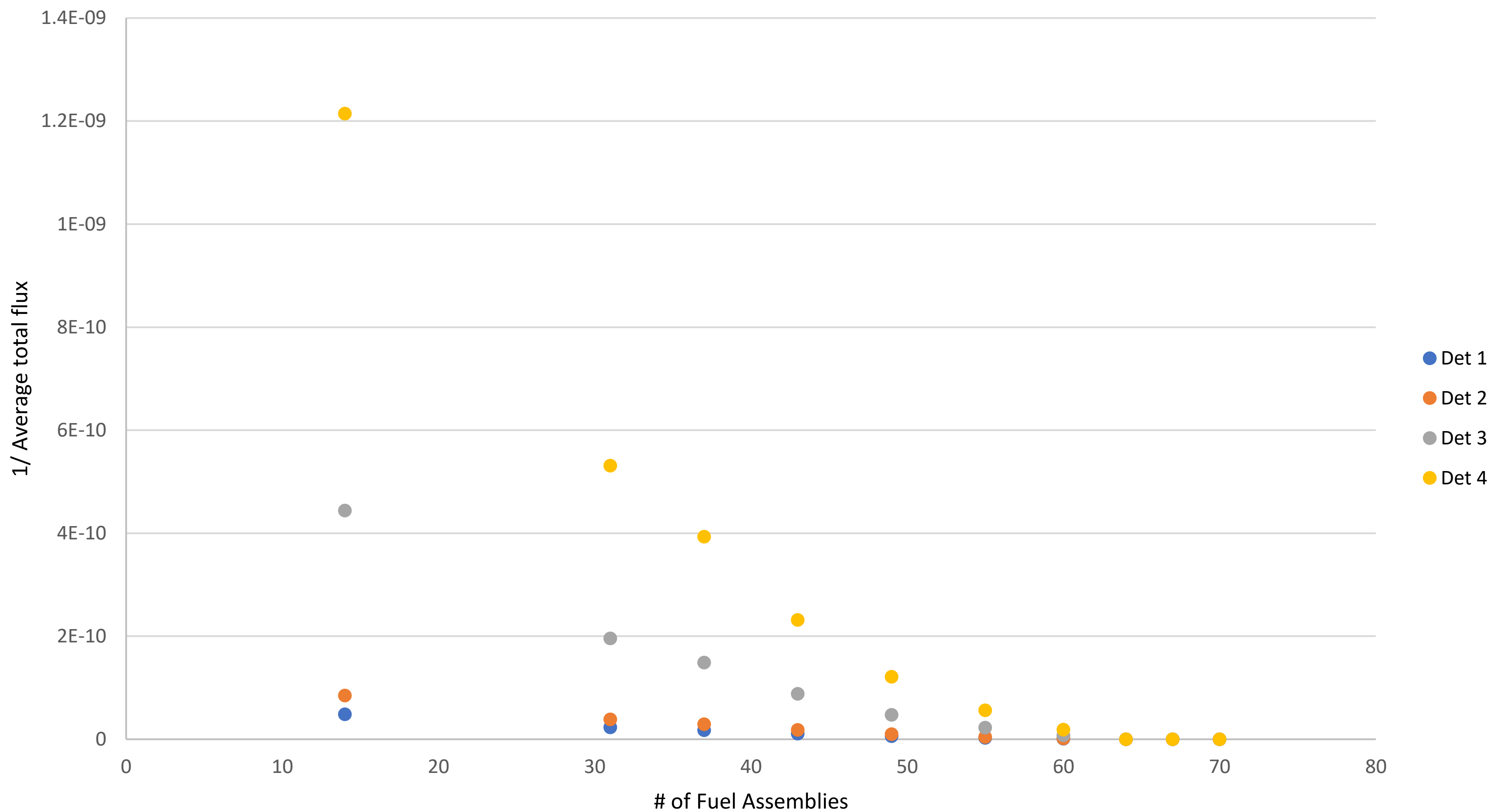

Figure 33. Wet critical experiment, CR "in" position, driver fuel subassemblies added as an inner blanket.

The dry critical experiment data points were clearly in descending order. However, the wet critical experiment data points look like descending order as shown in Figure 33, the last three points are not clear. So, these last three points were plotted on a separate scale to verify the 1/M curve. The last three data points of detector 1 and 2 were plotted as shown in Figure 34 and Figure 35, respectively.

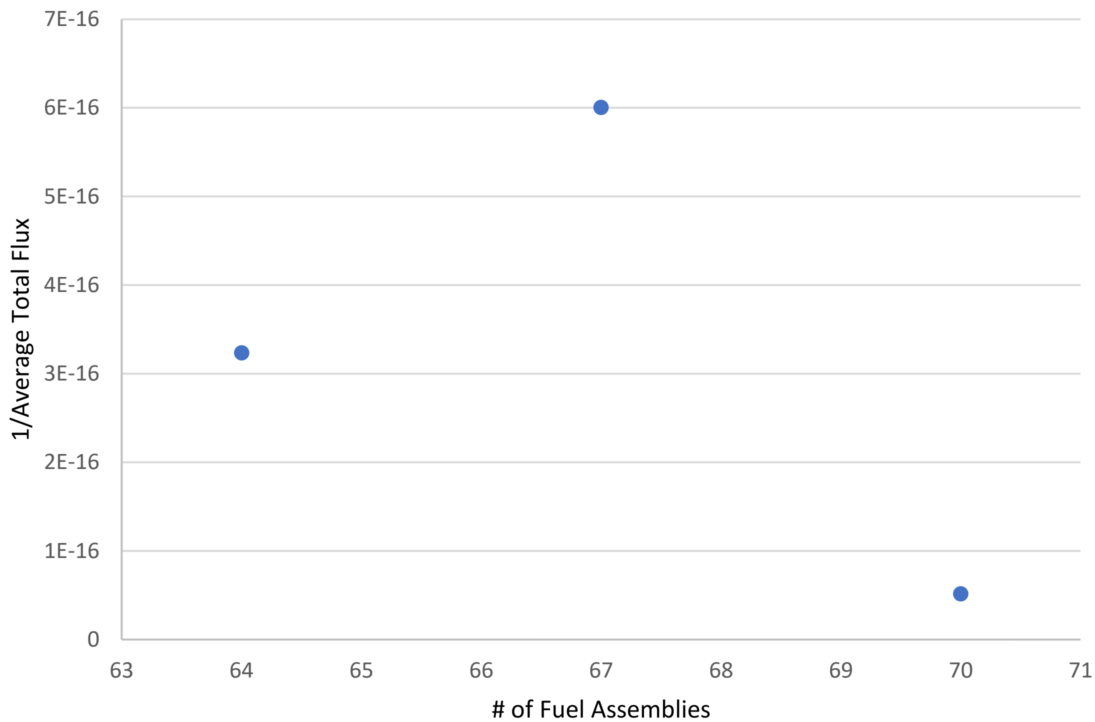

Figure 34. Wet critical experiment, CR "in", the last three points of detector 1.

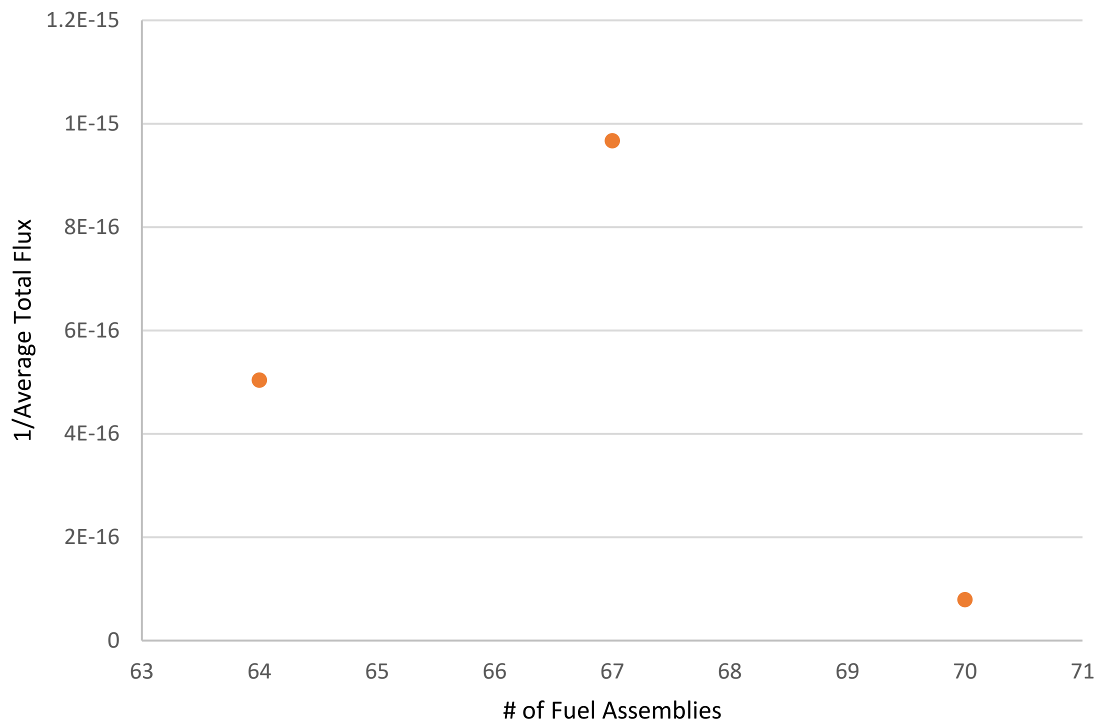

Figure 35. Wet critical experiment, CR "in", the last three points of detector 2.

In the second from the last fuel loading stage, the inverse flux value increased. Substituting enriched inner blanket assemblies by regular driver assembly did not work in wet critical experiment simulation. Further investigation was needed.

As mentioned in the literature, the inner blanket subassembly with enriched fuel was used for further parametric study. Both dry and wet critical experiments were repeated with an enriched inner blanket subassembly. The difference between the previous enriched inner blanket assembly is that the enrichment is not 48.0wt% ^{235}U. The enriched inner blanket assembly now had the same amount of ^{235}U, which is 2.82 kg of ^{235}U per assembly. The rest of the fuel consisted of pure ^{238}U. The total amount of uranium in each inner blanket and outer blanket assemblies was calculated to be 47.1 kg. The dry critical experiment simulation results are plotted as shown in Figure 36.

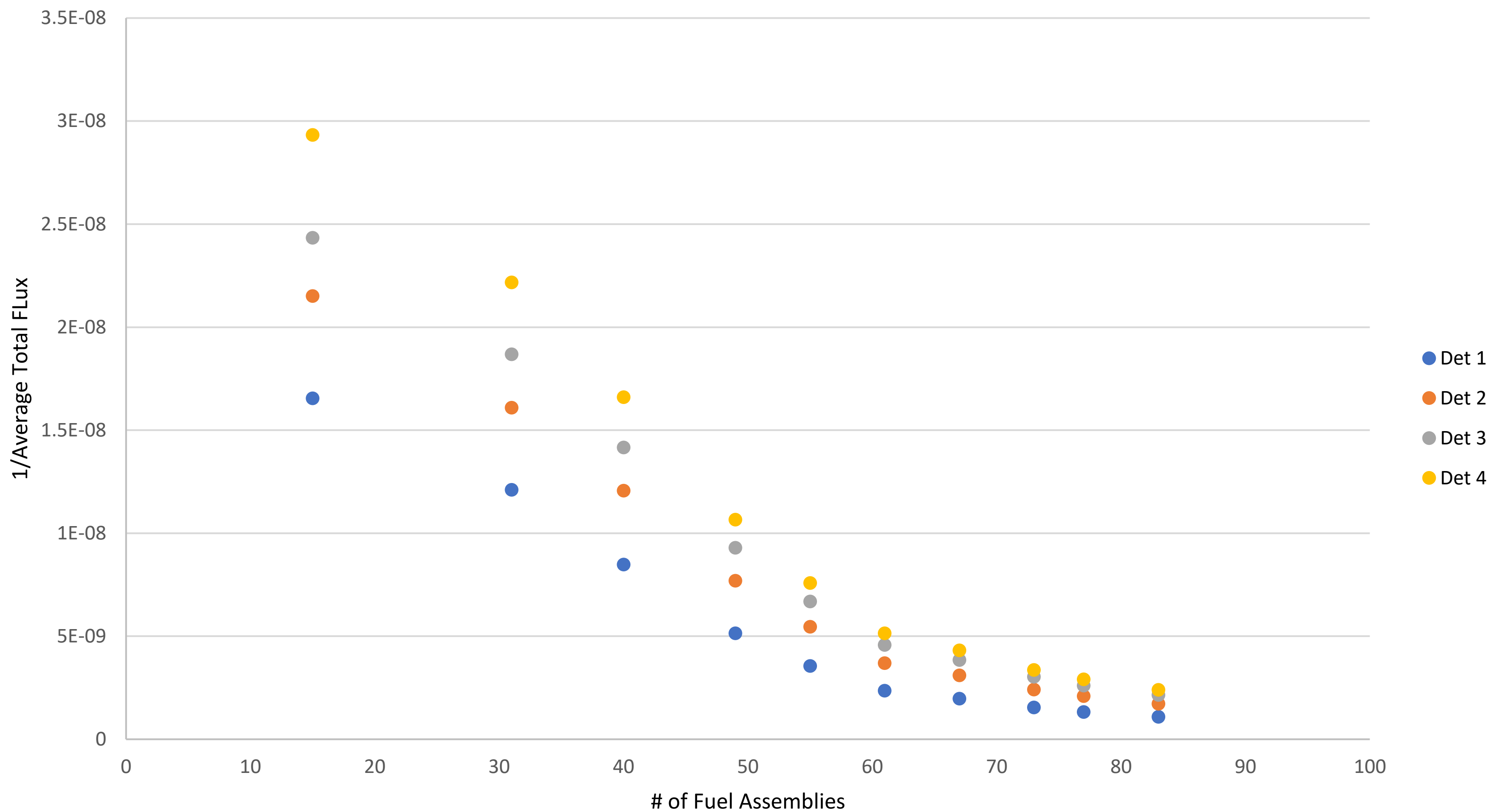

Figure 36. Dry critical experiment, CR "in" position, with enriched inner blanket.

The shape of the simulated detector response was very similar to the measured results. The detector 2 was chosen randomly to verify the 1/M shape. The 1/M plot of simulated detector 2 response and measured detector 2 results are shown in Figure 37 and Figure 38, respectively.

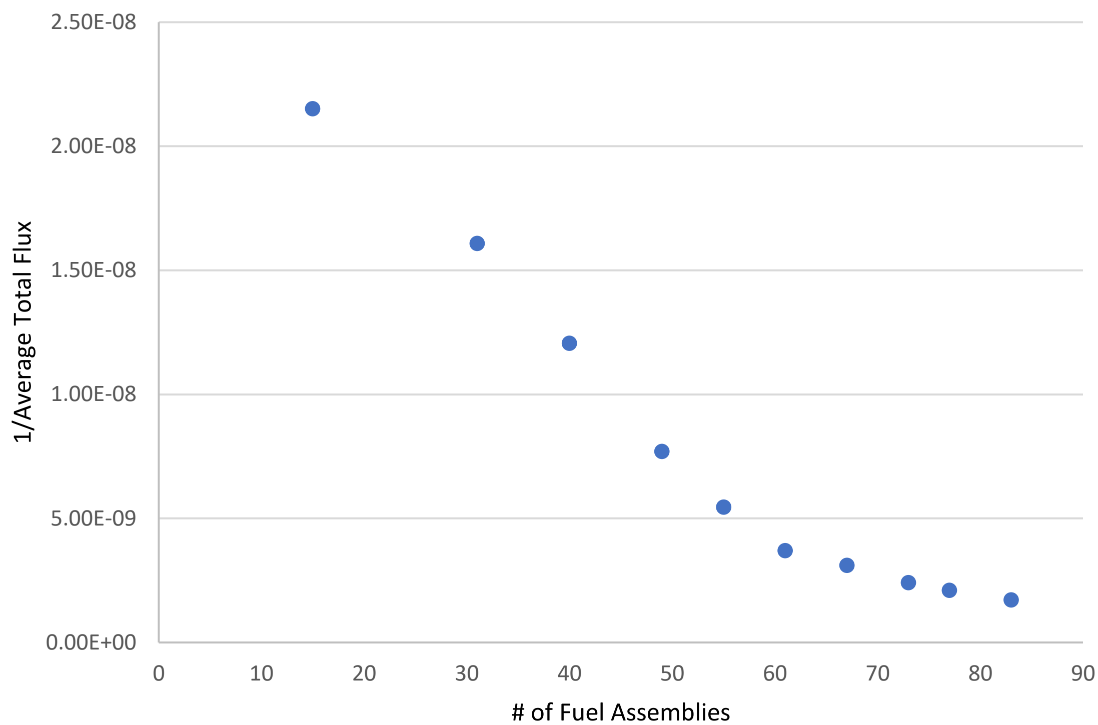

Figure 37. Simulated detector 2 response.

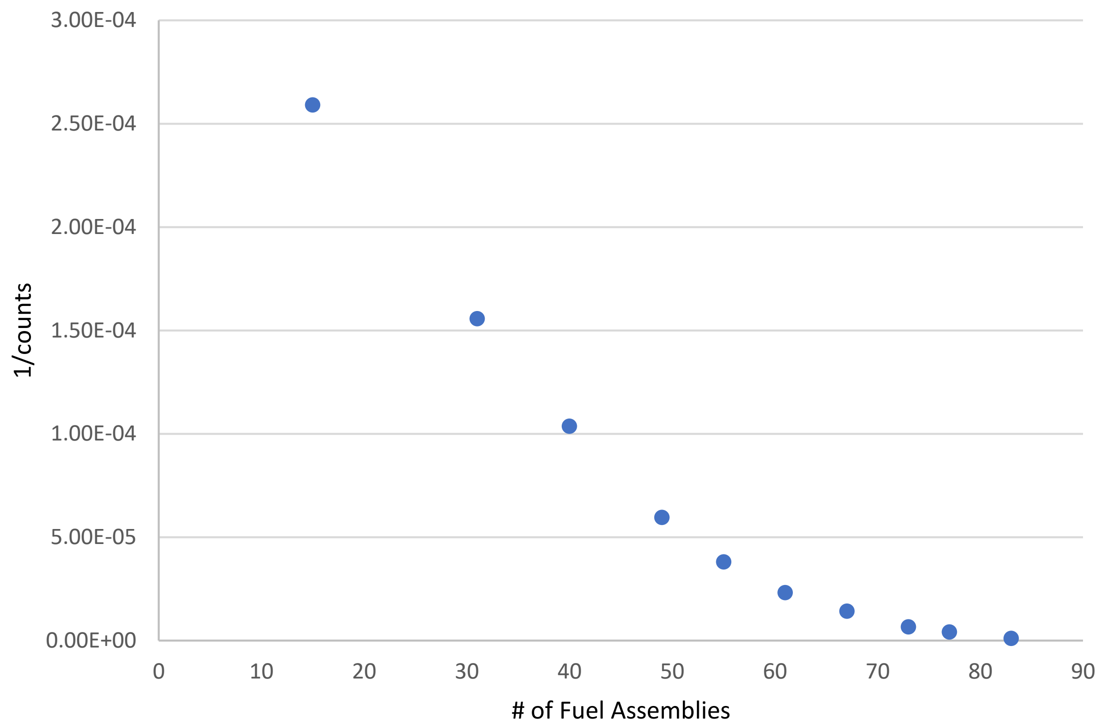

Figure 38. Measured detector 2 response.

Since the Y-axis values are not the same, the data normalized for comparison. The normalized detector 2 response is plotted in Figure 39.

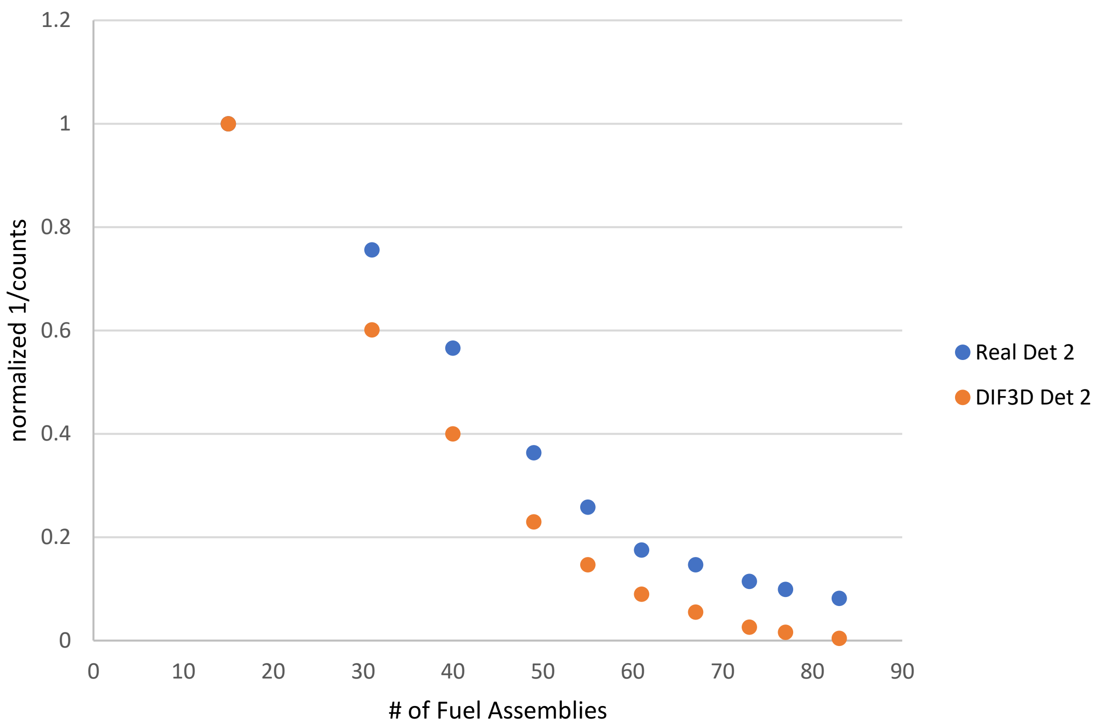

Figure 39. The normalized detector 2 responses.

Since the dry critical simulation results looked more like a curve (Figure 36) than a straight line (Figure 32), the wet critical experiment was simulated with same enriched inner blanket subassemblies. The 1/M curve of the wet critical experiment with control rod "in" position is shown in Figure 40. The detectors 1 and 2 were randomly chosen to verify whether there was a flaw in the flux behavior as before. The detector 1 and 4 results are shown in Figure 41 and Figure 42, respectively.

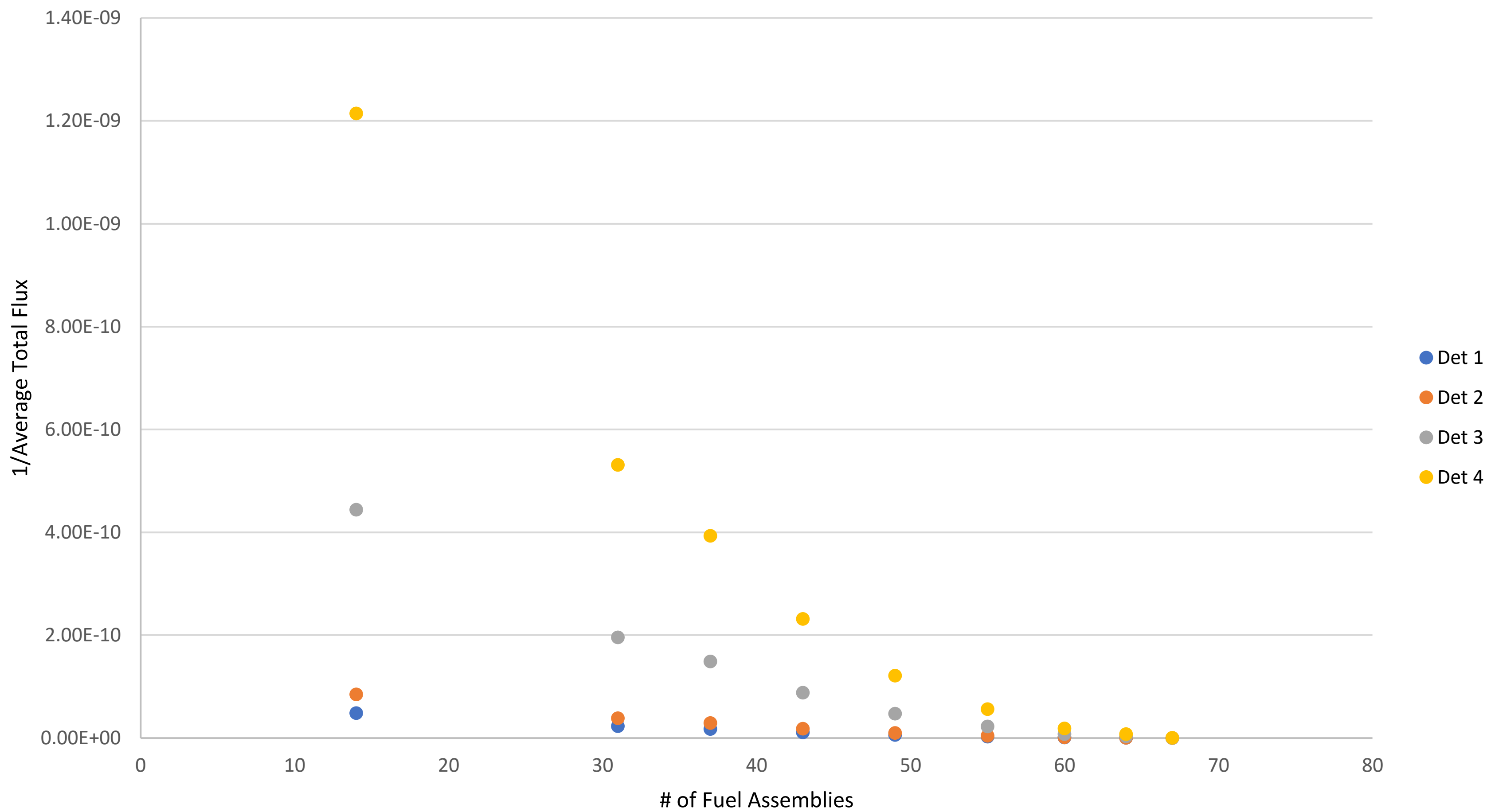

Figure 40. Wet critical experiment, CR "in" position, with enriched inner blanket.

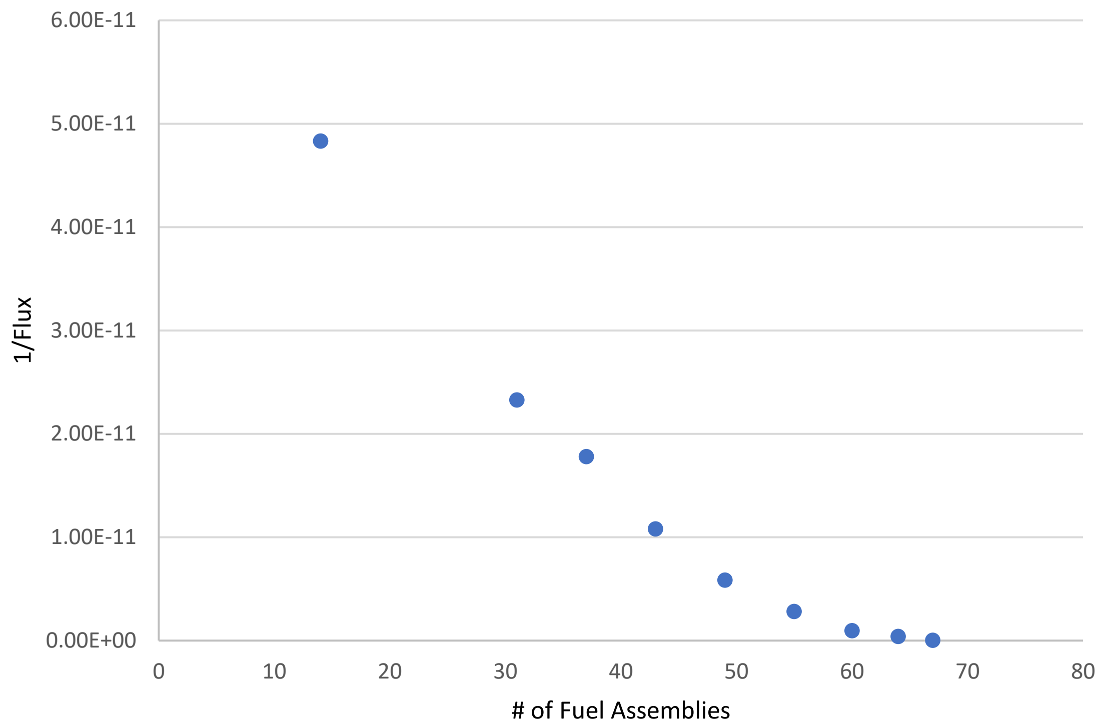

Figure 41. Wet critical experiment, CR "in" position, the detector 1 response.

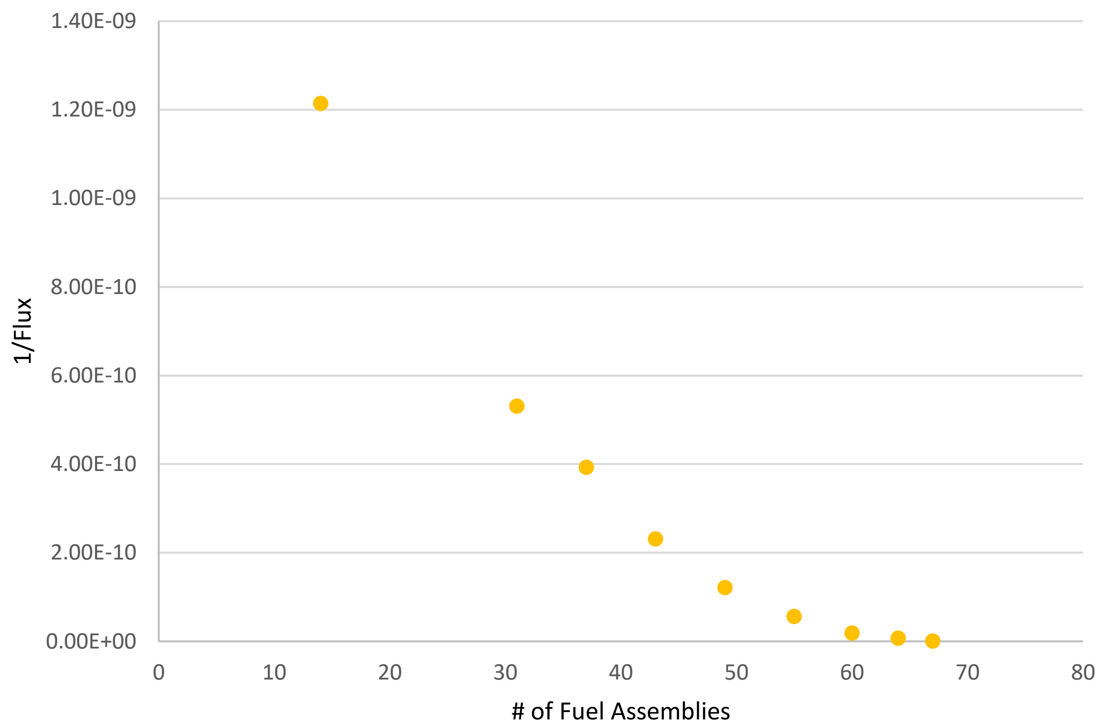

Figure 42. Wet critical experiment, CR "in" position, the detector 4 response.

To confirm continuous decrease in the inverse flux value, the last four points of detector 1 and 4 were plotted separately in Figure 43 and Figure 44, respectively.

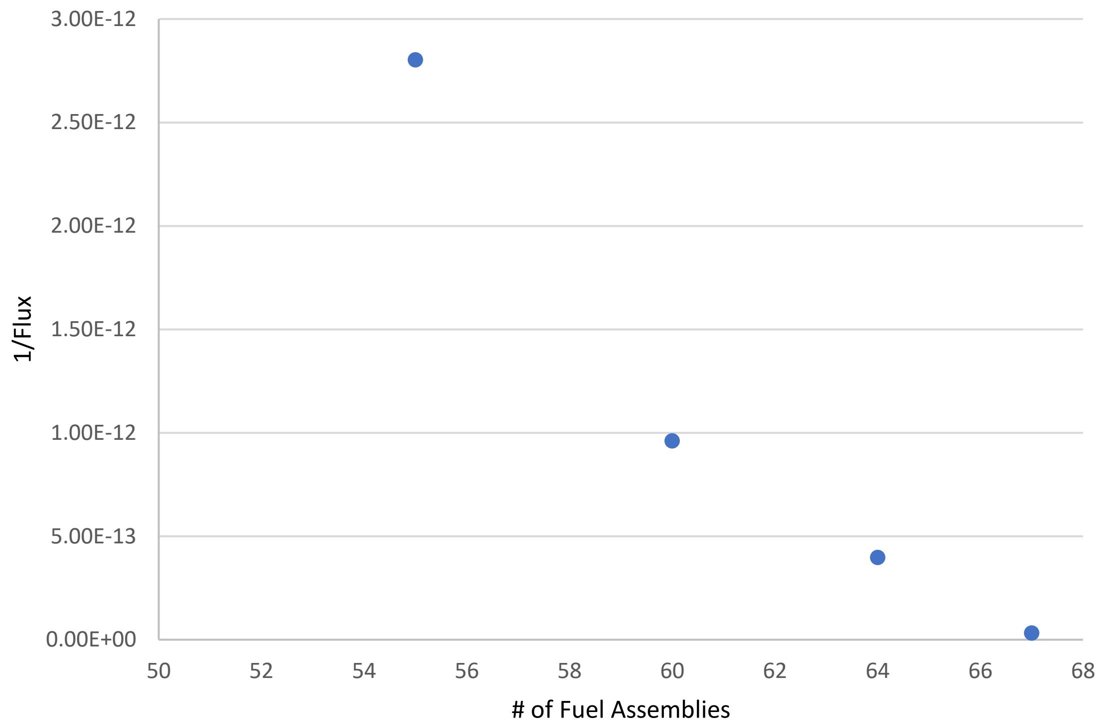

Figure 43. Wet critical experiment, CR "in", the last three points of detector 1.

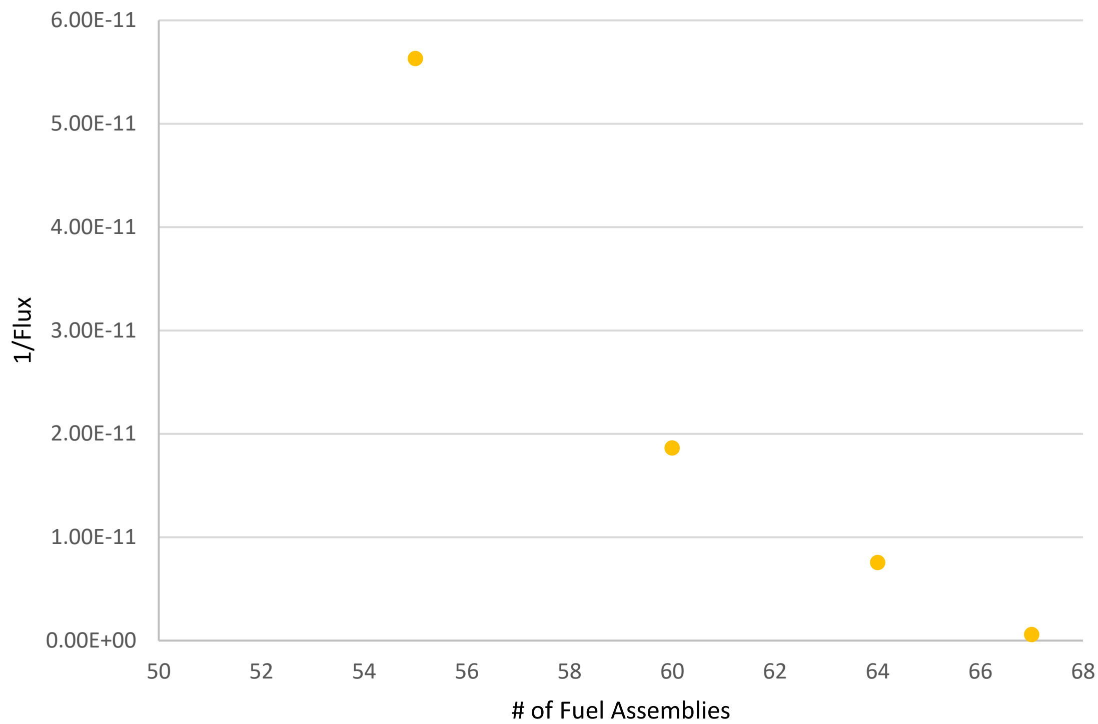

Figure 44. Wet critical experiment, CR "in", the last three points of detector 4.

Now that every data point in the dry and wet critical experiment were in descending orders and the shape looks more curve like, the enriched inner blanket assembly with 2.82 kg ^{235}U was used during approach-to-critical experiment simulation. With these results, the simulation of dry and wet critical approach-to-critical experiments were successful.

6. MSM Correction Factor

After simulating the approach-to-critical experiments, the measured results of the same experiment can be corrected by MSM correction factor as discussed in Section 2.

6.1 Calculating MSM Correction Factor

The MSM correction factor is calculated by Equation 11 (page 16) in each fuel loading stage. Every variable in this equation is calculated by DIF3D. Let's take the fuel loading stage 1 (Figure 13) and 2 (Figure 14) of dry critical control rods up position for example. The three parts, $\langle \phi^* S \rangle$, $\langle \phi^* \mathrm{F} \phi \rangle$, and $\langle \Sigma_d \phi \rangle$, of the Equation 11 will be evaluated separately in each stage.

$$\langle \phi^* S \rangle = \int_E \phi^*(E) S dV = \sum_{n=1}^{33} \phi^*(E_n) S V$$

$$\langle \phi^* \mathrm{F} \phi \rangle = \int_E \phi^*(E) \nu \Sigma_f(E) \phi(E) dV = \sum_{n=1}^{33} \phi^*(E_n) \nu \Sigma_f(E_n) \phi(E_n) V$$

$$\langle \Sigma_d \phi \rangle = \int_E \Sigma_d(E) \phi(E) dV = \sum_{n=1}^{33} \Sigma_d(E_n) \phi(E_n) V$$

The calculated values are given in Table 11.

Table 11. The Calculated Values of Each Variable*

	$\langle \phi^* S \rangle$	$\langle \phi^* \mathrm{F} \phi \rangle$	$\langle \Sigma_d \phi \rangle_1$	$\langle \Sigma_d \phi \rangle_2$	$\langle \Sigma_d \phi \rangle_3$	$\langle \Sigma_d \phi \rangle_4$
Stage 1	9.75E+14	8.04E+20	3.64E+08	4.97 E+08	7.68 E+08	7.70 E+08
Stage 2	9.87E+14	1.86E+21	4.69E+08	6.23 E+08	9.46 E+08	9.31 E+08

*Flux is arbitrary from the DIF3D calculation

The calculated correction factors for each detector are shown in Table 12.

Table 12. MSM Correction Factor for Each Detector

	Detector 1	Detector 2	Detector 3	Detector 4
Stage 1	0.56576	0.54928	0.54019	0.52977
Stage 2	0.40486	0.36229	0.35256	0.35254

The 1/M value of the measured data is corrected by multiplying it by the ratio of MSM correction factors. Both measured and corrected 1/M values are shown in Table 13.

Table 13. Detector Response before and after MSM Correction

	Detector 1	Detector 2	Detector 3	Detector 4
Measured 1/M	0.22389	0.60125	0.48245	0.44528
Corrected 1/M	0.12667	0.33026	0.26062	0.23590

The range of the corrected 1/M values is 0.20359 and the range of uncorrected 1/M value is 0.37736. The data points got closer which is the purpose of MSM. The MSM correction factors were calculated for each detector at each stage of the approach-to-critical experiments.

6.2 Applying MSM Correction on ASM results

The measured detector response of EBR-II reactor dry and wet critical experiment data was corrected using MSM correction factors. Table 14 and Table 15 show the measured 1/M value, MSM correction factor, and corrected 1/M value of dry and wet critical experiments with control rods “in” position, respectively. Table 16 and Table 17 show the measured 1/M value, MSM correction factor, and corrected 1/M value of dry and wet critical experiments with control rods “out/down” position, respectively.

Table 14. Dry Critical Experiment, CR "in", MSM Correction

# of fuel assemblies	Measured 1/M Value				Correction Factors				MSM Corrected 1/M Value			
	Det 1	Det 2	Det 3	Det 4	Det 1	Det 2	Det 3	Det 4	Det 1	Det 2	Det 3	Det 4
31	0.2239	0.6012	0.4825	0.4453	0.5658	0.5493	0.5402	0.5298	0.1267	0.3303	0.2606	0.2359
40	0.1502	0.4000	0.3022	0.2785	0.4049	0.3623	0.3526	0.3525	0.0608	0.1449	0.1065	0.0982
49	0.0878	0.2299	0.1678	0.1513	0.2870	0.2375	0.2255	0.2325	0.0252	0.0546	0.0378	0.0352
55	0.0565	0.1468	0.1048	0.0938	0.2463	0.1964	0.1843	0.1930	0.0139	0.0288	0.0193	0.0181
61	0.0345	0.0898	0.0630	0.0561	0.1941	0.1497	0.1389	0.1476	0.0067	0.0134	0.0088	0.0083
67	0.0217	0.0552	0.0374	0.0330	0.1714	0.1310	0.1213	0.1294	0.0037	0.0072	0.0045	0.0043
73	0.0102	0.0257	0.0172	0.0146	0.1539	0.1171	0.0907	0.1157	0.0016	0.0030	0.0016	0.0017
77	0.0065	0.0162	0.0106	0.0089	0.1409	0.1058	0.0976	0.1049	0.0009	0.0017	0.0010	0.0009
83	0.0018	0.0043	0.0028	0.0023	0.1216	0.0914	0.0839	0.0906	0.0002	0.0004	0.0002	0.0002

Table 15. Wet Critical Experiment, CR "in", MSM Correction

# of fuel assemblies	Measured 1/M Value					Correction Factors					MSM Corrected 1/M Value				
	Det 1	Det 2	Det 3	Det 4	Det 5	Det 1	Det 2	Det 3	Det 4	Det 5	Det 1	Det 2	Det 3	Det 4	Det 5
31	0.3857	0.3778	0.3742	0.4361	0.4898	1.1410	1.1410	1.0015	1.0273	0.9971	0.4401	0.4310	0.3747	0.4480	0.4883
37	0.2590	0.2629	0.2568	0.3166	0.3651	1.2369	1.2369	0.9747	1.0015	1.0537	0.3203	0.3252	0.2503	0.3171	0.3847
43	0.1695	0.1678	0.1689	0.2170	0.2664	1.0432	1.0432	0.8283	0.8460	0.8027	0.1769	0.1750	0.1399	0.1835	0.2138
49	0.0936	0.0940	0.0943	0.1264	0.1629	0.6444	0.6444	0.5171	0.5268	0.4539	0.0603	0.0606	0.0488	0.0666	0.0740
55	0.0478	0.0472	0.0472	0.0721	0.0896	0.7029	0.7029	0.5668	0.5767	0.4712	0.0336	0.0332	0.0267	0.0416	0.0422
60	0.0229	0.0226	0.0227	0.0389	0.0480	0.4738	0.4738	0.3842	0.3907	0.3044	0.0108	0.0107	0.0087	0.0152	0.0146
64	0.0102	0.0097	0.0100	0.0141	0.0252	0.4056	0.4056	0.3324	0.3379	0.2551	0.0041	0.0039	0.0033	0.0048	0.0064
67	0.0022	0.0036	0.0037	0.0052	0.0150	0.5532	0.5532	0.4749	0.4831	0.3581	0.0012	0.0020	0.0018	0.0025	0.0054

Table 16. Dry Critical Experiment, CR "out", MSM Correction

# of fuel assemblies	Measured 1/M Value				Correction Factors				MSM Corrected 1/M Value			
	Det 1	Det 2	Det 3	Det 4	Det 1	Det 2	Det 3	Det 4	Det 1	Det 2	Det 3	Det 4
31	0.2380	0.6223	0.4088	0.3605	0.4423	0.4416	0.4360	0.4447	0.1053	0.2748	0.1782	0.1603
40	0.1665	0.4283	0.2553	0.2232	0.3067	0.2864	0.2808	0.2908	0.0511	0.1227	0.0717	0.0649
49	0.1048	0.2624	0.1489	0.1267	0.2318	0.2031	0.1951	0.2072	0.0243	0.0533	0.0291	0.0263
55	0.0723	0.1795	0.0994	0.0860	0.2132	0.1807	0.1715	0.1851	0.0154	0.0324	0.0171	0.0159
61	0.0500	0.1233	0.0676	0.0571	0.1863	0.1533	0.1441	0.1575	0.0093	0.0189	0.0097	0.0090
67	0.0349	0.0844	0.0447	0.0373	0.1287	0.1048	0.0983	0.1079	0.0045	0.0088	0.0044	0.0040
73	0.0200	0.0477	0.0250	0.0202	0.1471	0.1190	0.1109	0.1227	0.0029	0.0057	0.0028	0.0025
77	0.0157	0.0371	0.0191	0.0152	0.1384	0.1106	0.1034	0.1144	0.0022	0.0041	0.0020	0.0017
83	0.0107	0.0240	0.0126	0.0100	0.1249	0.0999	0.0930	0.1033	0.0013	0.0024	0.0012	0.0010
87	0.0079		0.0091	0.0073	0.1192	0.0945	0.0883	0.0980	0.0009		0.0008	0.0007

Table 17. Wet Critical Experiment, CR "out", MSM Correction

# of fuel assemblies	Measured 1/M Value					Correction Factors					MSM Corrected 1/M Value				
	Det 1	Det 2	Det 3	Det 4	Det 5	Det 1	Det 2	Det 3	Det 4	Det 5	Det 1	Det 2	Det 3	Det 4	Det 5
31	0.2700	0.2615	0.2582	0.2731	0.2981	0.6722	0.6722	0.6899	0.6811	0.5822	0.1815	0.1758	0.1782	0.1861	0.1736
37	0.1843	0.1882	0.1797	0.1927	0.2153	0.5391	0.5391	0.5629	0.5530	0.4571	0.0993	0.1014	0.1012	0.1065	0.0984
43	0.1292	0.1275	0.1230	0.1379	0.1629	0.4236	0.4236	0.4462	0.4356	0.3284	0.0547	0.0540	0.0549	0.0601	0.0535
49	0.0771	0.0775	0.0743	0.0873	0.1049	0.3615	0.3615	0.3847	0.3746	0.2574	0.0279	0.0280	0.0286	0.0327	0.0270
55	0.0450	0.0440	0.0436	0.0551	0.0645	0.3224	0.3224	0.3448	0.3353	0.2197	0.0145	0.0142	0.0150	0.0185	0.0142
60	0.0290	0.0283	0.0279	0.0404	0.0443	0.2715	0.2715	0.2919	0.2837	0.1786	0.0079	0.0077	0.0082	0.0115	0.0079
64	0.0195	0.0186	0.0185		0.0311	0.2418	0.2418	0.2626	0.2551	0.1555	0.0047	0.0045	0.0049		0.0048
67	0.0140	0.0138	0.0139	0.0172	0.0243	0.2236	0.2236	0.2547	0.2475	0.1466	0.0031	0.0031	0.0035	0.0042	0.0036
70	0.0105	0.0103	0.0104	0.0138	0.0176	0.2108	0.2108	0.2400	0.2333	0.1395	0.0022	0.0022	0.0025	0.0032	0.0025

The measured detector response and corresponding MSM correction of the dry critical experiment with control rod "in" position are shown in Figure 45 and Figure 46, respectively. However, while the data points got closer, it was difficult to see it. The last six data points are plotted separately on Figure 47 and Figure 48. The last four data points are plotted separately on Figure 50 and Figure 51.

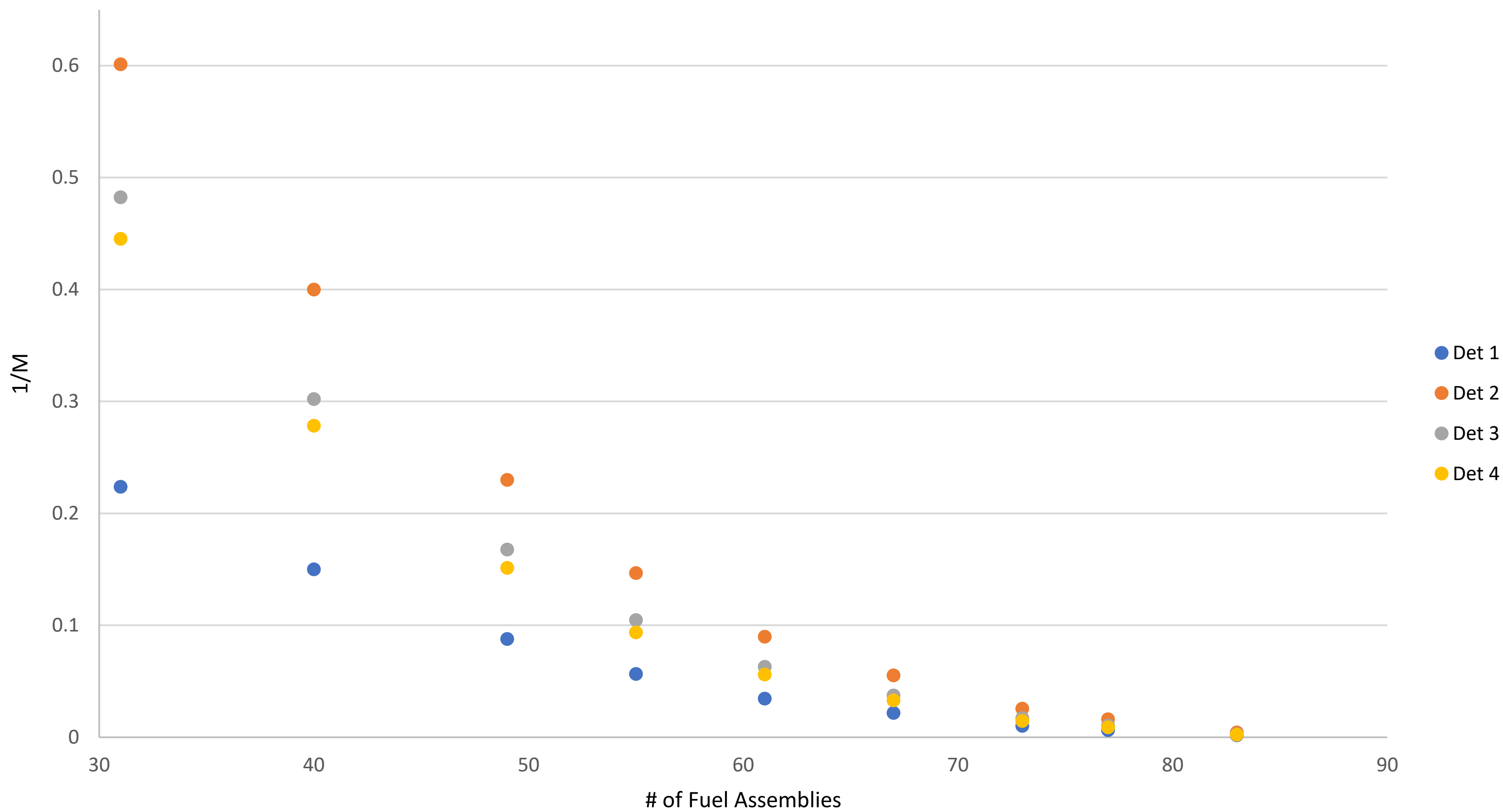

Figure 45. Dry critical experiment, CR “in” position, measured detector response.

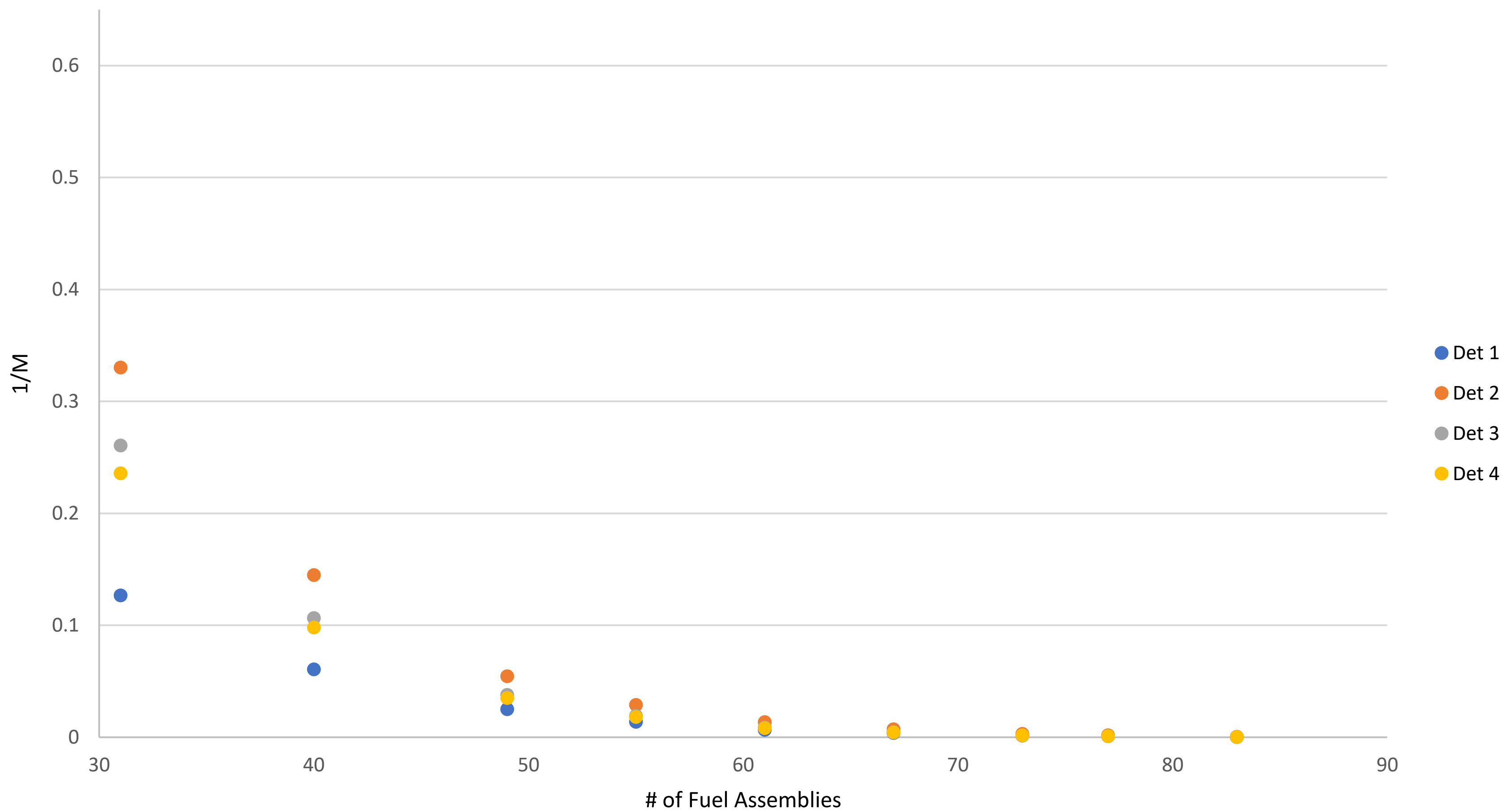

Figure 46. Dry critical experiment, CR “in” position, the detector response after MSM correction.

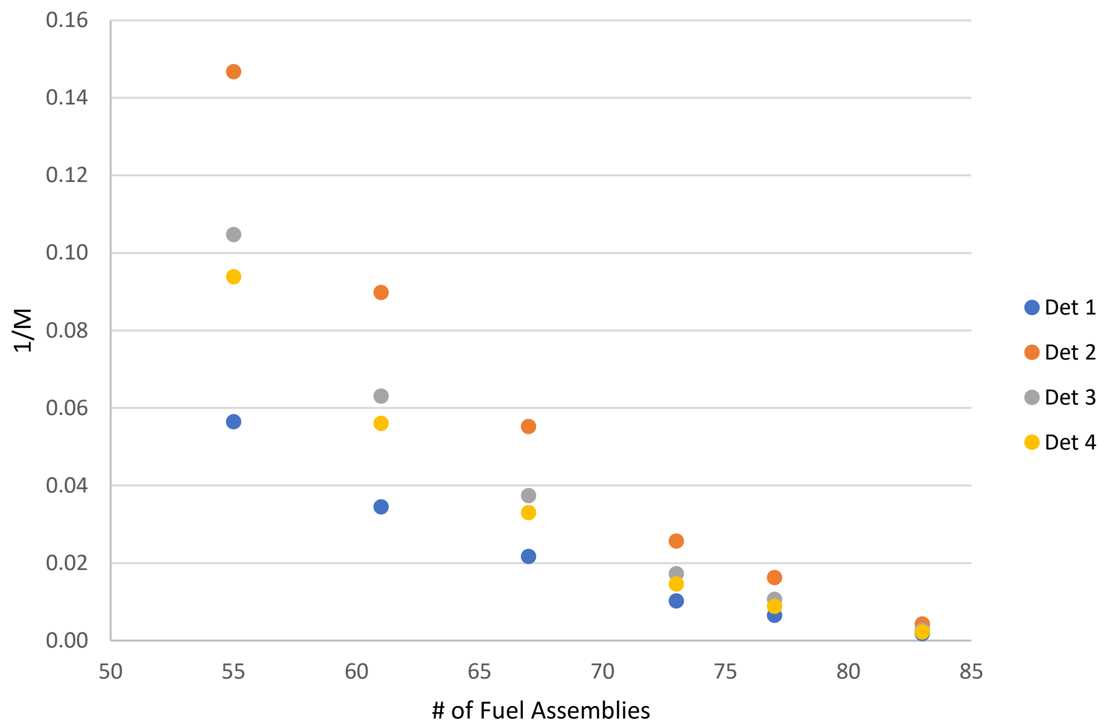

Figure 47. Dry critical experiment, CR “in”, last six measured data points.

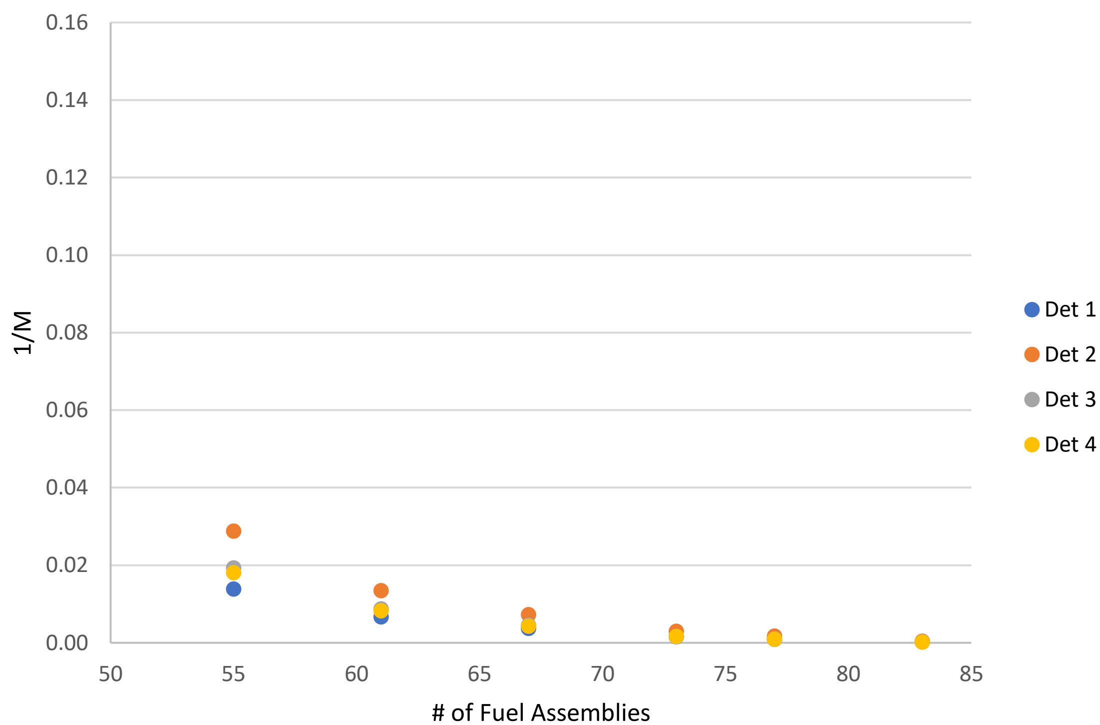

Figure 48. Dry critical experiment, CR “in”, last six MSM corrected data points.

As shown in Figure 49, the corrected 1/M plot of the last six points is amplified to show better detector 1/M locations.

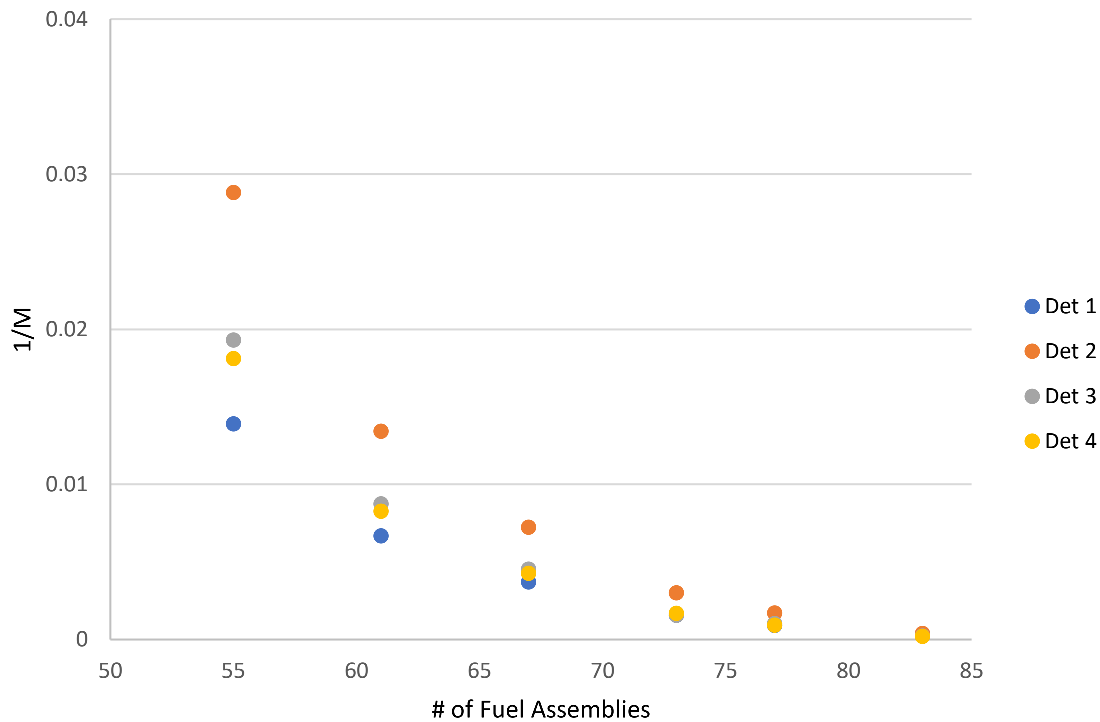

Figure 49. Dry critical experiment, CR “in”, amplified the last six MSM corrected data points.

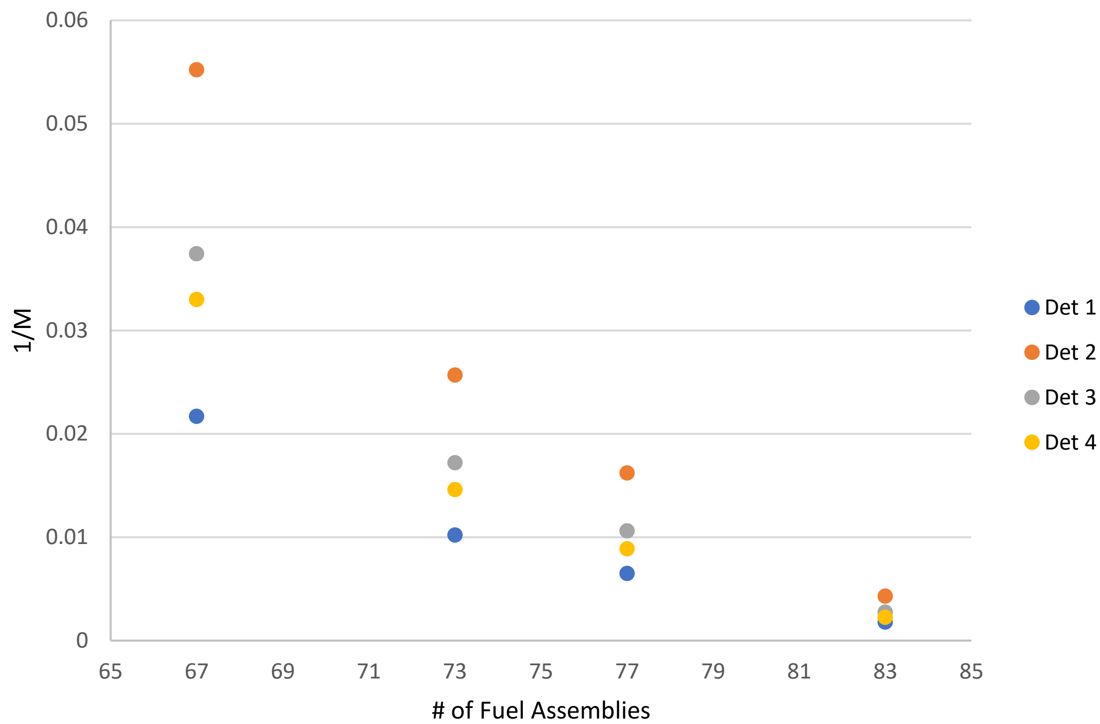

Figure 50. Dry critical experiment, CR “in”, last four measured data points.

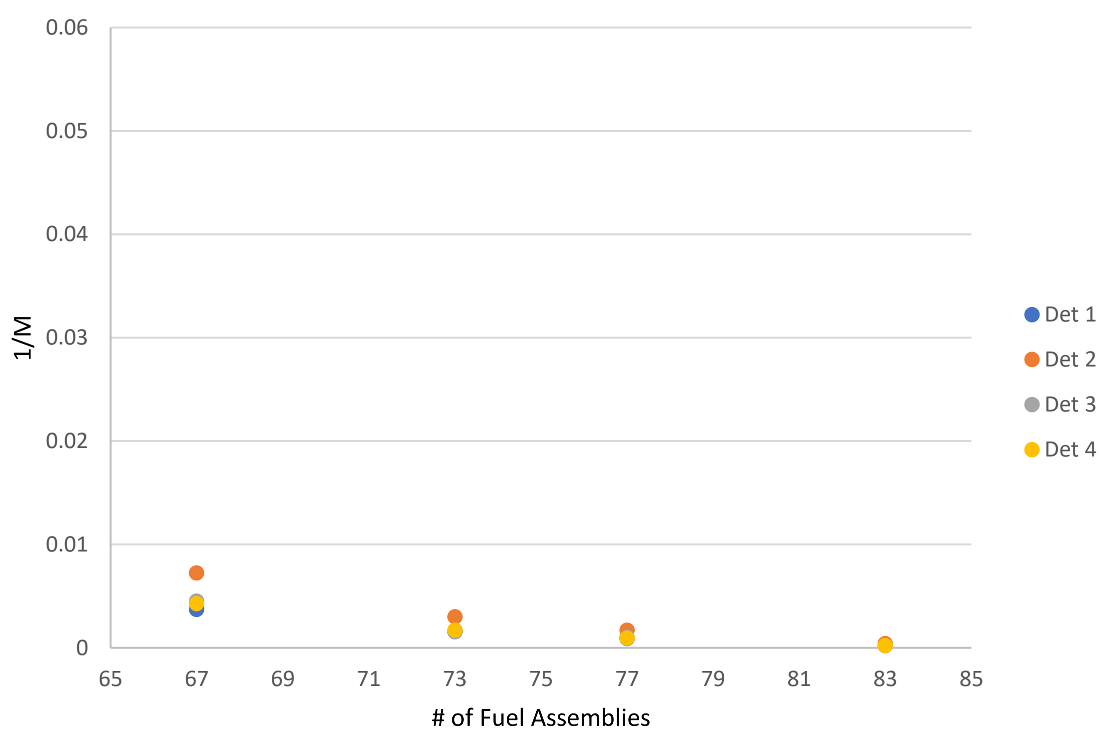

Figure 51. Dry critical experiment, CR “in”, last four MSM corrected data points.

As shown in Figure 52, the corrected 1/M plot of the last four points is amplified to show better detector 1/M locations.

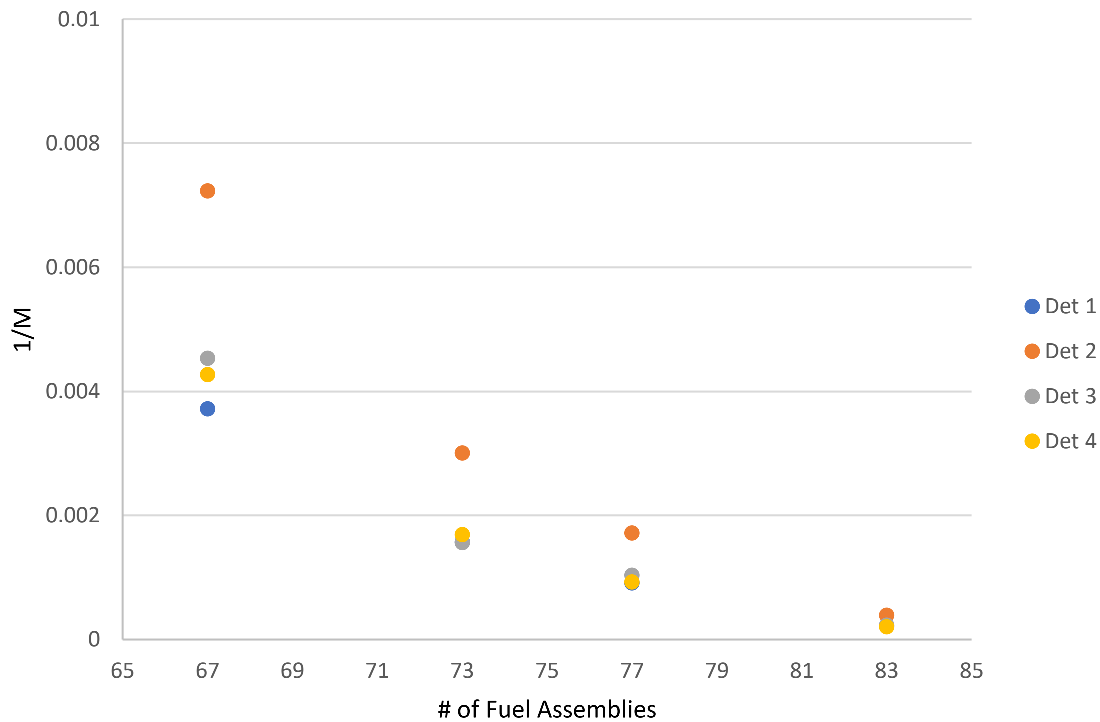

Figure 52. Dry critical experiment, CR "in", amplified the last four MSM corrected data points.

The measured detector response and corresponding MSM correction of the dry critical experiment with control rod "out" position are shown in Figure 53 and Figure 54, respectively. However, while the data points got closer, it was difficult to see it. The last seven data points are plotted separately on Figure 55 and Figure 56. The last four data points are plotted separately on Figure 58 and Figure 59.

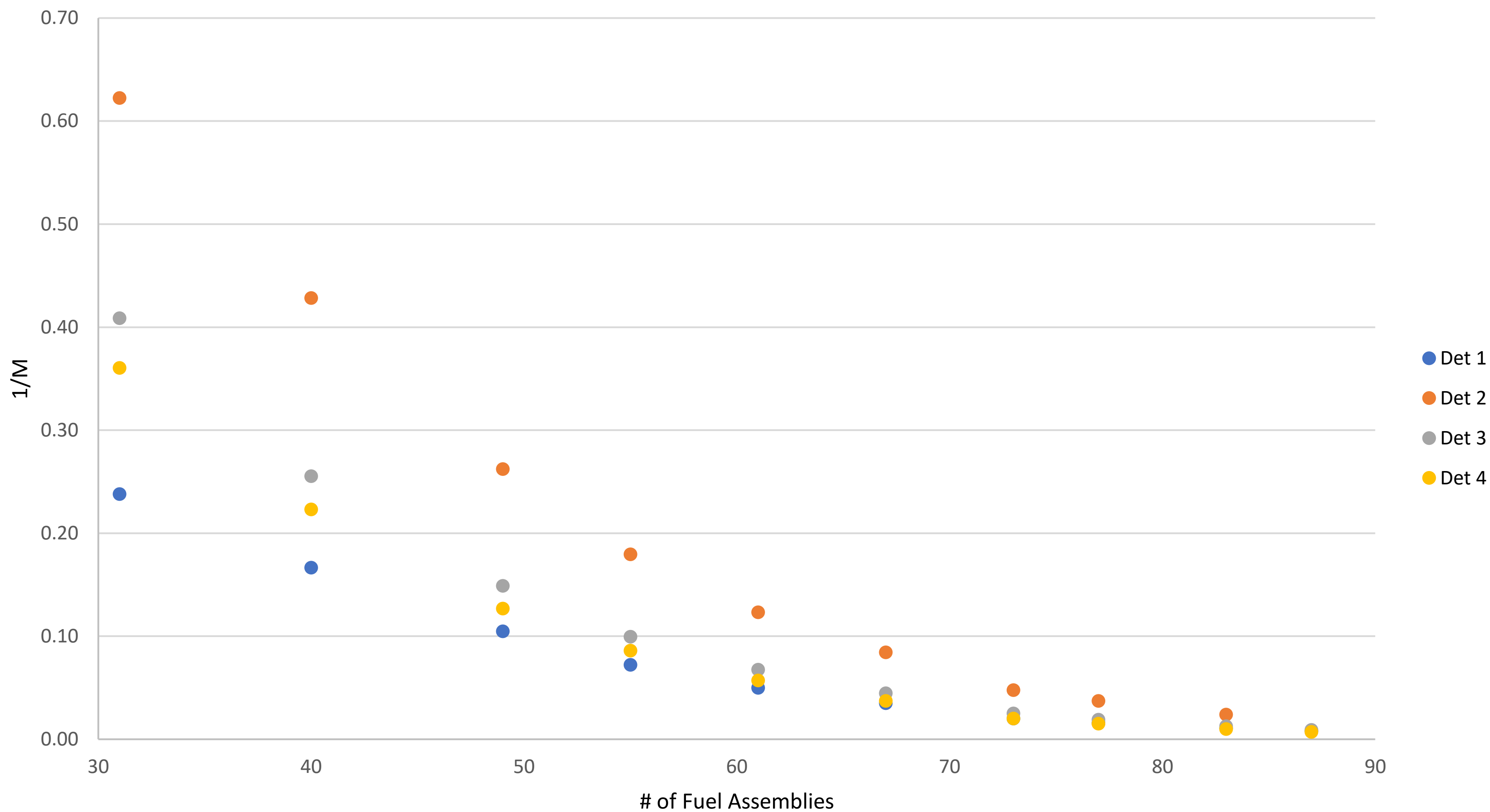

Figure 53. Dry critical experiment, CR “out” position, measured detector response.

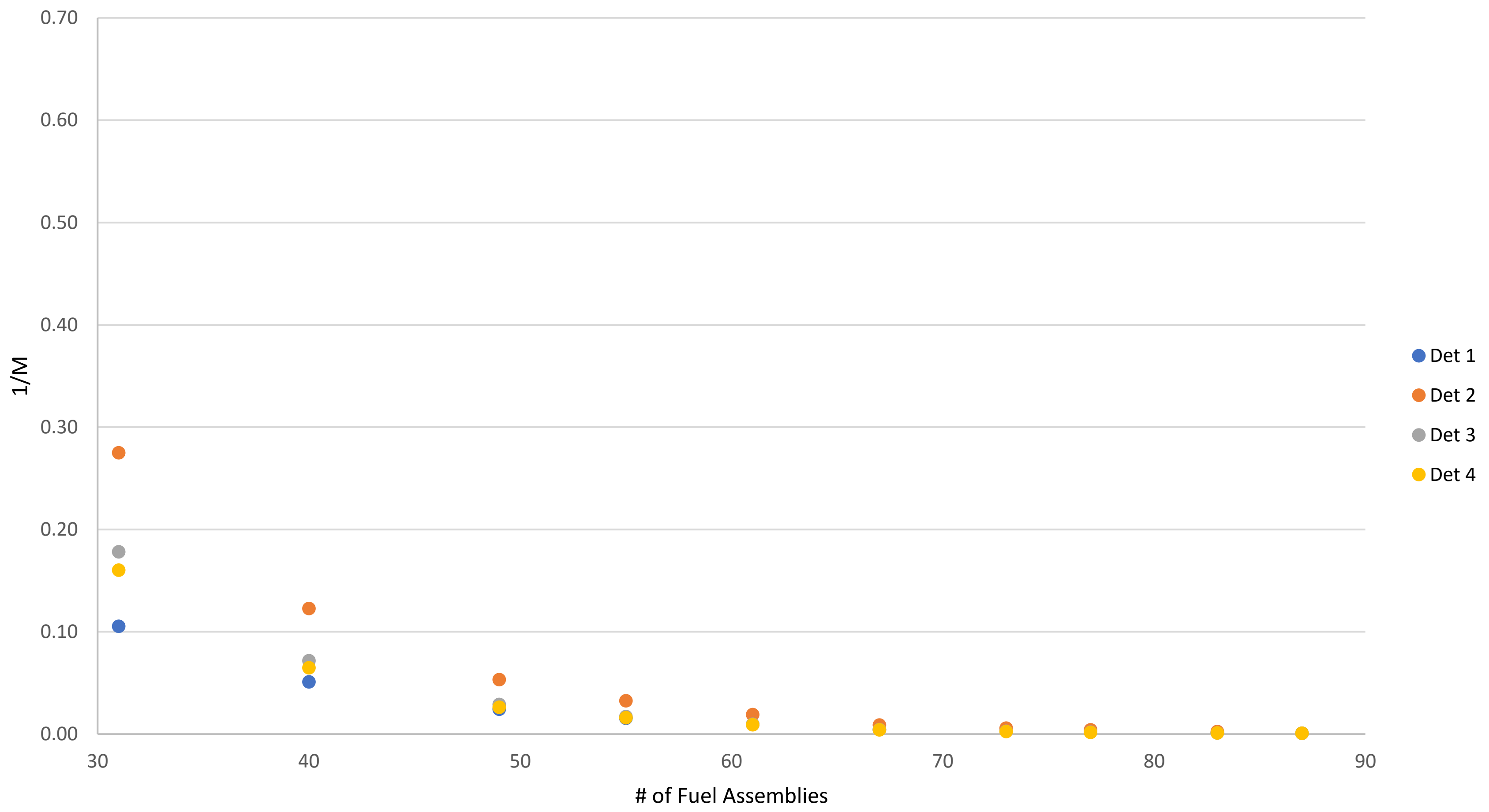

Figure 54. Dry critical experiment, CR “out” position, the detector response after MSM correction.

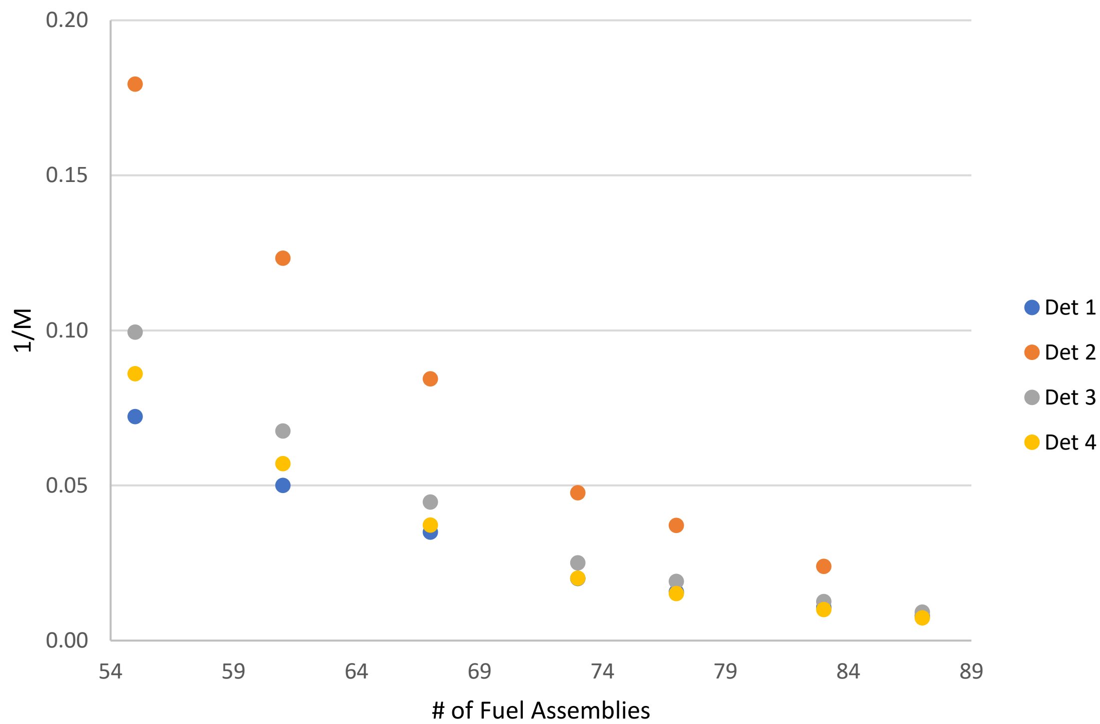

Figure 55. Dry critical experiment, CR “out”, last seven measured data points.

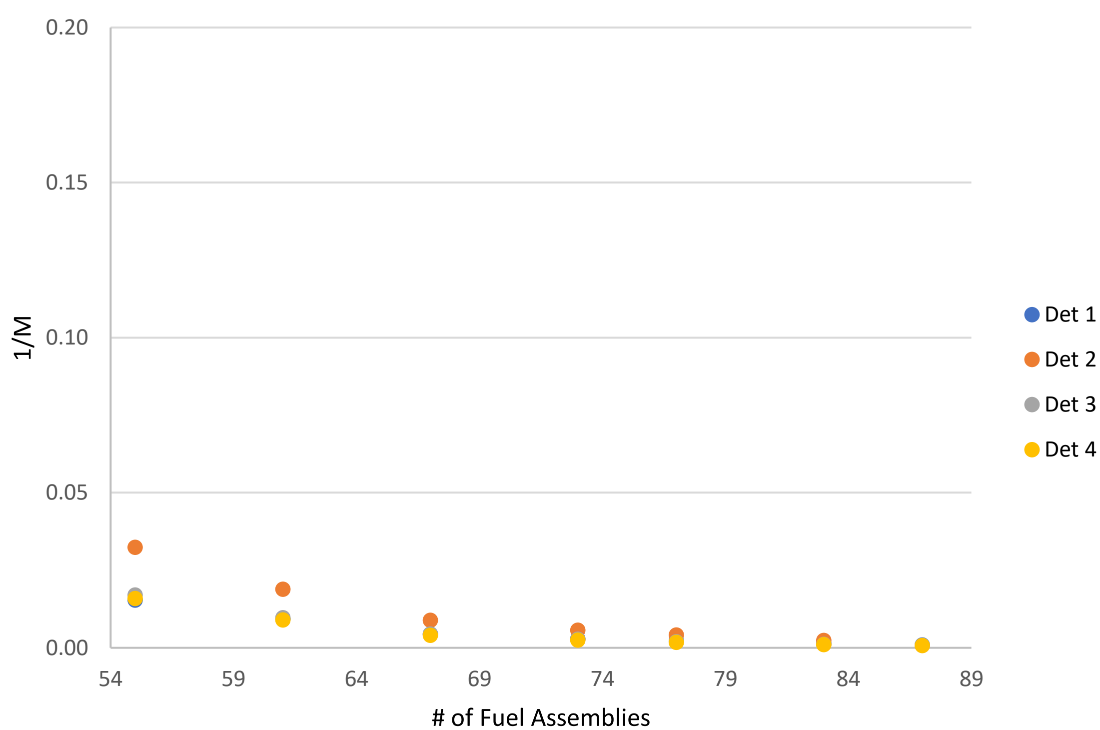

Figure 56. Dry critical experiment, CR “out”, last seven MSM corrected data points.

As shown in Figure 57, the corrected 1/M plot of the last seven points is amplified to show better detector 1/M locations.

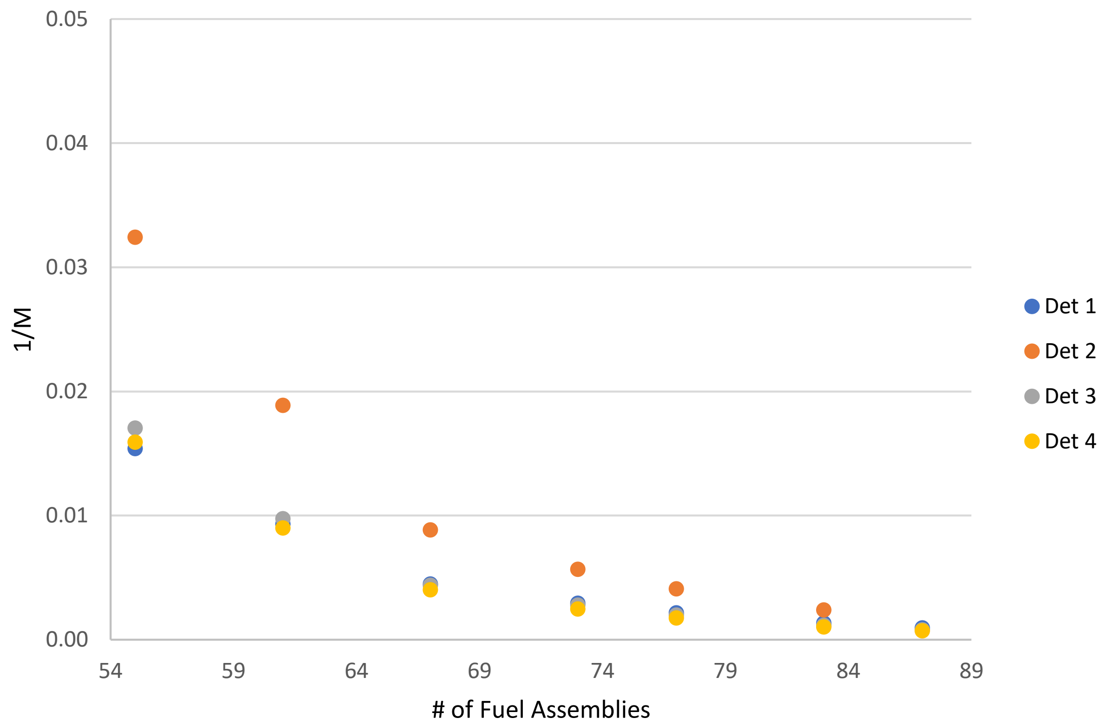

Figure 57. Dry critical experiment, CR “out”, amplified the last seven MSM corrected data points.

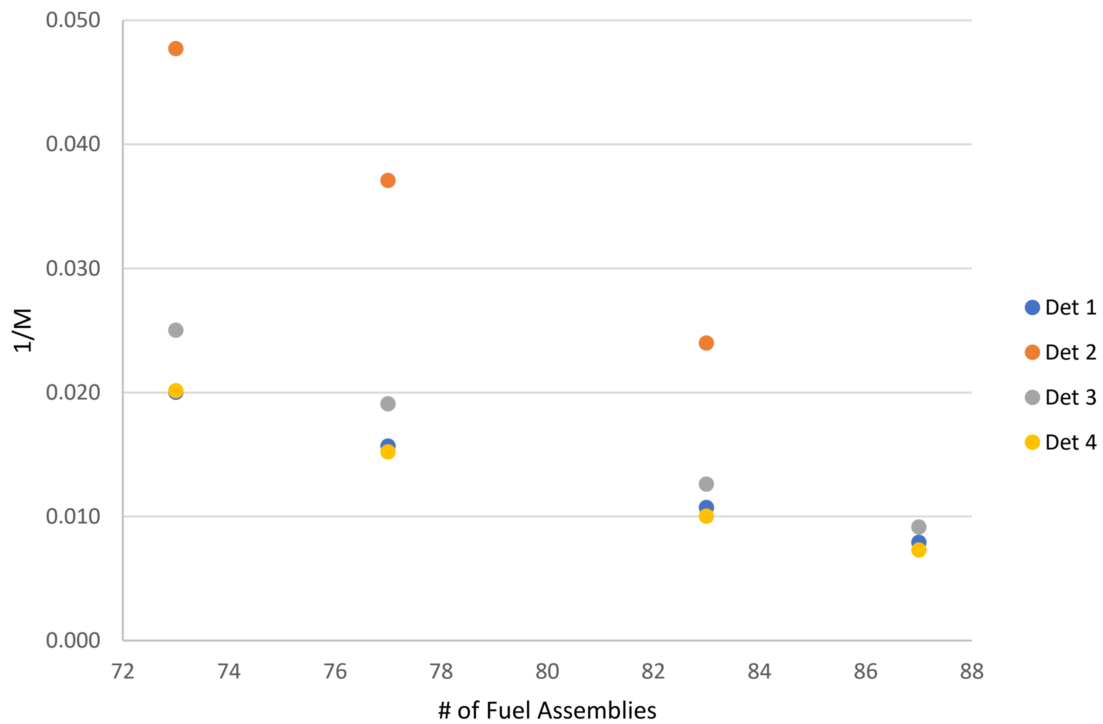

Figure 58. Dry critical experiment, CR “out”, last four measured data points.

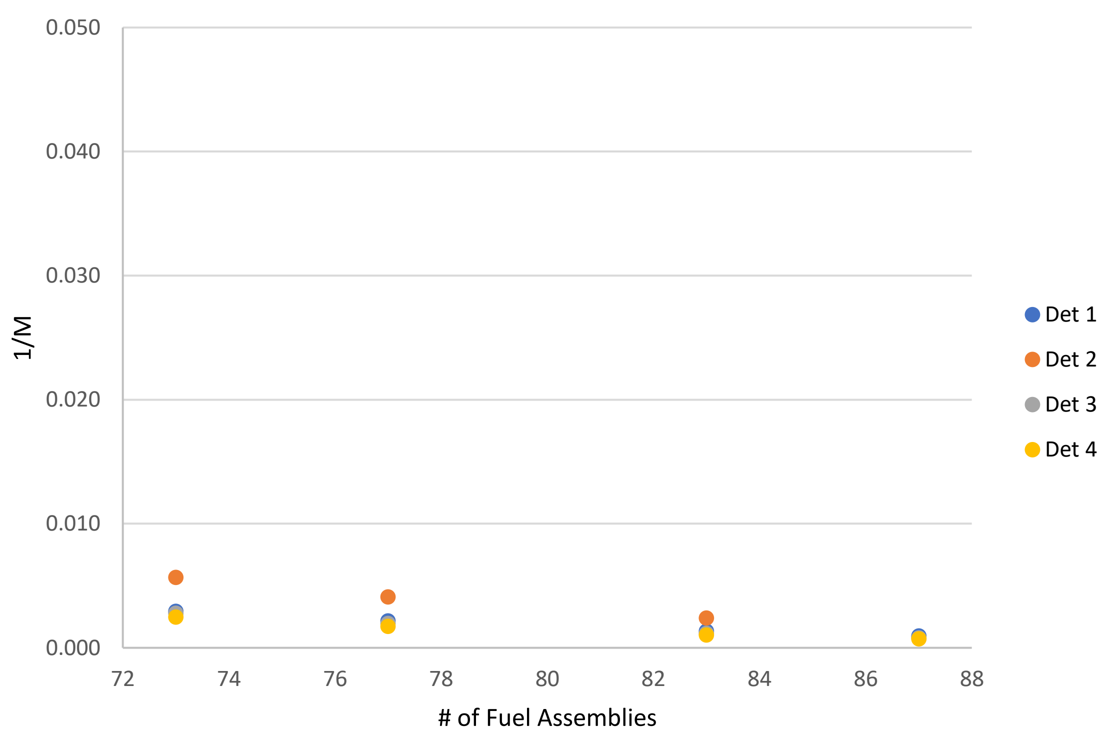

Figure 59. Dry critical experiment, CR “out”, last four MSM corrected data points.

As shown in Figure 60, the corrected 1/M plot of the last four points is amplified to show better detector 1/M locations.

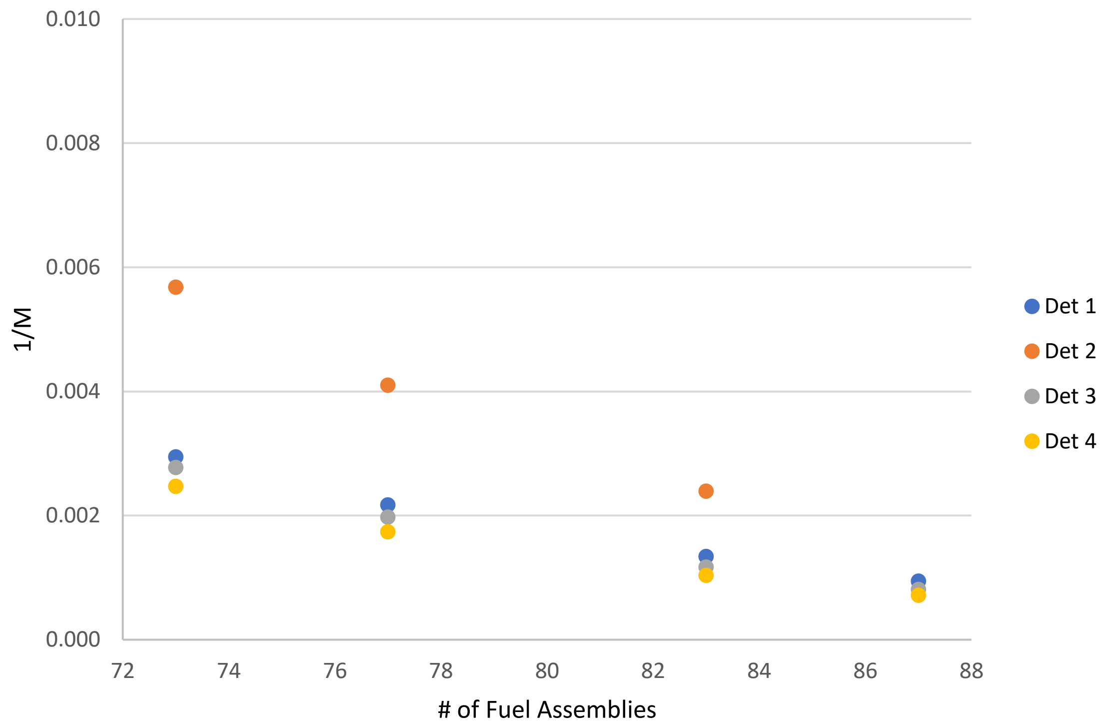

Figure 60. Dry critical experiment, CR “out”, amplified the last four MSM corrected data points.

The measured detector response and corresponding MSM correction of the wet critical experiment with control rod “in” position are shown in Figure 61 and Figure 62, respectively. However, while the data points got closer, it was difficult to see it. The last five data points are plotted separately on Figure 63 and Figure 64. The last three data points are plotted separately on Figure 66 and Figure 67.

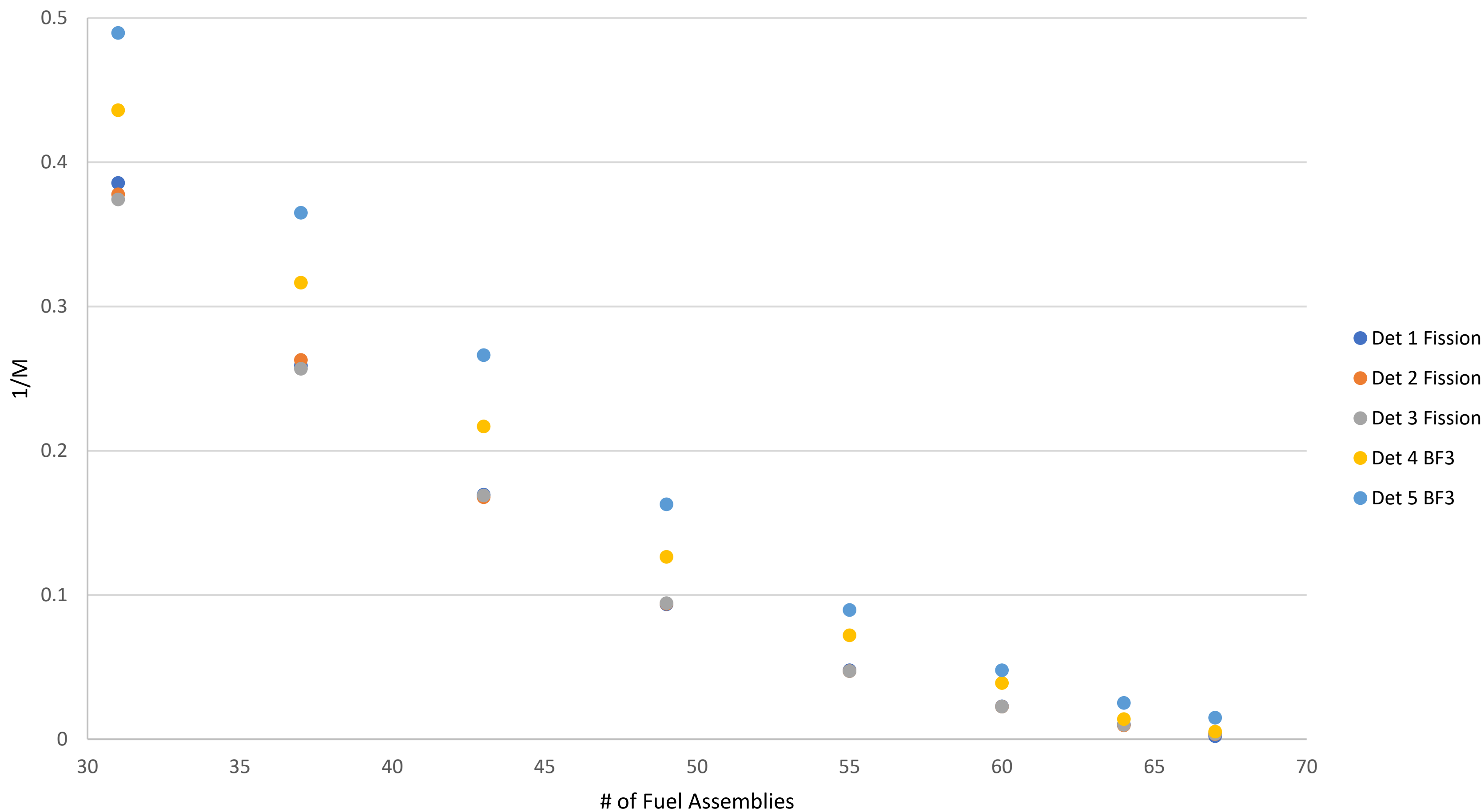

Figure 61. Wet critical experiment, CR “in” position, measured detector response.

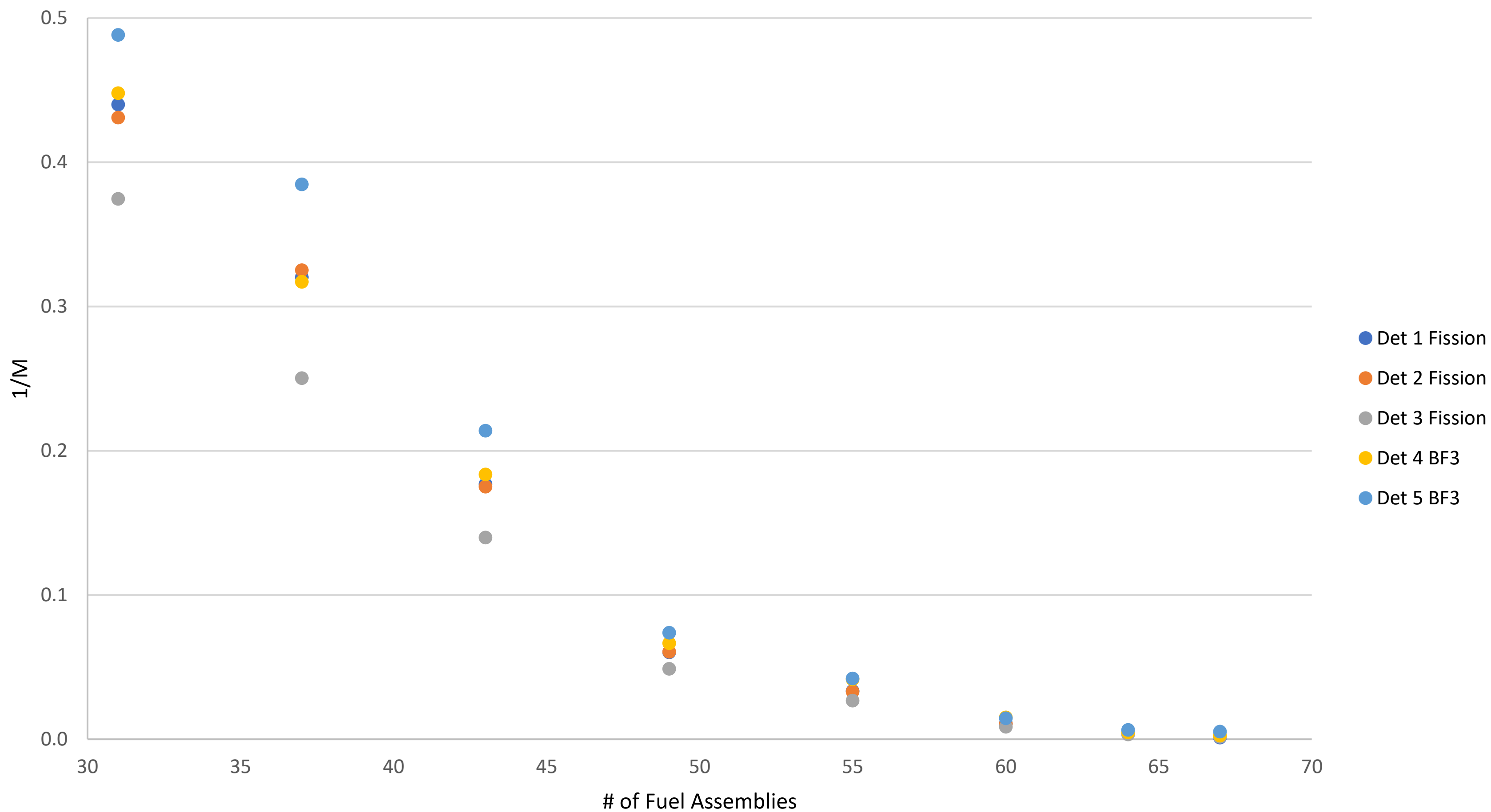

Figure 62.Wet critical experiment, CR “in” position, the detector response after MSM correction.

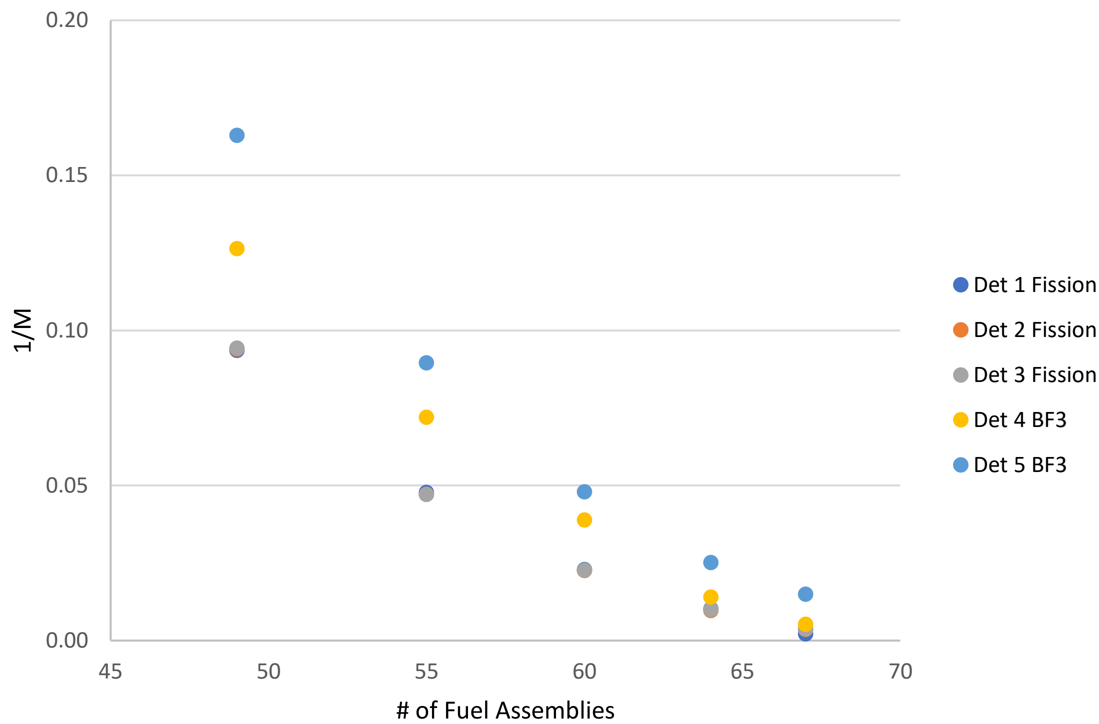

Figure 63. Wet critical experiment, CR “in”, last five measured data points.

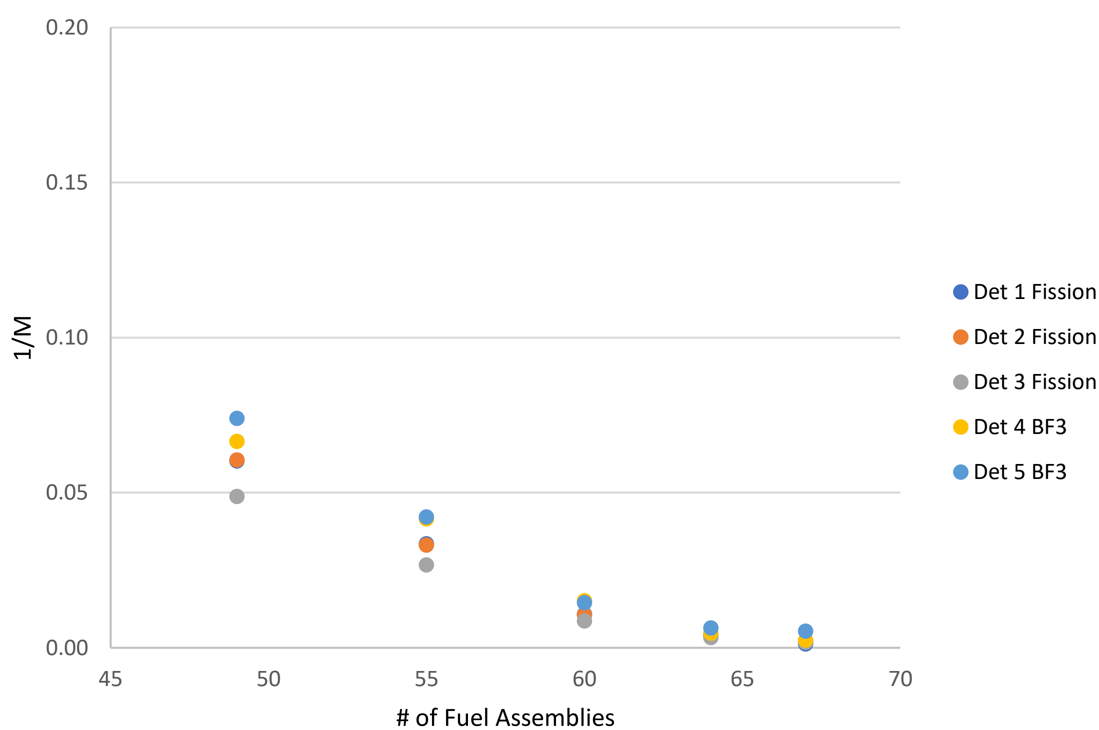

Figure 64. Wet critical experiment, CR “in”, last five MSM corrected data points.

As shown in Figure 65, the corrected 1/M plot of the last five points is amplified to show better detector 1/M locations.

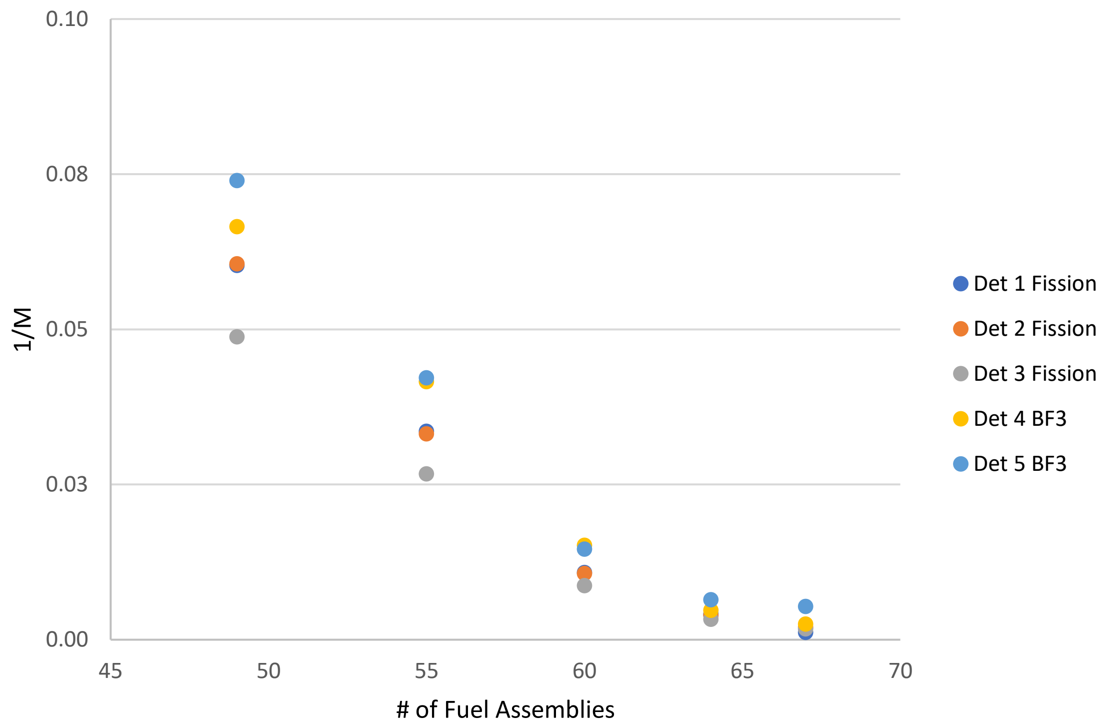

Figure 65. Wet critical experiment, CR “in”, amplified the last five MSM corrected data points.

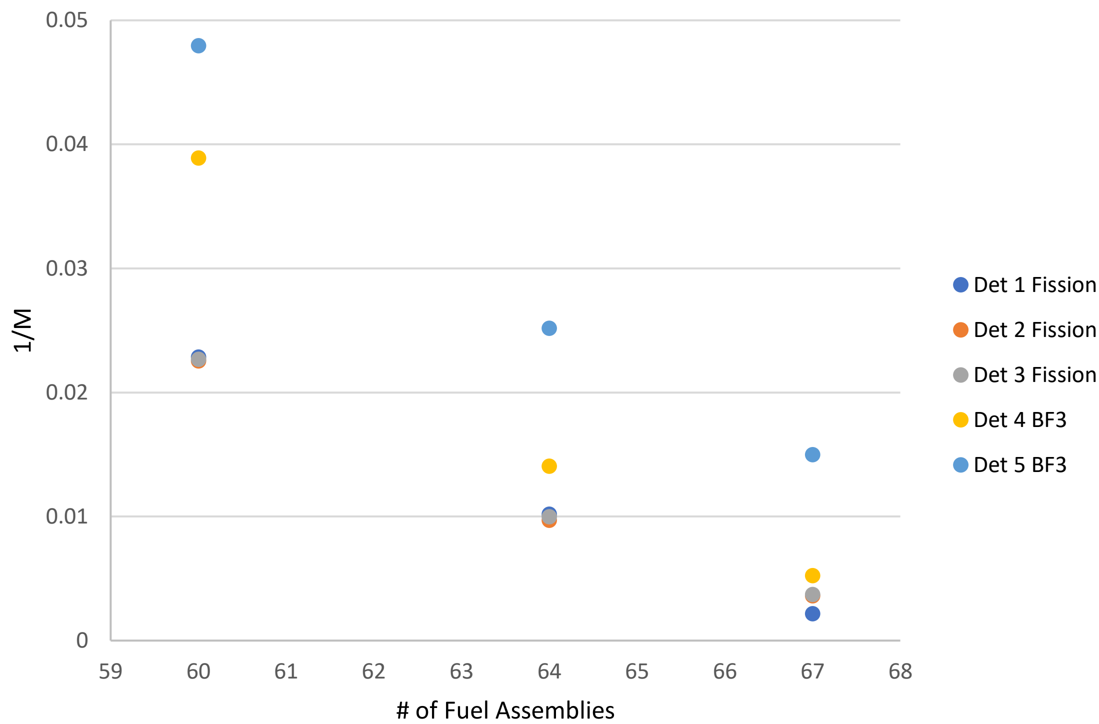

Figure 66. Wet critical experiment, CR “in”, last three measured data points.

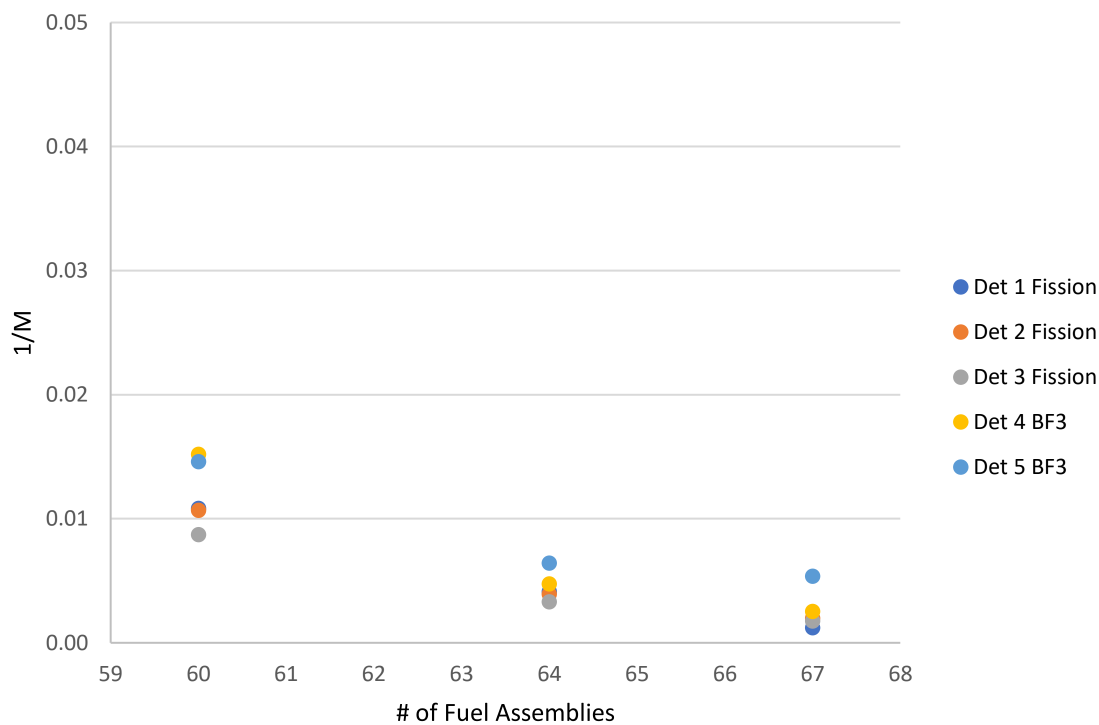

Figure 67. Wet critical experiment, CR “in”, last five MSM corrected data points.

As shown in Figure 68, the corrected 1/M plot of the last three points is amplified to show better detector 1/M locations.

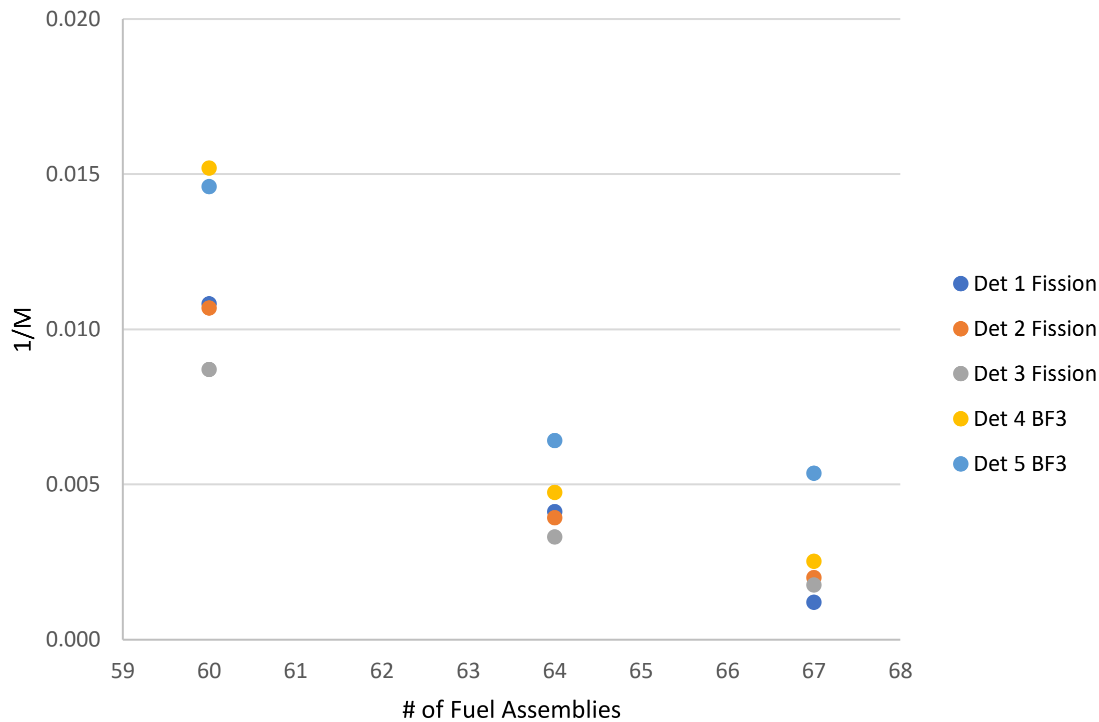

Figure 68. Wet critical experiment, CR "in", amplified the last five MSM corrected data points.

The measured detector response and corresponding MSM correction of the wet critical experiment with control rod "out" position are shown in Figure 69 and Figure 70, respectively. However, while the data points got closer, it was difficult to see it. The last six data points are plotted separately on Figure 71 and Figure 72. The last three data points are plotted separately on Figure 74 and Figure 75.

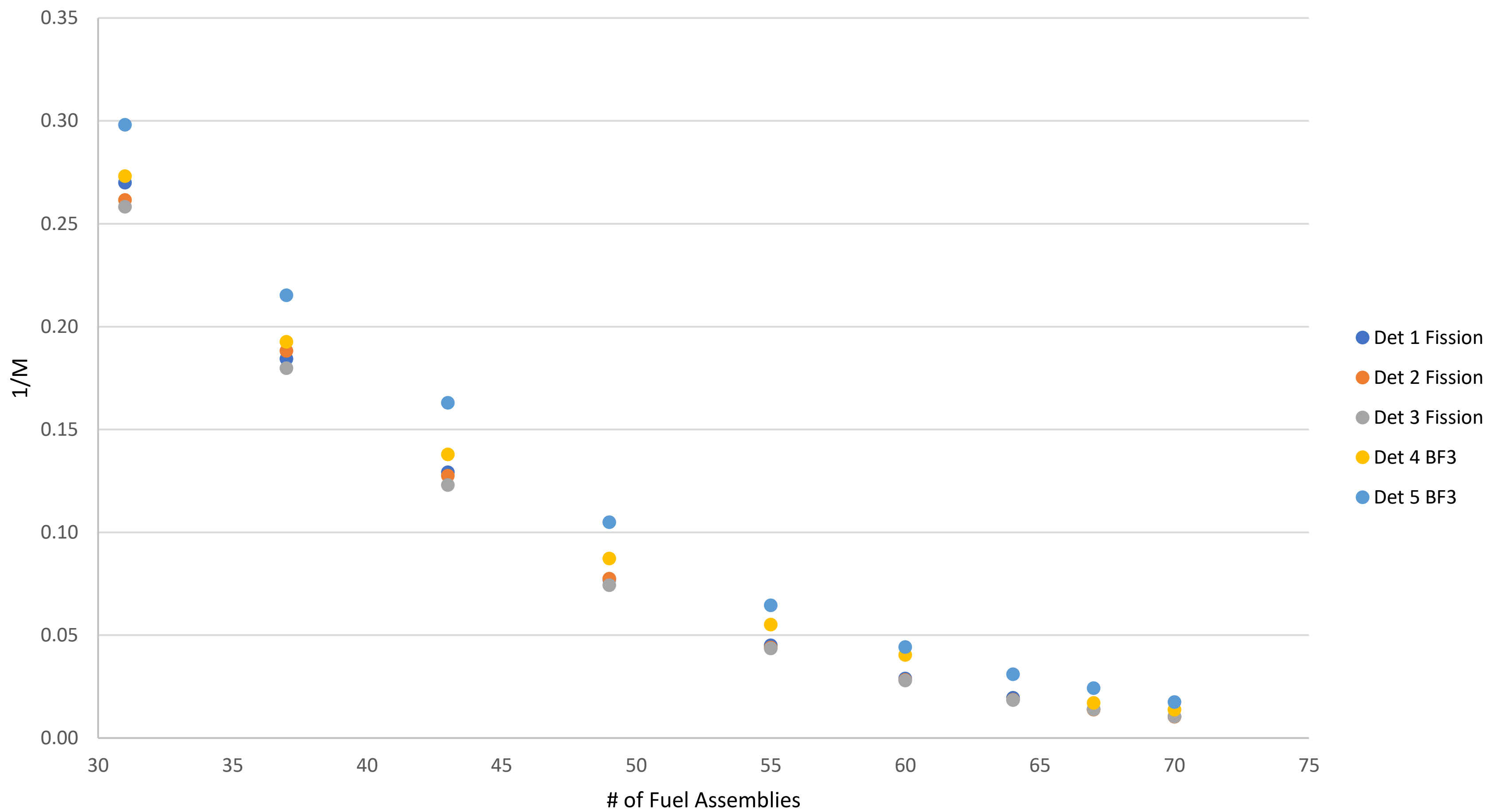

Figure 69. Wet critical experiment, CR “out” position, measured detector response.

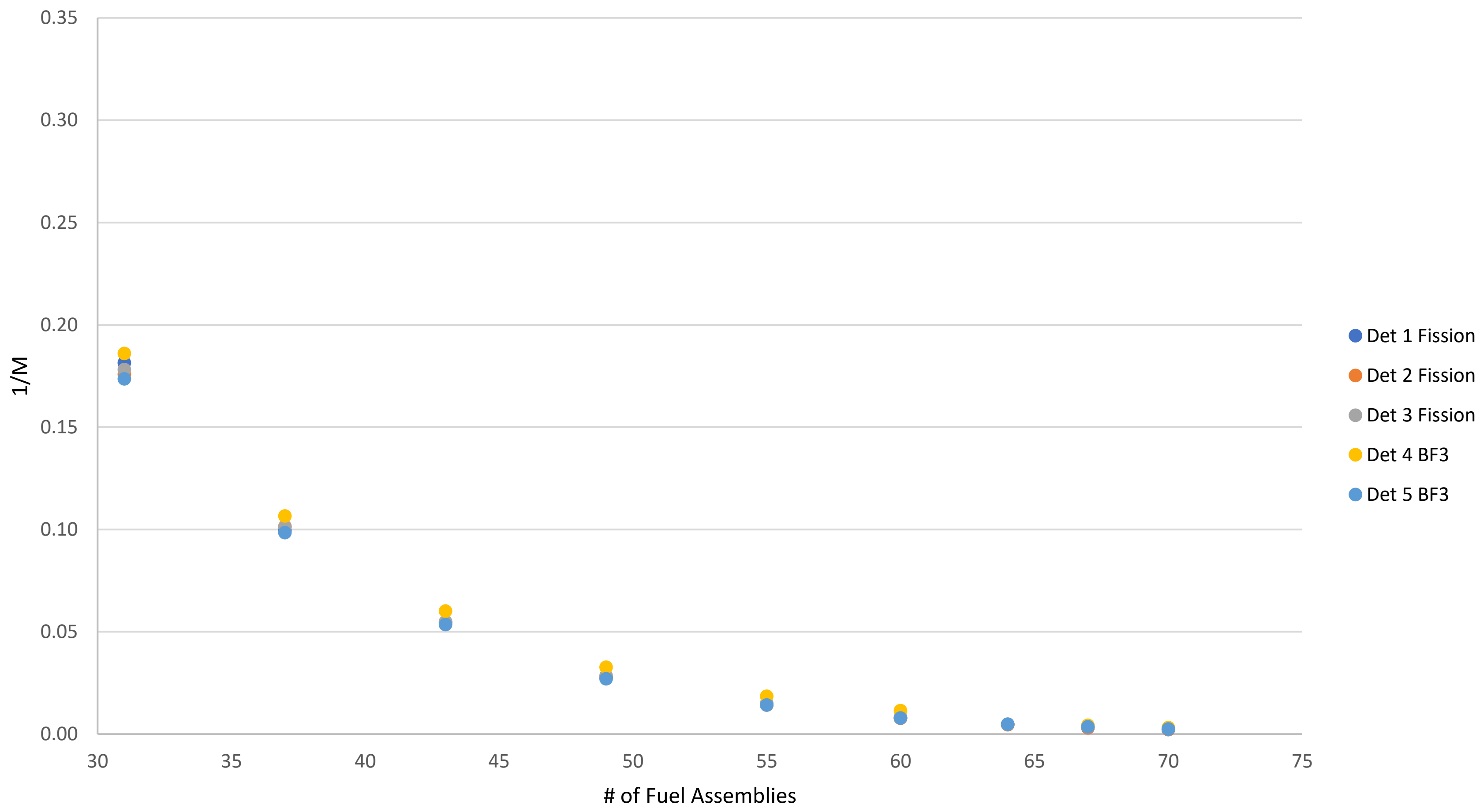

Figure 70. Wet critical experiment, CR “out” position, the detector response after MSM correction.

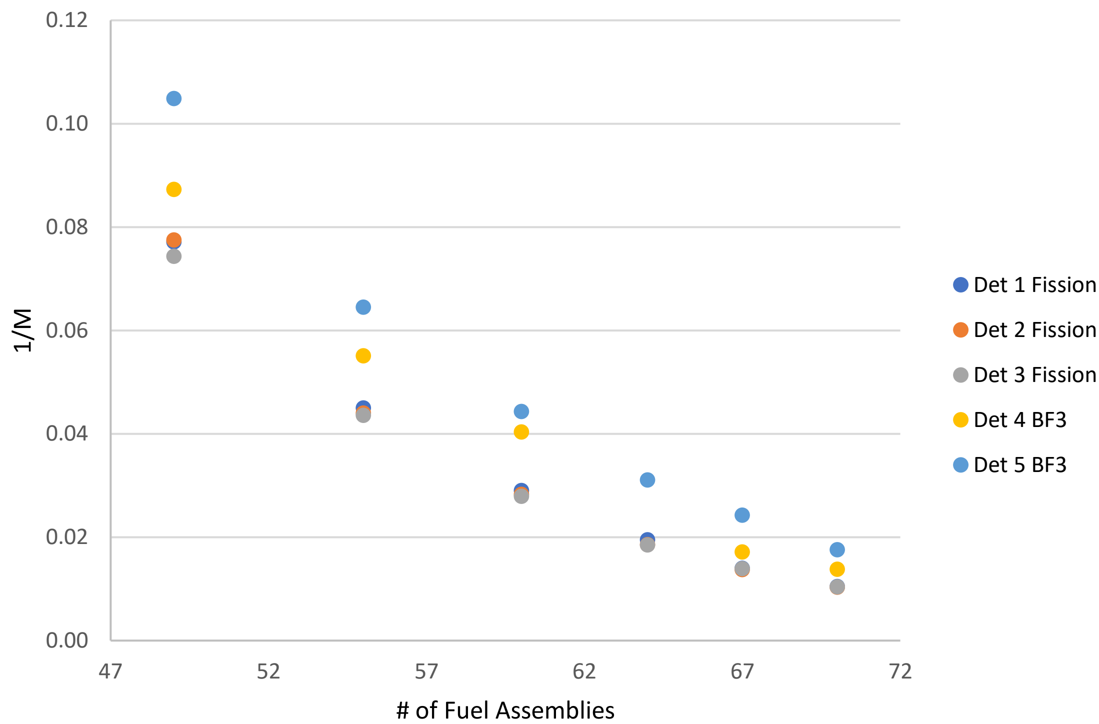

Figure 71**.** Wet critical experiment, CR “out”, last six measured data points.

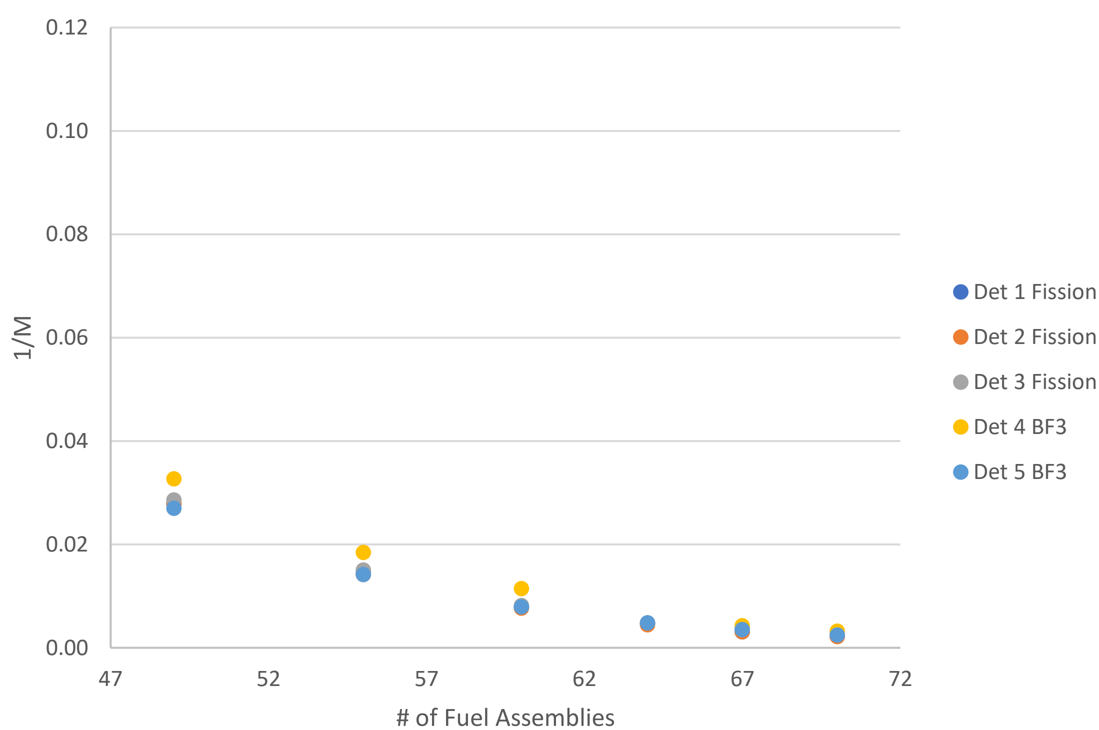

Figure 72**.** Wet critical experiment, CR “out”, last six MSM corrected data points.

As shown in Figure 73, the corrected 1/M plot of the last six points is amplified to show better detector 1/M locations.

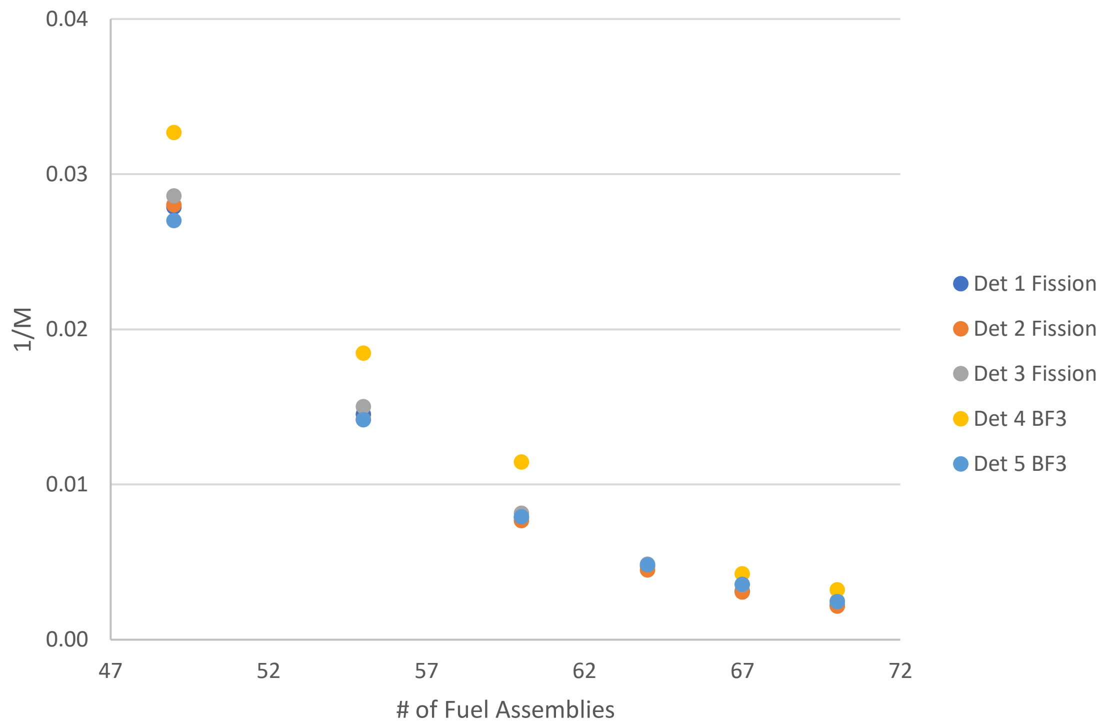

Figure 73. Wet critical experiment, CR “out”, amplified the last six MSM corrected data points.

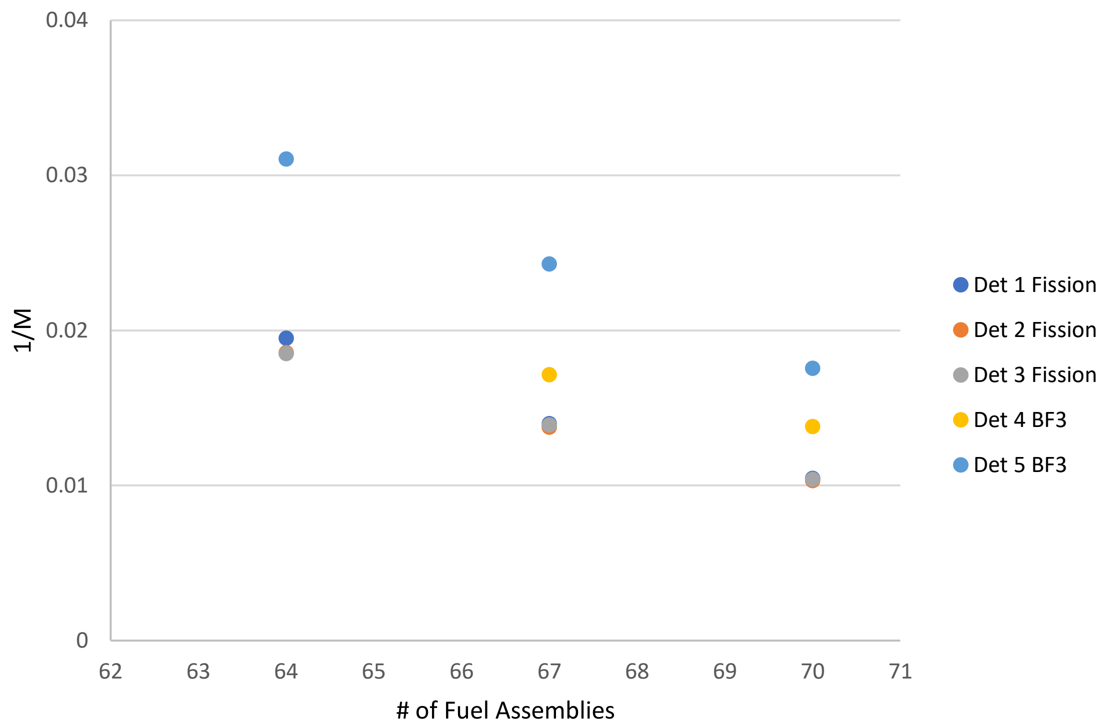

Figure 74. Wet critical experiment, CR “out”, last three measured data points.

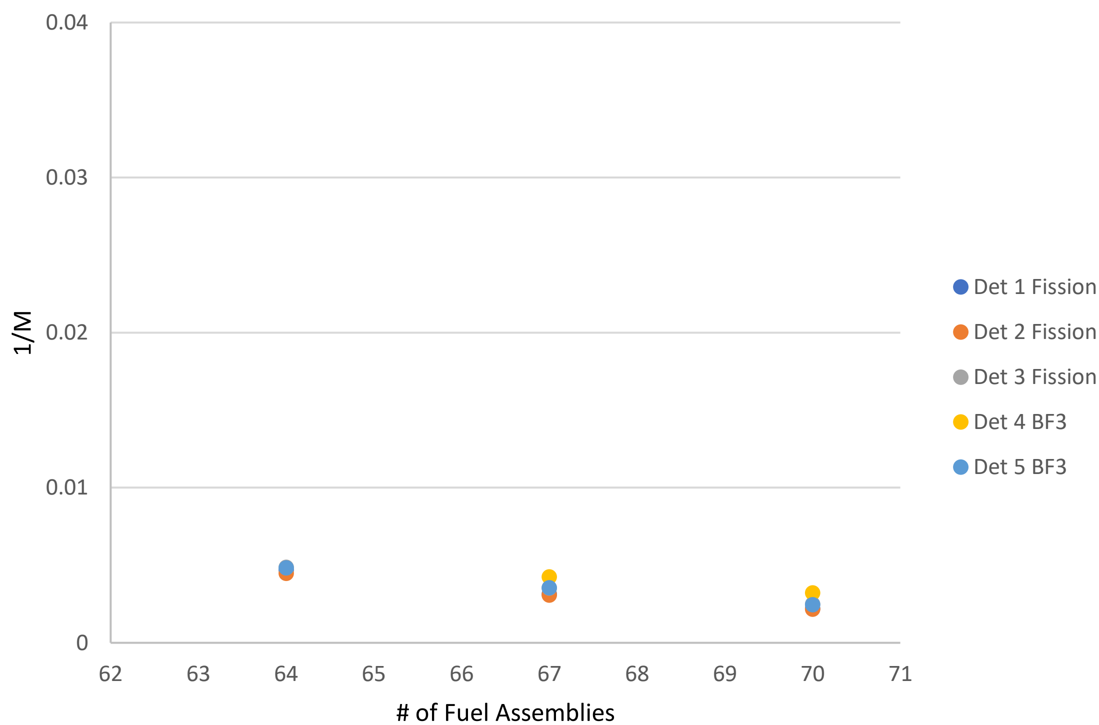

Figure 75. Wet critical experiment, CR “out”, last three MSM corrected data points.

As shown in Figure 76, the corrected 1/M plot of the last six points is amplified to show better detector 1/M locations.

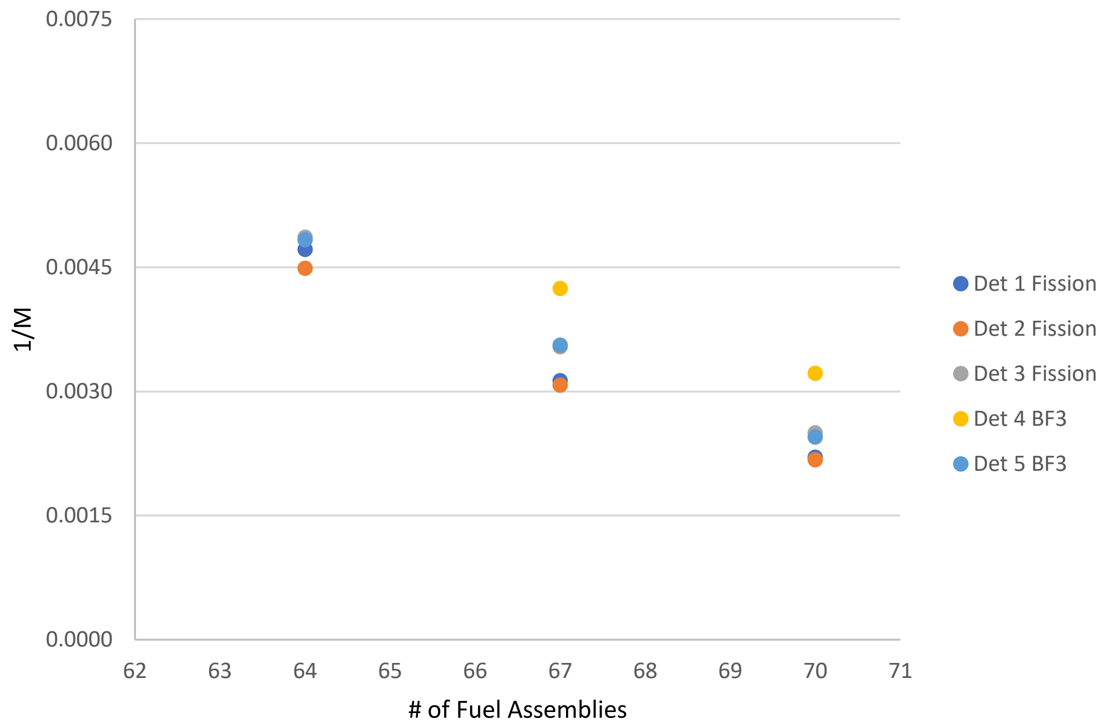

Figure 76. Wet critical experiment, CR “out”, amplified the last three MSM corrected data points.

6.3 The Improvement Factor

The improvement factor (IF) is a quantity that represents the quality of the application of MSM correction. The IF is calculated from the data point range. According to 1/M, extrapolation of any two consecutive points will give the predicted number of fuel assemblies required for a reactor to go critical. Since there is more than one detector in the system, we get more than one prediction for criticality. The range of this criticality prediction is important. For example, Figure 77 shows that two detectors each have different 1/M values predicting criticality at two different points.

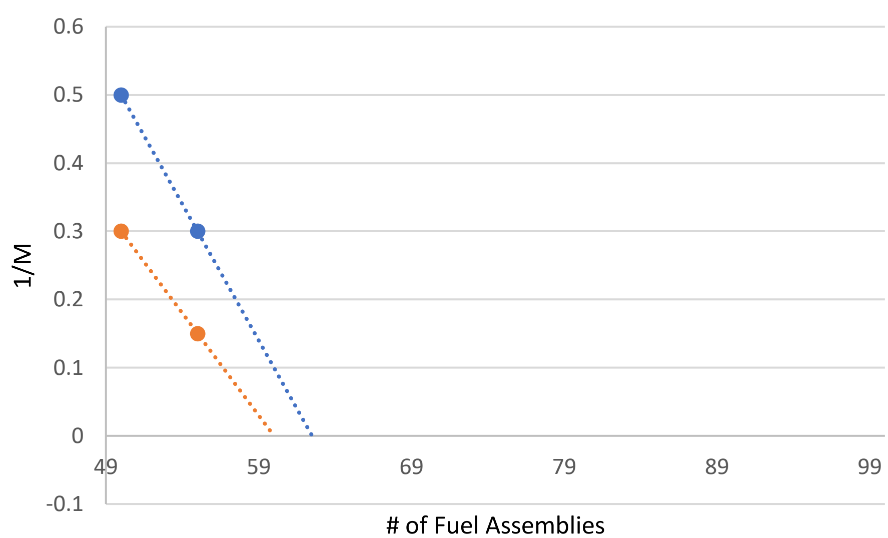

Figure 77. Two detectors response at two different stages before MSM correction.

The orange detector predicts 60 fuel assemblies to go critical and blue detector predicts 62.5 fuel assemblies to go critical. The range is 2.5. In the EBR-II case, we have more than two detectors. In which case, we take the difference between the maximum and minimum predicted values. Although, this range is important, the 1/M range also important. The IF is a ratio of MSM and ASM factors. The MSM and ASM factors are multiplication of three numbers; range in criticality prediction, range in first reactor configuration and range in second reactor configuration. he improvement factor is shown in Equation 17.

$$IF = \frac{MSM\ Factor}{ASM\ Factor} \tag{47}$$

$$ASM\ Factor = A * B * C \tag{58}$$

Where:

A – Maximum distance between first data points on ASM plot

B – Maximum distance between second data points on ASM plot

C – Maximum distance between predicted criticality on ASM plot

$$MSM\ Factor = A' * B' * C' \tag{69}$$

Where:

A' – Maximum distance between first data points on MSM plot

B' – Maximum distance between second data points on MSM plot

C' – Maximum distance between predicted criticality on MSM plot

From the example that was used for the range of the criticality prediction, the range in first and second configuration can be calculated. It is the difference between the minimum and maximum points in each configuration. Thus, the range in the first configuration is 0.2 and the range in second configuration is 0.15. Hence, the ASM factor is equal to 0.075. The optimal quantity is zero for both ASM and MSM factors.

Now assume we had MSM correction on the previous ASM example. Figure 78 shows the corrected 1/M values for each detector at each stage. The range in criticality prediction is 1.25. The range got shorter by applying MSM correction, but it does not always work in our favor. Sometimes the range gets bigger. That is why this range cannot quantify the quality of MSM correction alone.

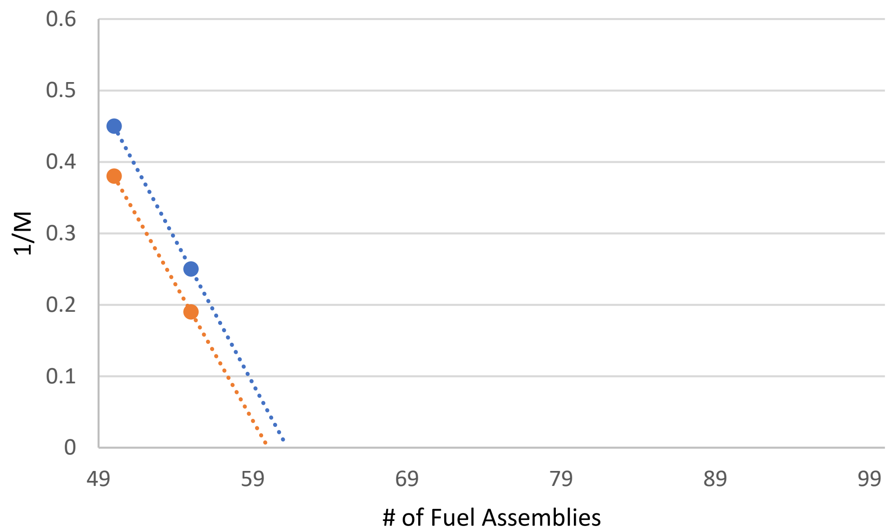

Figure 78. Two detectors response at two different stages after MSM correction.

The range in first and second configurations became 0.07 and 0.06, respectively. Hence, the MSM factor is equal to 0.00525 and the IF is 0.07. If the IF was equal to 1, there was no improvement. If the IF is less than 1, the MSM correction was applied successfully. However, the smaller the IF, better the correction. In theory, the best value for IF is 0. If the IF is greater than 1, the MSM correction to the existing ASM is failed.

The Table 18 shows the IF of the EBR-II dry and wet critical experiments. As the values indicate, overall MSM correction was applied very well. The first two points of the wet critical experiment with control rod “in” position, was not corrected well.

Table 18. The Improvement Factor

	Dry Crit. Rods “out”	Dry Crit. Rods “in”	Wet Crit. Rods “out”	Wet Crit. Rods “in”
Loading 3 and 4	0.046	0.114	0.025	1.199
Loading 4 and 5	0.030	0.050	0.006	1.155
Loading 5 and 6	0.043	0.038	0.016	0.206
Loading 6 and 7	0.018	0.022	0.026	0.049
Loading 7 and 8	0.004	0.009	0.021	0.031
Loading 8 and 9	0.021	0.021	0.002	0.012
Loading 9 and 10	0.010	0.031	0.003	0.013
Loading 10 and 11	0.007	0.005	0.007	
Loading 11 and 12	0.011			

7. Summary and Conclusion

Every nuclear reactor starts with a subcritical configuration and slowly approaches criticality. Traditionally, the ASM method was used to predict criticality. However, this method has a weakness. The more precise method, called MSM, was developed to improve ASM. This research was focused on applying MSM correction on measured ASM results of the dry and wet critical experiments of EBR-II reactor. There are four sets of measured data of EBR-II experiments: dry critical experiment with all control rods inserted and removed, wet critical experiment with all control rods inserted and removed.

The MSM corrections of dry critical experiments (both control rods inserted and removed positions) were successful. The data points of 1/M curve get closer to each other and the improvement factor is below 1.

The MSM corrections of wet critical experiments were successful except the first two data points of control rods inserted configuration. When starting the wet critical experiment, the k_{eff} was close to zero and count rate was about 100 counts per minute. The difference between dry and wet critical experiments is that the neutron detectors were located in different positions. The neutron detectors in dry critical experiments were in the reactor core specifically in inner blanket and outer blanket subassemblies. The neutron detectors in the wet critical experiment were located in the J-thimbles outside of the core. The DIF3D was not able to model the detectors outside of the core. Thus, the detector locations in the wet critical experiments were in the very outer row of the outer blanket region. They were located such that the reactor core, DIF3D detector, and actual detector in a line and the DIF3D detector was as close as possible to the actual detector.

As seen on measured 1/M plots, every detector predicts different criticality. The MSM method corrects these detector responses and predicts better criticality. To apply this technique on a reactor startup, the DIF3D simulation must be done beforehand because every simulation took between 3 to 6 hours on INL HPC. Doing simulation after taking every count rate is impractical. Hence, the simulation of approach-to-critical and calculation of MSM correction factor should be done before reactor startup. With calculated MSM correction factors in each fuel loading stage, the count rates can be corrected right after it is taken and predict better criticality.

8. References

1. Leonard, K., "Experimental Breeder Reactor-II (EBR-II): An Integrated Experimental Fast Reactor Nuclear Power Station," 1st Edition, American Nuclear Society, 2008.
2. Blaise, P., et al. "Application of the Modified Source Multiplication (MSM) Technique to Subcritical Reactivity Worth Measurements in Thermal and Fast Reactor Systems," IEEE Transactions on Nuclear Science, vol. 58, no. 3, 01 June 2011, pp. 1166-1176.
3. Imel, G., et al. "The TRADE Source Multiplication Experiments," PHYSOR 2004 The Physics of Fuel Cycle and Advanced Nuclear Systems: Global Developments Chicago, Illinois, April 25-29, 2004, American Nuclear Society, Lagrange Park, IL, 2004.
4. Kim, M., "Application of the Modified Neutron Source Multiplication Method for a Measurement of Sub-criticality in AGN-201K Reactor,"
5. Truchet, G., et al. "Application of the modified neutron source multiplication method to the prototype FBR Monju." Annals of Nuclear Energy 51, January 2013.
6. Bell, G.I. and Glasstone, S. "*Nuclear Reactor Theory*", Litton Educational Publishing, Inc. (1970)
7. "EBR-II Dry Critical Experiments Experimental Results," Argonne National Laboratory, ANL-6462, February 1962.
8. "EBR-II Dry Critical Experiments Experimental Program, Experimental Procedures and Safety Consideration," Argonne National Laboratory, ANL-6299, February 1961.

9. “EBR-II Wet Critical Experiments,” Argonne National Laboratory, ANL-6864, October 1964.
10. Michael, A.S. “DIF3D11.0-VARIANT Manual”, Argonne National Lab ANL-SF-12-048, (2012)
11. KENO VI
12. MC^2
13. John R. Lamarsh., “Introduction to Nuclear Engineering”, 3rd edition, 2001.

Appendix A

Setting up INL HPC Account and Installing DIF3D

After setting a PIN, install ssh on Linux machine by:

sudo apt-get install ssh

Search a folder named "ssh". Open "ssh_config". In the very end of the file, add the following:

Host hpclogin hpclogin.inl.gov

User YourHpcUsername

HostName hpclogin.inl.gov

LocalForward 8080 hpcweb:88

Then save and close.

Now open Terminal and login to hpc by typing:

ssh YourUserName@hpclogin.inl.gov

enter your password which is your 8-DIGIT-PIN+6 digit token.

To copy a file from your computer, use SCP.

Open a new terminal and type following to copy a file:

scp fileLocation YourUserName@hpclogin.inl.gov:

enter the password.

The file will be copied to your home directory in hpc. You can move the file by "mv" command when you log in to hpc.

To get MCNP permission, go to the Request History link on RSICC's Customer Service homepage. Click on the "Request History" link and enter your RSICC Pass number and Password. Once you verify the information is correct, an email will be sent to the email address listed in your account. Forward this email to rsicc_licenses@inl.gov. You will receive an email from INL that you have a permission to use MCNP or other RSICC codes on HPC.

To use MCNP

First you need to log in to the server, falcon1, falcon2, bechler etc.

ssh falcon1

Inside falcon1, your directories are same as hpclogin.

Do the following commands based on your MCNP version.

module load use.exp_ctl

module load MCNP6/1.0-imvmklt-1.5.0

To see available options of MCNP type:

sub_mcnp6_1.0 -h

sub_mcnp6_1.0 -i inputfilenameOrLocation -w walltime -P projectname -x locationORnameOfthecrossection -n numberofbatch -N numberofcpu -j jobname

For example:

sub_mcnp6_1.0 -i EBRII.i -w 24:0:0 -P neup -x EBRII646dir -n 240 -N 24 -j EBR2

For DIF3D, you need to compile it on HPC.

First you will need to copy the DIF3D.tar.gz file to your HPC directory.

scp locationOfyourDIF3D.tar.gz YourUserName@hpclogin.inl.gov:

log in to your hpc account then extract the DIF3D.tar.gz file.

tar -xvzf DIF3D.tar.gz

After it is extracted, go into extracted folder and rename “Makefile.arch.export” to “Makefile.arch” rm “Makefile.arch.export” “Makefile.arch”

then open the file

vi Makefile.arch

hit “i”

replace everything by:

FC = gfortran

CC = gcc

LD = gfortran

CPPDEF = -DVERSION_STANDALONE -DFORCEFIXED -DISABLE_TIMING

FFLAGS = -02 -DMEMORY_LARGE -fpic

CFLAGS =

Hit “esc” and hit “:” then type “wq” and hit enter.

Now go to the folder named “src_DIF3D”

And type “make -j4”

It will compile dif3d on your hpc.

Copy the executable of dif3d which is named by “dif3d.x” to the location you want

cp -i dif3d.x locationYouWant

In order to run dif3d, you will need cross section file, input file and dif3d.x in a same location.

After you have all 3 of them in a same location, you will need a shell script to run dif3d on hpc. Create a text file and name it MyFile.sh

This file must contain the following:

#!/bin/bash

```
#PBS -N nameofyourwork

#PBS -j oe

#PBS -P neup

#PBS -l select=1:ncpus=1:mem=100gb

cd locationOfyourworkingfolder

./dif3d.x <inputfile.inp >outputfile
```

Copy this MyFile.sh from your computer to the hpc and then copy it to the directory where your dif3d.x and input files are.

Then log in to hpc and the log in to bechler bechler server by:

```
ssh bechler
```

now go into the directory where MyFile.sh is.

Type

```
qsub -l walltime=24:0:0 MyFile.sh
```

If you know that your work will take more than 24 hours, then increase it.

After submitting a job, you will receive a job ID number. You can check the status of your work by:

```
qstat jobIDnumber
```

Appendix B

Input deck of dry critical experiment with control rods “in” position, the last fuel loading configuration.

```
PRINT=NO
BLOCK=OLD
DATASET=ISOTXS
BLOCK=STP021,3
UNFORM=A.DIF3D
01        33 GROUP 3D PROBLEM
02    20000000 100000000
03        1     2     0  4500   500     0 1000000000 0 0 0 90
04        1     0     0    00   000    00   000     1     1
05           1.0E-5      1.0E-5      1.0E-5
06                 1.0       0.001        0.04  14.30000+6
  09        16    10           1.0E-5
  12   80801  33  -1  2  5  -1   1   3  0   0    0

12 80801 33
  12   80801  77
  12   80801  77  -1  2  5  -1   1   3  0   0    0
  12   40401  11  -1  0  0  -1   1   0  0   0    0

UNFORM=A.HMG4C
01         TURN OFF HMG4C EDITS
02    999999    1     0     0     0     1
DATASET=A.NIP3
01        33 GROUP FIXED-SOURCE TRANSPORT PROBLEM
  02             0     0250000     0 50000                      0     0
02             0     0 50000       50000     0     0     0     0     0
03           120
04             2     2     2     2     2     2
09        Z     1   60.000
09        Z     1  120.000
09        Z     1  121.944
09        Z     1  137.504
09        Z     1  157.504
09        Z     1  172.070
09        Z     1  178.737
09        Z     1  196.358
09        Z     1  198.263
09        Z     1  211.918
09        Z     1  213.823
09        Z     1  224.457
09        Z     1  231.918
09        Z     1  232.553
09        Z     1  233.823
09        Z     1  234.382
09        Z     1  234.458
09        Z     1  242.332
09        Z     1  249.942
09        Z     1  257.892
09        Z     1  269.942
```

```
09         Z     1  270.577
09         Z     1  277.892
09         Z     1  278.527
09         Z     1  281.689
09         Z     1  282.337
09         Z     1  287.722
09         Z     1  297.897
09         Z     1  312.817
09         Z     1  317.897
09         Z     1  318.437
09         Z     1  323.282
09         Z     1  327.409
09         Z     1  328.377
09         Z     1  334.312
09         Z     1  338.998
09         Z     1  348.377
09         Z     1  348.893
09         Z     1  364.453
09         Z     1  384.453
09         Z     1  388.998
09         Z     1  550.000

  DRIVER ASSEMBLY
  Lower Ext
  Lower Blanket Fuel Region
14         DEPB  NA23I  0.000761778
14         DEPB  U235N  0.000044937U238N  0.014745338
14         DEPB  FE__R  0.010127125NI__R  0.001628561CR__R  0.002604296
  Above Lower Blanket Fuel Region
 14         DEPBT NA23I  0.012141076
14         DEPBT FE__R  0.030510065NI__R  0.004906379CR__R  0.007845981
  Below Lower Blanket Fuel Region
 14         DEPBB NA23I  0.007284646
14         DEPBB FE__R  0.042714091NI__R  0.006868930CR__R  0.010984373
  MID Section
  Fuel Region
14         FUEL  NA23I  0.001379298
14         FUEL  FS__H  0.001783781U235N  0.006815427U238N  0.007266792
14         FUEL  FE__R  0.012225156NI__R  0.001965949CR__R  0.003143826
  Above Fuel region
 14         FUELT NA23I  0.012204748
14         FUELT FE__R  0.030350   NI__R  0.004880648CR__R  0.007804833
  Below Fuel region
 14         FUELB NA23I  0.011013176
14         FUELB FE__R  0.033344434NI__R  0.005362179CR__R  0.008574868

  Upper Ext
  Upper Blanket Fuel Region
14         DEPT  NA23I  0.000761778
14         DEPT  U235N  0.000044937U238N  0.014745338
14         DEPT  FE__R  0.010127125NI__R  0.001628561CR__R  0.002604296
  Above Upper Blanket Fuel Region
 14         DEPTT NA23I  0.022613070
14         DEPTT FE__R  0.004194342NI__R  0.000674500CR__R  0.001078619
  Below Upper Blanket Fuel Region
 14         DEPTB NA23I  0.012141080
```

```
14        DEPTB FE__R  0.03051006 NI__R  0.00490638 CR__R  0.00784598
 ss reflector very bottom piece
14        REFL  FE__R  0.06102013 NI__R  0.00981276 CR__R  0.01569196
 14        REFL  NA23I  0.02428215
```

EMPTY DRIVER ASSEMBLY

```
   Lower Ext
  Lower Blanket Fuel Region
 14        EDEPB NA23I  0.000761778
 14        DEPB  U235N  0.000044937U238N  0.014745338
14        EDEPB FE__R  0.010127125NI__R  0.001628561CR__R  0.002604296
  Above Lower Blanket Fuel Region
 14        EDEPBTNA23I  0.012141076
14        EDEPBTFE__R  0.030510065NI__R  0.004906379CR__R  0.007845981
  Below Lower Blanket Fuel Region
 14        EDEPBBNA23I  0.007284646
14        EDEPBBFE__R  0.042714091NI__R  0.006868930CR__R  0.010984373
  MID Section
  Fuel Region
14        EFUEL NA23I  0.001379298
 14        FUEL  FS__H  0.001783781U235N  0.006815427U238N  0.007266792
14        EFUEL FE__R  0.012225156NI__R  0.001965949CR__R  0.003143826
  Above Fuel region
 14        EFUELTNA23I  0.012204748
14        EFUELTFE__R  0.030350   NI__R  0.004880648CR__R  0.007804833
  Below Fuel region
 14        EFUELBNA23I  0.011013176
14        EFUELBFE__R  0.033344434NI__R  0.005362179CR__R  0.008574868

  Upper Ext
  Upper Blanket Fuel Region
 14        EDEPT NA23I  0.012660584
 14        DEPT  U235N  0.000044937U238N  0.014745338
14        EDEPT FE__R  0.010127125NI__R  0.001628561CR__R  0.002604296
  Above Upper Blanket Fuel Region
 14        EDEPTTNA23I  0.022611307
14        EDEPTTFE__R  0.004194342NI__R  0.000674500CR__R  0.001078619
  Below Upper Blanket Fuel Region
 14        EDEPTBNA23I  0.012141080
14        EDEPTBFE__R  0.03051006 NI__R  0.00490638 CR__R  0.00784598
 ss reflector very bottom piece
 14        REFL  FE__R  0.06102013 NI__R  0.00981276 CR__R  0.01569196
 14        REFL  NA23I  0.02428215
```

NaTURAL URANIUM DRIVER ASSEMBLY

```
   Lower Ext
  Lower Blanket Fuel Region
14        NDEPB NA23I  0.012660584
14        NDEPB U235N  0.000044937U238N  0.014745338
14        NDEPB FE__R  0.010127125NI__R  0.001628561CR__R  0.002604296
  Above Lower Blanket Fuel Region
14        NDEPBTNA23I  0.012141076
14        NDEPBTFE__R  0.030510065NI__R  0.004906379CR__R  0.007845981
```

Below Lower Blanket Fuel Region
14 NDEPBBNA23I 0.007284646
14 NDEPBBFE__R 0.042714091NI__R 0.006868930CR__R 0.010984373
MID Section
Fuel Region
14 NFUEL NA23I 0.011472559
14 NFUEL FS__H 0.001899031U235N 0.000108655U238N 0.014793094
14 NFUEL FE__R 0.012225156NI__R 0.001965949CR__R 0.003143826
Above Fuel region
14 NFUELTNA23I 0.012204748
14 NFUELTFE__R 0.030350 NI__R 0.004880648CR__R 0.007804833
Below Fuel region
14 NFUELBNA23I 0.011013176
14 NFUELBFE__R 0.033344434NI__R 0.005362179CR__R 0.008574868

Upper Ext
Upper Blanket Fuel Region
14 NDEPT NA23I 0.012660584
14 NDEPT U235N 0.000044937U238N 0.014745338
14 NDEPT FE__R 0.010127125NI__R 0.001628561CR__R 0.002604296
Above Upper Blanket Fuel Region
14 NDEPTTNA23I 0.022611307
14 NDEPTTFE__R 0.004194342NI__R 0.000674500CR__R 0.001078619
Below Upper Blanket Fuel Region
14 NDEPTBNA23I 0.012141080
14 NDEPTBFE__R 0.03051006 NI__R 0.00490638 CR__R 0.00784598

Just sodium above and below ALSO AROUND BLANKET REGION
14 SODI NA23I 0.02428215

INNER BLANKET REGION MATERIALS
Fuel Region
14 IBFR NA23I 0.001708712
14 IBFR U235N 0.000059186U238N 0.029160810
14 IBFR FE__R 0.011069454NI__R 0.001780099CR__R 0.002846625
Above Fuel Region
14 IBFRT NA23I 0.007155620
14 IBFRT FE__R 0.022825034NI__R 0.003670535CR__R 0.005869695
TOP of the INNER BLANKET
14 IBT NA23I 0.007284646
14 IBT FE__R 0.042714091NI__R 0.006868930CR__R 0.010984373

EMPTY INNER BLANKET

Fuel Region
14 EIBFR NA23I 0.004878860
14 IBFR U235N 0.005918609U238N 2.916081019
14 EIBFR FE__R 0.011069454NI__R 0.001780099CR__R 0.002846625
Above Fuel Region
14 EIBFRTNA23I 0.007155620
14 EIBFRTFE__R 0.022825034NI__R 0.003670535CR__R 0.005869695
TOP of the INNER BLANKET
14 EIBT NA23R 0.007284646
14 EIBT FE__R 0.042714091NI__R 0.006868930CR__R 0.010984373

ENRICHED INNER BLANKET REGION MATERIALS

```
  Fuel Region
14         IBEFR NA23B  0.001708712
14         IBEFR U235B  0.001769759U238B  0.027471844
14         IBEFR FE__B  0.011069454NI__B  0.001780099CR__B  0.002846625

  OUTER BLANKET REGION MATERIAL
  Fuel Region
 14         OBFR  NA23I  0.001708712U235N  0.000059186U238N  0.029160810
14         OBFR  FE__R  0.011069454NI__R  0.001780099CR__R  0.002846625
   Above Fuel Region
 14         OBFRT NA23I  0.007155620
14         OBFRT FE__R  0.022825034NI__R  0.003670535CR__R  0.005869695
  TOP of the INNER BLANKET
 14         OBT   NA23I  0.007284646
14         OBT   FE__R  0.042714091NI__R  0.006868930CR__R  0.010984373

  CONTROL ROD
  Fuel Region
14         CR    NA23I  0.006707   U235N  0.004568583U238N  0.004871146
14         CR    FS__H  0.001195721
14         CR    FE__R  0.013057054NI__R  0.002099728CR__R  0.003357757
  Above Fuel region
 14         CRT   NA23I  0.014251475
14         CRT   FE__R  0.025206714NI__R  0.004053537CR__R  0.006482169
  Below Fuel region
 14         CRB   NA23I  0.013452728
14         CRB   FE__R  0.027213933NI__R  0.004376322CR__R  0.006998346
  Void section above fuel
 14         VOID  NA23I  0.021228481
14         VOID  FE__R  0.007673761NI__R  0.001234031CR__R  0.001973387
  Poison instead of VOID
14         B4C   FE__X  1.35683E-02NA23X  1.20403E-02CR__X  3.98487E-03
14         B4C   NI__X  1.93593E-03B10_X  7.81500E-03C___X  9.76875E-03
14         B4C   B11_X  3.12609E-02
 Reflector above Void
 14         CRRF  NA23I  0.021228481
14         CRRF  FE__R  0.007673761NI__R  0.001234031CR__R  0.001973387

  Very top piece
 14         CRTP  NA23I  0.021853937
14         CRTP  FE__R  0.006102013NI__R  0.000981276CR__R  0.001569196

  Very bottom piece
 14         CRBP  NA23I  0.004856430
14         CRBP  FE__R  0.048816104NI__R  0.007850206CR__R  0.012553569

  Reflector on top and bottom
14         OREF  FE__R  0.488161040NI__R  0.078502060CR__R  0.125535690

 SOURCE ROD
 14         SOUR  NA23I  0.001709000
14         SOUR  FE__R  0.011069454NI__R  0.001780099CR__R  0.002846625

 DRIVER ASSEMBLY NAMING

15    DEPBB FR1BB
```

15 DEPB FR1B
15 DEPBT FR1BT
15 FUELB FR1FB
15 FUEL FR1F
15 FUELT FR1FT
15 DEPTB FR1TB
15 DEPT FR1T
15 DEPTT FR1TT

15 DEPBB R2BB
15 DEPB R2B
15 DEPBT R2BT
15 FUELB R2FB
15 FUEL R2F
15 FUELT R2FT
15 DEPTB R2TB
15 DEPT R2T
15 DEPTT R2TT

15 DEPBB R3BB
15 DEPB R3B
15 DEPBT R3BT
15 FUELB R3FB
15 FUEL R3F
15 FUELT R3FT
15 DEPTB R3TB
15 DEPT R3T
15 DEPTT R3TT

15 EDEPBBR4BB
15 EDEPB R4B
15 EDEPBTR4BT
15 EFUELBR4FB
15 EFUEL R4F
15 EFUELTR4FT
15 EDEPTBR4TB
15 EDEPT R4T
15 EDEPTTR4TT

15 DEPBB FR4BB
15 DEPB FR4B
15 DEPBT FR4BT
15 FUELB FR4FB
15 FUEL FR4F
15 FUELT FR4FT
15 DEPTB FR4TB
15 DEPT FR4T
15 DEPTT FR4TT

15 NDEPBBNR4BB
15 NDEPB NR4B
15 NDEPBTNR4BT
15 NFUELBNR4FB
15 NFUEL NR4F
15 NFUELTNR4FT
15 NDEPTBNR4TB

15 NDEPT NR4T
15 NDEPTTNR4TT

15 NDEPBBR5BB
15 NDEPB R5B
15 NDEPBTR5BT
15 NFUELBR5FB
15 NFUEL R5F
15 NFUELTR5FT
15 NDEPTBR5TB
15 NDEPT R5T
15 NDEPTTR5TT

15 DEPBB R5BB
15 DEPB R5B
15 DEPBT R5BT
15 FUELB R5FB
15 FUEL R5F
15 FUELT R5FT
15 DEPTB R5TB
15 DEPT R5T
15 DEPTT R5TT

15 REFL BOT
15 SODI BOTS
15 SODI TOPS

INNER BLANKET ASSEMBLY NAMING

15 DEPBB R6BB
15 IBFR R6F
15 IBFRT R6FT
15 IBT R6T

15 DEPBB FR6BB
15 IBEFR FR6F
15 IBFRT FR6FT
15 IBT FR6T

15 DEPBB R7BB
15 IBEFR R7F
15 IBFRT R7FT
15 IBT R7T
15 EIBFR R6DET
15 EIBFR R7DET

SODIUM AROUND BLANKET REGION
15 SODI EMPT

OUTER BLANKET ASSEMBLY NAMING
15 DEPBB R8BB
15 OBFR R8F
15 OBFRT R8FT
15 OBT R8T

15 DEPBB R9BB

15 OBFR R9F
15 OBFRT R9FT
15 OBT R9T

15 DEPBB R10BB
15 OBFR R10F
15 OBFRT R10FT
15 OBT R10T

15 DEPBB R11BB
15 OBFR R11F
15 OBFRT R11FT
15 OBT R11T

15 DEPBB R12BB
15 OBFR R12F
15 OBFRT R12FT
15 OBT R12T

15 DEPBB R13BB
15 OBFR R13F
15 OBFRT R13FT
15 OBT R13T

15 DEPBB R14BB
15 OBFR R14F
15 OBFRT R14FT
15 OBT R14T

15 DEPBB R15BB
15 OBFR R15F
15 OBFRT R15FT
15 OBT R15T

15 DEPBB R16BB
15 OBFR R16F
15 OBFRT R16FT
15 OBT R16T

15 OBFR R11DET
15 OBFR R13DET

CONTROL ASSEMBLY NAMING
15 CRBP CRBPA
15 CRB CRBA
15 CR CRA
15 CRT CRTA
15 VOID VOIDA
15 CRRF CRRFA
15 CRTP CRTPA

15 CRBP CRBPB
15 CRB CRBB
15 CR CRB
15 CRT CRTB

15 VOID VOIDB
15 CRRF CRRFB
15 CRTP CRTPB

15 CRBP CRBPC
15 CRB CRBC
15 CR CRC
15 CRT CRTC
15 VOID VOIDC
15 CRRF CRRFC
15 CRTP CRTPC

15 CRBP CRBPD
15 CRB CRBD
15 CR CRD
15 CRT CRTD
15 VOID VOIDD
15 CRRF CRRFD
15 CRTP CRTPD

15 CRBP CRBPE
15 CRB CRBE
15 CR CRE
15 CRT CRTE
15 VOID VOIDE
15 CRRF CRRFE
15 CRTP CRTPE

15 CRBP CRBPF
15 CRB CRBF
15 CR CRF
15 CRT CRTF
15 VOID VOIDF
15 CRRF CRRFF
15 CRTP CRTPF

15 CRBP CRBPG
15 CRB CRBG
15 CR CRG
15 CRT CRTG
15 B4C POISN
15 CRRF CRRFG
15 CRTP CRTPG

15 CRBP CRBPH
15 CRB CRBH
15 CR CRH
15 CRT CRTH
15 VOID VOIDH
15 CRRF CRRFH
15 CRTP CRTPH

15 CRBP CRBPI
15 CRB CRBI
15 CR CRI
15 CRT CRTI

```
15    VOID  VOIDI
15    CRRF  CRRFI
15    CRTP  CRTPI

15    CRBP  CRBPJ
15    CRB   CRBJ
15    CR    CRJ
15    CRT   CRTJ
15    VOID  VOIDJ
15    CRRF  CRRFJ
15    CRTP  CRTPJ

15    CRBP  CRBPK
15    CRB   CRBK
15    CR    CRK
15    CRT   CRTK
15    VOID  VOIDK
15    CRRF  CRRFK
15    CRTP  CRTPK

15    CRBP  CRBPL
15    CRB   CRBL
15    CR    CRL
15    CRT   CRTL
15    VOID  VOIDL
15    CRRF  CRRFL
15    CRTP  CRTPL

15    OREF  OREF
15    OREF  OREF8
15    OREF  OREF9
15    OREF  OREF10
15    OREF  OREF11
15    OREF  OREF12
15    OREF  OREF13
15    OREF  OREF14
15    OREF  OREF15
15    OREF  OREF16
15    OREF  OREF17
15    OREF  OREF18
15    OREF  OREF19
15    OREF  OREF20
15    OREF  OREF21
15    OREF  OREF22
15    OREF  OREF23
15    OREF  OREF24
15    OREF  OREF25

15    SOUR  SOURC1
15    SOUR  SOURB
15    SOUR  SOURT

19    SOURC1     1    662.517546E+07
  19    SOURC1     1    33         1.0
29            5.80898     25     3
```

DRIVER REGION

30	OREF	01			0.0	60.000
30	BOTS	01			60.000	120.000
30	BOT	01			120.000	172.070
30	FR1BB	01			172.070	178.737
30	FR1B	01			178.737	224.457
30	FR1BT	01			224.457	232.553
30	FR1FB	01			232.553	234.458
30	FR1F	01			234.458	270.577
30	FR1FT	01			270.577	278.527
30	FR1TB	01			278.527	281.689
30	FR1T	01			281.689	327.409
30	FR1TT	01			327.409	338.998
30	TOPS	01			338.998	388.998
30	OREF	01			388.998	550.000
30	OREF	02			0.0	60.000
30	BOTS	02			60.000	120.000
30	BOT	02			120.000	172.070
30	R2BB	02			172.070	178.737
30	R2B	02			178.737	224.457
30	R2BT	02			224.457	232.553
30	R2FB	02			232.553	234.458
30	R2F	02			234.458	270.577
30	R2FT	02			270.577	278.527
30	R2TB	02			278.527	281.689
30	R2T	02			281.689	327.409
30	R2TT	02			327.409	338.998
30	TOPS	02			338.998	388.998
30	OREF	02			388.998	550.000
30	OREF	03			0.0	60.000
30	BOTS	03			60.000	120.000
30	BOT	03			120.000	172.070
30	R3BB	03			172.070	178.737
30	R3B	03			178.737	224.457
30	R3BT	03			224.457	232.553
30	R3FB	03			232.553	234.458
30	R3F	03			234.458	270.577
30	R3FT	03			270.577	278.527
30	R3TB	03			278.527	281.689
30	R3T	03			281.689	327.409
30	R3TT	03			327.409	338.998
30	TOPS	03			338.998	388.998
30	OREF	03			388.998	550.000

Safety

30	OREF	03	1	1	0.0	60.000
30	BOTS	03	1	1	60.000	157.504
30	CRBPA	03	1	1	157.504	231.918
30	CRBA	03	1	1	231.918	233.823
30	CRA	03	1	1	233.823	269.942
30	CRTA	03	1	1	269.942	277.892
30	VOIDA	03	1	1	277.892	317.897
30	CRRFA	03	1	1	317.897	348.377

30	CRTPA	03	1	1	348.377	384.453
30	TOPS	03	1	1	384.453	388.998
30	OREF	03	1	1	388.998	550.000
30	OREF	03	2	6	0.0	60.000
30	BOTS	03	2	6	60.000	120.000
30	BOT	03	2	6	120.000	172.070
30	R3BB	03	2	6	172.070	178.737
30	R3B	03	2	6	178.737	224.457
30	R3BT	03	2	6	224.457	232.553
30	R3FB	03	2	6	232.553	234.458
30	R3F	03	2	6	234.458	270.577
30	R3FT	03	2	6	270.577	278.527
30	R3TB	03	2	6	278.527	281.689
30	R3T	03	2	6	281.689	327.409
30	R3TT	03	2	6	327.409	338.998
30	TOPS	03	2	6	338.998	388.998
30	OREF	03	2	6	388.998	550.000
30	OREF	03	7	7	0.0	60.000
30	BOTS	03	7	7	60.000	157.504
30	CRBPA	03	7	7	157.504	231.918
30	CRBA	03	7	7	231.918	233.823
30	CRA	03	7	7	233.823	269.942
30	CRTA	03	7	7	269.942	277.892
30	VOIDA	03	7	7	277.892	317.897
30	CRRFA	03	7	7	317.897	348.377
30	CRTPA	03	7	7	348.377	384.453
30	TOPS	03	7	7	384.453	388.998
30	OREF	03	7	7	388.998	550.000
30	OREF	03	8	12	0.0	60.000
30	BOTS	03	8	12	60.000	120.000
30	BOT	03	8	12	120.000	172.070
30	R3BB	03	8	12	172.070	178.737
30	R3B	03	8	12	178.737	224.457
30	R3BT	03	8	12	224.457	232.553
30	R3FB	03	8	12	232.553	234.458
30	R3F	03	8	12	234.458	270.577
30	R3FT	03	8	12	270.577	278.527
30	R3TB	03	8	12	278.527	281.689
30	R3T	03	8	12	281.689	327.409
30	R3TT	03	8	12	327.409	338.998
30	TOPS	03	8	12	338.998	388.998
30	OREF	03	8	12	388.998	550.000
30	OREF	04			0.0	60.000
30	BOTS	04			60.000	120.000
30	BOT	04			120.000	172.070
30	FR4BB	04			172.070	178.737
30	FR4B	04			178.737	224.457
30	FR4BT	04			224.457	232.553
30	FR4FB	04			232.553	234.458
30	FR4F	04			234.458	270.577
30	FR4FT	04			270.577	278.527
30	FR4TB	04			278.527	281.689

30	FR4T	04			281.689	327.409
30	FR4TT	04			327.409	338.998
30	TOPS	04			338.998	388.998
30	OREF	04			388.998	550.000
30	OREF	05			0.0	60.000
30	BOTS	05	1	1	60.000	157.504
30	CRBPA	05	1	1	157.504	231.918
30	CRBA	05	1	1	231.918	233.823
30	CRA	05	1	1	233.823	269.942
30	CRTA	05	1	1	269.942	277.892
30	VOIDA	05	1	1	277.892	317.897
30	CRRFA	05	1	1	317.897	348.377
30	CRTPA	05	1	1	348.377	384.453
30	TOPS	05	1	1	384.453	388.998
30	OREF	05			388.998	550.000
30	BOTS	05	2	2	60.000	120.000
30	BOT	05	2	2	120.000	172.070
30	R5BB	05	2	2	172.070	178.737
30	R5B	05	2	2	178.737	224.457
30	R5BT	05	2	2	224.457	232.553
30	R5FB	05	2	2	232.553	234.458
30	R5F	05	2	2	234.458	270.577
30	R5FT	05	2	2	270.577	278.527
30	R5TB	05	2	2	278.527	281.689
30	R5T	05	2	2	281.689	327.409
30	R5TT	05	2	2	327.409	338.998
30	TOPS	05	2	2	338.998	388.998
30	BOTS	05	3	3	60.000	157.504
30	CRBPB	05	3	3	157.504	231.918
30	CRBB	05	3	3	231.918	233.823
30	CRB	05	3	3	233.823	269.942
30	CRTB	05	3	3	269.942	277.892
30	VOIDB	05	3	3	277.892	317.897
30	CRRFB	05	3	3	317.897	348.377
30	CRTPB	05	3	3	348.377	384.453
30	TOPS	05	3	3	384.453	388.998
30	BOTS	05	4	4	60.000	120.000
30	BOT	05	4	4	120.000	172.070
30	R5BB	05	4	4	172.070	178.737
30	R5B	05	4	4	178.737	224.457
30	R5BT	05	4	4	224.457	232.553
30	R5FB	05	4	4	232.553	234.458
30	R5F	05	4	4	234.458	270.577
30	R5FT	05	4	4	270.577	278.527
30	R5TB	05	4	4	278.527	281.689
30	R5T	05	4	4	281.689	327.409
30	R5TT	05	4	4	327.409	338.998
30	TOPS	05	4	4	338.998	388.998

Control rod 3 - 12 fully up

30	BOTS	05	5	5	60.000	157.504

30	CRBPC	05	5	5	157.504	231.918
30	CRBC	05	5	5	231.918	233.823
30	CRC	05	5	5	233.823	269.942
30	CRTC	05	5	5	269.942	277.892
30	VOIDC	05	5	5	277.892	317.897
30	CRRFC	05	5	5	317.897	348.377
30	CRTPC	05	5	5	348.377	384.453
30	TOPS	05	5	5	384.453	388.998
30	BOTS	05	6	6	60.000	120.000
30	BOT	05	6	6	120.000	172.070
30	R5BB	05	6	6	172.070	178.737
30	R5B	05	6	6	178.737	224.457
30	R5BT	05	6	6	224.457	232.553
30	R5FB	05	6	6	232.553	234.458
30	R5F	05	6	6	234.458	270.577
30	R5FT	05	6	6	270.577	278.527
30	R5TB	05	6	6	278.527	281.689
30	R5T	05	6	6	281.689	327.409
30	R5TT	05	6	6	327.409	338.998
30	TOPS	05	6	6	338.998	388.998
30	BOTS	05	7	7	60.000	157.504
30	CRBPD	05	7	7	157.504	231.918
30	CRBD	05	7	7	231.918	233.823
30	CRD	05	7	7	233.823	269.942
30	CRTD	05	7	7	269.942	277.892
30	VOIDD	05	7	7	277.892	317.897
30	CRRFD	05	7	7	317.897	348.377
30	CRTPD	05	7	7	348.377	384.453
30	TOPS	05	7	7	384.453	388.998
30	BOTS	05	8	8	60.000	120.000
30	BOT	05	8	8	120.000	172.070
30	R5BB	05	8	8	172.070	178.737
30	R5B	05	8	8	178.737	224.457
30	R5BT	05	8	8	224.457	232.553
30	R5FB	05	8	8	232.553	234.458
30	R5F	05	8	8	234.458	270.577
30	R5FT	05	8	8	270.577	278.527
30	R5TB	05	8	8	278.527	281.689
30	R5T	05	8	8	281.689	327.409
30	R5TT	05	8	8	327.409	338.998
30	TOPS	05	8	8	338.998	388.998
30	BOTS	05	9	9	60.000	157.504
30	CRBPE	05	9	9	157.504	231.918
30	CRBE	05	9	9	231.918	233.823
30	CRE	05	9	9	233.823	269.942
30	CRTE	05	9	9	269.942	277.892
30	VOIDE	05	9	9	277.892	317.897
30	CRRFE	05	9	9	317.897	348.377
30	CRTPE	05	9	9	348.377	384.453
30	TOPS	05	9	9	384.453	388.998
30	BOTS	05	10	10	60.000	120.000

30	BOT	05	10	10	120.000	172.070
30	R5BB	05	10	10	172.070	178.737
30	R5B	05	10	10	178.737	224.457
30	R5BT	05	10	10	224.457	232.553
30	R5FB	05	10	10	232.553	234.458
30	R5F	05	10	10	234.458	270.577
30	R5FT	05	10	10	270.577	278.527
30	R5TB	05	10	10	278.527	281.689
30	R5T	05	10	10	281.689	327.409
30	R5TT	05	10	10	327.409	338.998
30	TOPS	05	10	10	338.998	388.998
30	BOTS	05	11	11	60.000	157.504
30	CRBPF	05	11	11	157.504	231.918
30	CRBF	05	11	11	231.918	233.823
30	CRF	05	11	11	233.823	269.942
30	CRTF	05	11	11	269.942	277.892
30	VOIDF	05	11	11	277.892	317.897
30	CRRFF	05	11	11	317.897	348.377
30	CRTPF	05	11	11	348.377	384.453
30	TOPS	05	11	11	384.453	388.998
30	BOTS	05	12	12	60.000	120.000
30	BOT	05	12	12	120.000	172.070
30	R5BB	05	12	12	172.070	178.737
30	R5B	05	12	12	178.737	224.457
30	R5BT	05	12	12	224.457	232.553
30	R5FB	05	12	12	232.553	234.458
30	R5F	05	12	12	234.458	270.577
30	R5FT	05	12	12	270.577	278.527
30	R5TB	05	12	12	278.527	281.689
30	R5T	05	12	12	281.689	327.409
30	R5TT	05	12	12	327.409	338.998
30	TOPS	05	12	12	338.998	388.998
30	BOTS	05	13	13	60.000	157.504
30	CRBPG	05	13	13	157.504	231.918
30	CRBG	05	13	13	231.918	233.823
30	CRG	05	13	13	233.823	269.942
30	CRTG	05	13	13	269.942	287.722
30	POISN	05	13	13	287.722	323.282
30	CRRFG	05	13	13	323.282	348.377
30	CRTPG	05	13	13	348.377	384.453
30	TOPS	05	13	13	384.453	388.998
30	BOTS	05	14	14	60.000	120.000
30	BOT	05	14	14	120.000	172.070
30	R5BB	05	14	14	172.070	178.737
30	R5B	05	14	14	178.737	224.457
30	R5BT	05	14	14	224.457	232.553
30	R5FB	05	14	14	232.553	234.458
30	R5F	05	14	14	234.458	270.577
30	R5FT	05	14	14	270.577	278.527
30	R5TB	05	14	14	278.527	281.689
30	R5T	05	14	14	281.689	327.409
30	R5TT	05	14	14	327.409	338.998

30	TOPS	05	14	14	338.998	388.998
30	BOTS	05	15	15	60.000	157.504
30	CRBPH	05	15	15	157.504	231.918
30	CRBH	05	15	15	231.918	233.823
30	CRH	05	15	15	233.823	269.942
30	CRTH	05	15	15	269.942	277.892
30	VOIDH	05	15	15	277.892	317.897
30	CRRFH	05	15	15	317.897	348.377
30	CRTPH	05	15	15	348.377	384.453
30	TOPS	05	15	15	384.453	388.998
30	BOTS	05	16	16	60.000	120.000
30	BOT	05	16	16	120.000	172.070
30	R5BB	05	16	16	172.070	178.737
30	R5B	05	16	16	178.737	224.457
30	R5BT	05	16	16	224.457	232.553
30	R5FB	05	16	16	232.553	234.458
30	R5F	05	16	16	234.458	270.577
30	R5FT	05	16	16	270.577	278.527
30	R5TB	05	16	16	278.527	281.689
30	R5T	05	16	16	281.689	327.409
30	R5TT	05	16	16	327.409	338.998
30	TOPS	05	16	16	338.998	388.998
30	BOTS	05	17	17	60.000	157.504
30	CRBPI	05	17	17	157.504	231.918
30	CRBI	05	17	17	231.918	233.823
30	CRI	05	17	17	233.823	269.942
30	CRTI	05	17	17	269.942	277.892
30	VOIDI	05	17	17	277.892	317.897
30	CRRFI	05	17	17	317.897	348.377
30	CRTPI	05	17	17	348.377	384.453
30	TOPS	05	17	17	384.453	388.998
30	BOTS	05	18	18	60.000	120.000
30	BOT	05	18	18	120.000	172.070
30	R5BB	05	18	18	172.070	178.737
30	R5B	05	18	18	178.737	224.457
30	R5BT	05	18	18	224.457	232.553
30	R5FB	05	18	18	232.553	234.458
30	R5F	05	18	18	234.458	270.577
30	R5FT	05	18	18	270.577	278.527
30	R5TB	05	18	18	278.527	281.689
30	R5T	05	18	18	281.689	327.409
30	R5TT	05	18	18	327.409	338.998
30	TOPS	05	18	18	338.998	388.998
30	BOTS	05	19	19	60.000	157.504
30	CRBPJ	05	19	19	157.504	231.918
30	CRBJ	05	19	19	231.918	233.823
30	CRJ	05	19	19	233.823	269.942
30	CRTJ	05	19	19	269.942	277.892
30	VOIDJ	05	19	19	277.892	317.897
30	CRRFJ	05	19	19	317.897	348.377
30	CRTPJ	05	19	19	348.377	384.453

30	TOPS	05	19	19	384.453	388.998
30	BOTS	05	20	20	60.000	120.000
30	BOT	05	20	20	120.000	172.070
30	R5BB	05	20	20	172.070	178.737
30	R5B	05	20	20	178.737	224.457
30	R5BT	05	20	20	224.457	232.553
30	R5FB	05	20	20	232.553	234.458
30	R5F	05	20	20	234.458	270.577
30	R5FT	05	20	20	270.577	278.527
30	R5TB	05	20	20	278.527	281.689
30	R5T	05	20	20	281.689	327.409
30	R5TT	05	20	20	327.409	338.998
30	TOPS	05	20	20	338.998	388.998
30	BOTS	05	21	21	60.000	157.504
30	CRBPK	05	21	21	157.504	231.918
30	CRBK	05	21	21	231.918	233.823
30	CRK	05	21	21	233.823	269.942
30	CRTK	05	21	21	269.942	277.892
30	VOIDK	05	21	21	277.892	317.897
30	CRRFK	05	21	21	317.897	348.377
30	CRTPK	05	21	21	348.377	384.453
30	TOPS	05	21	21	384.453	388.998
30	BOTS	05	22	22	60.000	120.000
30	BOT	05	22	22	120.000	172.070
30	R5BB	05	22	22	172.070	178.737
30	R5B	05	22	22	178.737	224.457
30	R5BT	05	22	22	224.457	232.553
30	R5FB	05	22	22	232.553	234.458
30	R5F	05	22	22	234.458	270.577
30	R5FT	05	22	22	270.577	278.527
30	R5TB	05	22	22	278.527	281.689
30	R5T	05	22	22	281.689	327.409
30	R5TT	05	22	22	327.409	338.998
30	TOPS	05	22	22	338.998	388.998
30	BOTS	05	23	23	60.000	157.504
30	CRBPL	05	23	23	157.504	231.918
30	CRBL	05	23	23	231.918	233.823
30	CRL	05	23	23	233.823	269.942
30	CRTL	05	23	23	269.942	277.892
30	VOIDL	05	23	23	277.892	317.897
30	CRRFL	05	23	23	317.897	348.377
30	CRTPL	05	23	23	348.377	384.453
30	TOPS	05	23	23	384.453	388.998
30	BOTS	05	24	24	60.000	120.000
30	BOT	05	24	24	120.000	172.070
30	R5BB	05	24	24	172.070	178.737
30	R5B	05	24	24	178.737	224.457
30	R5BT	05	24	24	224.457	232.553
30	R5FB	05	24	24	232.553	234.458
30	R5F	05	24	24	234.458	270.577
30	R5FT	05	24	24	270.577	278.527

30	R5TB	05	24	24	278.527	281.689
30	R5T	05	24	24	281.689	327.409
30	R5TT	05	24	24	327.409	338.998
30	TOPS	05	24	24	338.998	388.998

INNER BLANKET REGION

30	OREF	06	1	5	0.0	60.000
30	OREF	06	1	5	388.998	550.000
30	BOTS	06	1	5	60.000	120.000
30	BOT	06	1	5	120.000	172.070
30	FR6BB	06	1	5	172.070	178.737
30	FR6F	06	1	5	178.737	318.437
30	FR6FT	06	1	5	318.437	334.312
30	FR6T	06	1	5	334.312	338.998
30	TOPS	06	1	5	338.998	388.998
30	OREF	06	6	6	0.0	60.000
30	OREF	06	6	6	388.998	550.000
30	BOTS	06	6	6	60.000	120.000
30	BOT	06	6	6	120.000	172.070
30	R6BB	06	6	6	172.070	178.737
30	R6F	06	6	6	178.737	318.437
30	R6FT	06	6	6	318.437	334.312
30	R6T	06	6	6	334.312	338.998
30	TOPS	06	6	6	338.998	388.998
30	OREF	06	7	10	0.0	60.000
30	OREF	06	7	10	388.998	550.000
30	BOTS	06	7	10	60.000	120.000
30	BOT	06	7	10	120.000	172.070
30	FR6BB	06	7	10	172.070	178.737
30	FR6F	06	7	10	178.737	318.437
30	FR6FT	06	7	10	318.437	334.312
30	FR6T	06	7	10	334.312	338.998
30	TOPS	06	7	10	338.998	388.998
30	OREF	06	11	11	0.0	60.000
30	OREF	06	11	11	388.998	550.000
30	BOTS	06	11	11	60.000	120.000
30	BOT	06	11	11	120.000	172.070
30	R6BB	06	11	11	172.070	178.737
30	R6DET	06	11	11	178.737	318.437
30	R6FT	06	11	11	318.437	334.312
30	R6T	06	11	11	334.312	338.998
30	TOPS	06	11	11	338.998	388.998
30	OREF	06	12	24	0.0	60.000
30	OREF	06	12	24	388.998	550.000
30	BOTS	06	12	24	60.000	120.000
30	BOT	06	12	24	120.000	172.070
30	FR6BB	06	12	24	172.070	178.737
30	FR6F	06	12	24	178.737	318.437
30	FR6FT	06	12	24	318.437	334.312
30	FR6T	06	12	24	334.312	338.998
30	TOPS	06	12	24	338.998	388.998

30	OREF	06	25	26	0.0	60.000
30	OREF	06	25	26	388.998	550.000
30	BOTS	06	25	26	60.000	120.000
30	BOT	06	25	26	120.000	172.070
30	R6BB	06	25	26	172.070	178.737
30	R6F	06	25	26	178.737	318.437
30	R6FT	06	25	26	318.437	334.312
30	R6T	06	25	26	334.312	338.998
30	TOPS	06	25	26	338.998	388.998

30	OREF	06	27	30	0.0	60.000
30	OREF	06	27	30	388.998	550.000
30	BOTS	06	27	30	60.000	120.000
30	BOT	06	27	30	120.000	172.070
30	FR6BB	06	27	30	172.070	178.737
30	FR6F	06	27	30	178.737	318.437
30	FR6FT	06	27	30	318.437	334.312
30	FR6T	06	27	30	334.312	338.998
30	TOPS	06	27	30	338.998	388.998

30	OREF	07	0.0	60.000
30	OREF	07	388.998	550.000
30	BOTS	07	60.000	120.000
30	BOT	07	120.000	172.070
30	R7BB	07	172.070	178.737
30	R7F	07	178.737	318.437
30	R7FT	07	318.437	334.312
30	R7T	07	334.312	338.998
30	TOPS	07	338.998	388.998

30	OREF	07	1	6	0.0	60.000
30	OREF	07	1	6	388.998	550.000
30	BOTS	07	1	6	60.000	120.000
30	BOT	07	1	6	120.000	172.070
30	R7BB	07	1	6	172.070	178.737
30	R7F	07	1	6	178.737	318.437
30	R7FT	07	1	6	318.437	334.312
30	R7T	07	1	6	334.312	338.998
30	TOPS	07	1	6	338.998	388.998

30	OREF	07	7	7	0.0	60.000
30	OREF	07	7	7	388.998	550.000
30	BOTS	07	7	7	60.000	120.000
30	BOT	07	7	7	120.000	172.070
30	R7BB	07	7	7	172.070	178.737
30	R7DET	07	7	7	178.737	318.437
30	R7FT	07	7	7	318.437	334.312
30	R7T	07	7	7	334.312	338.998
30	TOPS	07	7	7	338.998	388.998

30	OREF	07	8	28	0.0	60.000
30	OREF	07	8	28	388.998	550.000

```
30    BOTS   07    8   28     60.000    120.000
30    BOT    07    8   28    120.000    172.070
30    R7BB   07    8   28    172.070    178.737
30    R7F    07    8   28    178.737    318.437
30    R7FT   07    8   28    318.437    334.312
30    R7T    07    8   28    334.312    338.998
30    TOPS   07    8   28    338.998    388.998

30    OREF   07   29   29      0.0       60.000
30    OREF   07   29   29    388.998    550.000
30    BOTS   07   29   29     60.000    120.000
30    BOT    07   29   29    120.000    172.070
30    R7BB   07   29   29    172.070    178.737
30    SOURB  07   29   29    178.737    234.458
30    SOURC1 07   29   29    234.458    270.577
30    SOURT  07   29   29    270.577    318.437
30    R7FT   07   29   29    318.437    334.312
30    R7T    07   29   29    334.312    338.998
30    TOPS   07   29   29    338.998    388.998

30    OREF   07   30   36      0.0       60.000
30    OREF   07   30   36    388.998    550.000

30    BOTS   07   30   36     60.000    120.000
30    BOT    07   30   36    120.000    172.070
30    R7BB   07   30   36    172.070    178.737
30    R7F    07   30   36    178.737    318.437
30    R7FT   07   30   36    318.437    334.312
30    R7T    07   30   36    334.312    338.998
30    TOPS   07   30   36    338.998    388.998

  OUTER BLANKET REGION
30    OREF8   08                 0.0       60.000
30    OREF8   08               388.998    550.000
30    BOTS    08                60.000    120.000
30    BOT     08               120.000    172.070
30    R8BB    08               172.070    178.737
30    R8F     08               178.737    318.437
30    R8FT    08               318.437    334.312
30    R8T     08               334.312    338.998
30    TOPS    08               338.998    388.998

30    OREF9   09                 0.0       60.000
30    OREF9   09               388.998    550.000
30    BOTS    09                60.000    120.000
30    BOT     09               120.000    172.070
30    R9BB    09               172.070    178.737
30    R9F     09               178.737    318.437
30    R9FT    09               318.437    334.312
30    R9T     09               334.312    338.998
30    TOPS    09               338.998    388.998

30    OREF10  10                 0.0       60.000
30    OREF10  10               388.998    550.000
30    BOTS    10                60.000    120.000
30    BOT     10               120.000    172.070
```

30	R10BB	10			172.070	178.737
30	R10F	10			178.737	318.437
30	R10FT	10			318.437	334.312
30	R10T	10			334.312	338.998
30	TOPS	10			338.998	388.998

30	OREF11	11			0.0	60.000
30	OREF11	11			388.998	550.000
30	BOTS	11	1	23	60.000	120.000
30	BOT	11	1	23	120.000	172.070
30	R11BB	11	1	23	172.070	178.737
30	R11F	11	1	23	178.737	318.437
30	R11FT	11	1	23	318.437	334.312
30	R11T	11	1	23	334.312	338.998
30	TOPS	11	1	23	338.998	388.998

30	BOTS	11	24	24	60.000	120.000
30	BOT	11	24	24	120.000	172.070
30	R11BB	11	24	24	172.070	178.737
30	R11DET	11	24	24	178.737	318.437
30	R11FT	11	24	24	318.437	334.312
30	R11T	11	24	24	334.312	338.998
30	TOPS	11	24	24	338.998	388.998

30	BOTS	11	25	60	60.000	120.000
30	BOT	11	25	60	120.000	172.070
30	R11BB	11	25	60	172.070	178.737
30	R11F	11	25	60	178.737	318.437
30	R11FT	11	25	60	318.437	334.312
30	R11T	11	25	60	334.312	338.998
30	TOPS	11	25	60	338.998	388.998

30	OREF12	12			0.0	60.000
30	OREF12	12			388.998	550.000
30	BOTS	12			60.000	120.000
30	BOT	12			120.000	172.070
30	R12BB	12			172.070	178.737
30	R12F	12			178.737	318.437
30	R12FT	12			318.437	334.312
30	R12T	12			334.312	338.998
30	TOPS	12			338.998	388.998

30	OREF13	13			0.0	60.000
30	OREF13	13			388.998	550.000
30	BOTS	13	1	17	60.000	120.000
30	BOT	13	1	17	120.000	172.070
30	R13BB	13	1	17	172.070	178.737
30	R13F	13	1	17	178.737	318.437
30	R13FT	13	1	17	318.437	334.312
30	R13T	13	1	17	334.312	338.998
30	TOPS	13	1	17	338.998	388.998

30	BOTS	13	18	18	60.000	120.000
30	BOT	13	18	18	120.000	172.070
30	R13BB	13	18	18	172.070	178.737
30	R13DET	13	18	18	178.737	318.437

30	R13FT	13	18	18	318.437	334.312
30	R13T	13	18	18	334.312	338.998
30	TOPS	13	18	18	338.998	388.998

30	BOTS	13	19	72	60.000	120.000
30	BOT	13	19	72	120.000	172.070
30	R13BB	13	19	72	172.070	178.737
30	R13F	13	19	72	178.737	318.437
30	R13FT	13	19	72	318.437	334.312
30	R13T	13	19	72	334.312	338.998
30	TOPS	13	19	72	338.998	388.998

30	OREF14	14			0.0	60.000
30	OREF14	14			388.998	550.000
30	BOTS	14			60.000	120.000
30	BOT	14			120.000	172.070
30	R14BB	14			172.070	178.737
30	R14F	14			178.737	318.437
30	R14FT	14			318.437	334.312
30	R14T	14			334.312	338.998
30	TOPS	14			338.998	388.998

30	OREF15	15			0.0	60.000
30	OREF15	15			388.998	550.000
30	EMPT	15	1	2	60.000	388.998
30	BOTS	15	3	13	60.000	120.000
30	BOT	15	3	13	120.000	172.070
30	R15BB	15	3	13	172.070	178.737
30	R15F	15	3	13	178.737	318.437
30	R15FT	15	3	13	318.437	334.312
30	R15T	15	3	13	334.312	338.998
30	TOPS	15	3	13	338.998	388.998
30	EMPT	15	14	16	60.000	388.998
30	BOTS	15	17	27	60.000	120.000
30	BOT	15	17	27	120.000	172.070
30	R15BB	15	17	27	172.070	178.737
30	R15F	15	17	27	178.737	318.437
30	R15FT	15	17	27	318.437	334.312
30	R15T	15	17	27	334.312	338.998
30	TOPS	15	17	27	338.998	388.998
30	EMPT	15	28	30	60.000	388.998
30	BOTS	15	31	41	60.000	120.000
30	BOT	15	31	41	120.000	172.070
30	R15BB	15	31	41	172.070	178.737
30	R15F	15	31	41	178.737	318.437
30	R15FT	15	31	41	318.437	334.312
30	R15T	15	31	41	334.312	338.998
30	TOPS	15	31	41	338.998	388.998
30	EMPT	15	42	44	60.000	388.998
30	BOTS	15	45	55	60.000	120.000
30	BOT	15	45	55	120.000	172.070
30	R15BB	15	45	55	172.070	178.737
30	R15F	15	45	55	178.737	318.437

30	R15FT	15	45	55	318.437	334.312
30	R15T	15	45	55	334.312	338.998
30	TOPS	15	45	55	338.998	388.998
30	EMPT	15	56	58	60.000	388.998
30	BOTS	15	59	69	60.000	120.000
30	BOT	15	59	69	120.000	172.070
30	R15BB	15	59	69	172.070	178.737
30	R15F	15	59	69	178.737	318.437
30	R15FT	15	59	69	318.437	334.312
30	R15T	15	59	69	334.312	338.998
30	TOPS	15	59	69	338.998	388.998
30	EMPT	15	70	72	60.000	388.998
30	BOTS	15	73	83	60.000	120.000
30	BOT	15	73	83	120.000	172.070
30	R15BB	15	73	83	172.070	178.737
30	R15F	15	73	83	178.737	318.437
30	R15FT	15	73	83	318.437	334.312
30	R15T	15	73	83	334.312	338.998
30	TOPS	15	73	83	338.998	388.998
30	EMPT	15	84	84	60.000	388.998

30	OREF16	16			0.0	60.000
30	OREF16	16			388.998	550.000
30	EMPT	16	1	6	60.000	388.998
30	BOTS	16	7	10	60.000	120.000
30	BOT	16	7	10	120.000	172.070
30	R16BB	16	7	10	172.070	178.737
30	R16F	16	7	10	178.737	318.437
30	R16FT	16	7	10	318.437	334.312
30	R16T	16	7	10	334.312	338.998
30	TOPS	16	7	10	338.998	388.998
30	EMPT	16	11	21	60.000	388.998
30	BOTS	16	22	25	60.000	120.000
30	BOT	16	22	25	120.000	172.070
30	R16BB	16	22	25	172.070	178.737
30	R16F	16	22	25	178.737	318.437
30	R16FT	16	22	25	318.437	334.312
30	R16T	16	22	25	334.312	338.998
30	TOPS	16	22	25	338.998	388.998
30	EMPT	16	26	36	60.000	388.998
30	BOTS	16	37	40	60.000	120.000
30	BOT	16	37	40	120.000	172.070
30	R16BB	16	37	40	172.070	178.737
30	R16F	16	37	40	178.737	318.437
30	R16FT	16	37	40	318.437	334.312
30	R16T	16	37	40	334.312	338.998
30	TOPS	16	37	40	338.998	388.998
30	EMPT	16	41	51	60.000	388.998
30	BOTS	16	52	55	60.000	120.000
30	BOT	16	52	55	120.000	172.070
30	R16BB	16	52	55	172.070	178.737
30	R16F	16	52	55	178.737	318.437
30	R16FT	16	52	55	318.437	334.312
30	R16T	16	52	55	334.312	338.998
30	TOPS	16	52	55	338.998	388.998
30	EMPT	16	56	66	60.000	388.998

30	BOTS	16	67	70	60.000	120.000
30	BOT	16	67	70	120.000	172.070
30	R16BB	16	67	70	172.070	178.737
30	R16F	16	67	70	178.737	318.437
30	R16FT	16	67	70	318.437	334.312
30	R16T	16	67	70	334.312	338.998
30	TOPS	16	67	70	338.998	388.998
30	EMPT	16	71	81	60.000	388.998
30	BOTS	16	71	81	60.000	120.000
30	BOT	16	71	81	120.000	172.070
30	R16BB	16	71	81	172.070	178.737
30	R16F	16	71	81	178.737	318.437
30	R16FT	16	71	81	318.437	334.312
30	R16T	16	71	81	334.312	338.998
30	TOPS	16	71	81	338.998	388.998
30	EMPT	16	82	85	60.000	388.998
30	BOTS	16	86	90	60.000	120.000
30	BOT	16	86	90	120.000	172.070
30	R16BB	16	86	90	172.070	178.737
30	R16F	16	86	90	178.737	318.437
30	R16FT	16	86	90	318.437	334.312
30	R16T	16	86	90	334.312	338.998
30	TOPS	16	86	90	338.998	388.998

30	OREF17	17	0.0	550.000
30	OREF18	18	0.0	550.000
30	OREF19	19	0.0	550.000
30	OREF20	20	0.0	550.000
30	OREF21	21	0.0	550.000
30	OREF22	22	0.0	550.000
30	OREF23	23	0.0	550.000
30	OREF24	24	0.0	550.000
30	OREF25	25	0.0	550.000